National Library
of Canada

Acquisitions and
Bibliographic Services Branch

395 Wellington Street
Ottawa, Ontario
K1A 0N4

Bibliothèque nationale
du Canada

Direction des acquisitions et
des services bibliographiques

395, rue Wellington
Ottawa (Ontario)
K1A 0N4

Your file Votre référence

Our file Notre référence

NOTICE

The quality of this microform is heavily dependent upon the quality of the original thesis submitted for microfilming. Every effort has been made to ensure the highest quality of reproduction possible.

If pages are missing, contact the university which granted the degree.

Some pages may have indistinct print especially if the original pages were typed with a poor typewriter ribbon or if the university sent us an inferior photocopy.

Reproduction in full or in part of this microform is governed by the Canadian Copyright Act, R.S.C. 1970, c. C-30, and subsequent amendments.

AVIS

La qualité de cette microforme dépend grandement de la qualité de la thèse soumise au microfilmage. Nous avons tout fait pour assurer une qualité supérieure de reproduction.

S'il manque des pages, veuillez communiquer avec l'université qui a conféré le grade.

La qualité d'impression de certaines pages peut laisser à désirer, surtout si les pages originales ont été dactylographiées à l'aide d'un ruban usé ou si l'université nous a fait parvenir une photocopie de qualité inférieure.

La reproduction, même partielle, de cette microforme est soumise à la Loi canadienne sur le droit d'auteur, SRC 1970, c. C-30, et ses amendements subséquents.

Canada

University of Alberta

Simple One and Three-Dimensional Finite Element Methods for Low Frequency Duct Acoustics

by

©

Bradley P. Semeniuk

A thesis submitted to the Faculty of Graduate Studies and Research in partial fulfillment of the requirements for the degree of **Master of Science**.

Department of Mechanical Engineering

Edmonton, Alberta
Spring 1993

National Library
of Canada

Acquisitions and
Bibliographic Services Branch

395 Wellington Street
Ottawa, Ontario
K1A 0N4

The author has granted an irrevocable non-exclusive licence allowing the National Library of Canada to reproduce, loan, distribute or sell copies of his/her thesis by any means and in any form or format, making this thesis available to interested persons.

The author retains ownership of the copyright in his/her thesis. Neither the thesis nor substantial extracts from it may be printed or otherwise reproduced without his/her permission.

Bibliothèque nationale
du Canada

Direction des acquisitions et
des services bibliographiques

395, rue Wellington
Ottawa (Ontario)
K1A 0N4

Your file Votre référence

Our file Notre référence

L'auteur a accordé une licence irrévocable et non exclusive permettant à la Bibliothèque nationale du Canada de reproduire, prêter, distribuer ou vendre des copies de sa thèse de quelque manière et sous quelque forme que ce soit pour mettre des exemplaires de cette thèse à la disposition des personnes intéressées.

L'auteur conserve la propriété du droit d'auteur qui protège sa thèse. Ni la thèse ni des extraits substantiels de celle-ci ne doivent être imprimés ou autrement reproduits sans son autorisation.

ISBN 0-315-82049-7

Canada

University of Alberta
Release Form

Name of Author:	**Bradley P. Semeniuk**
Title of Thesis:	**Simple One and Three-Dimension Finite Element Methods for Low Frequency Duct Acoustics**
Degree:	**Master of Science**
Year this degree granted:	**1993**

Permission is hereby granted to the **University of Alberta Library** to reproduce single copies of this thesis and to lend or sell such copies for private, scholarly, or scientific research purposes only.

The author reserves all other publication and other rights in association with the copyright in the thesis, and except as hereinbefore provided neither the thesis nor any substantial portion thereof may be printed or otherwise reproduced in any material form whatever without the author's prior written permission.

B. P. Semeniuk

Bradley P. Semeniuk
#17 Anderson Court
Leduc, Alberta
Canada
T9E 5H4

Date: April 16, 1993

University of Alberta

Faculty of Graduate Studies and Research

The undersigned certify that they have read, and recommend to the Faculty of Graduate Studies and Research for acceptance, a thesis entitled **Simple One and Three-Dimensional Finite Element Methods for Low Frequency Duct Acoustics** submitted by **Bradley P. Semeniuk** in partial fulfillment of the requirements for the degree of **Master of Science**.

Dr. A. Craggs (Supervisor)

JR Colbourne

Dr. J.R. Colbourne

Ken Fyfe

Dr. K.R. Fyfe

F.E. Vermeulen

Dr. F.E. Vermeulen

Date: April 16, 1993

Abstract

Two finite elements are presented here to study low frequency duct acoustics; a quadratic one-dimensional element and a linear isoparametric three-dimensional element. With the goal of developing simple finite element methods for the acoustics engineer, the computer programs developed are implemented on desktop computers.

The one-dimensional element was developed to study plane wave acoustics in rigid and flexible walled ducts with stationary flow. Its accuracy was tested by determining the natural frequencies of a standing wave in a rigid closed tube and a flexible walled tube with mass and stiffness controlled flexible walls. Very few elements were needed to calculate the sixth natural frequency with significant accuracy. To demonstrate the usefulness of the element in approximating various one-dimensional systems, sudden and gradual area changes, expansion chambers, Helmholtz resonators, sidebranches, junctions and curved pipe sections were all modelled using the element. These systems could all be accurately modelled by the element as long as the system was purely one-dimensional; offset systems and junctions with angle dependent sidebranches could not be modelled using this element.

A linear isoparametric three-dimensional element was formulated with the specific purpose of analysing plane wave, dipole and quadrupole mode propagation and attenuation in ducts using the procedure of chain assembling the elements in the axial direction. Mode cut-off frequencies could be predicted with an accuracy of 10.27% because of the linear approximation in the transverse direction of the duct. A linear isoparametric two-dimensional surface element was coupled to the three-dimensional element to allow the approximation of mass and stiffness controlled locally reacting flexible walls.

Sources of aerodynamic sound such as turbulence may represented by equivalent dipole and quadrupole sources. A hybrid element known as the *hypercube* was formulated to model aerodynamic sound sources by constraining the inner faces of the element with equivalent dipoles and quadrupoles. Various sound sources in a straight duct section were considered where it was found that sound propagation was independent of source configuration if the dimensions of the source were small compared with the acoustic wavelength.

Acknowledgements

The author wishes to thank his supervisor, Dr. A. Craggs, for his assistance and guidance in the preparation of this thesis and the Department of Mechanical Engineering for its support during the author's graduate student career. The author would also like to thank the Natural Sciences and Engineering Research Council for its financial support through operating grant No. A7431 held by A. Craggs.

Contents

CHAPTER 1

Introduction 1

CHAPTER 2

A One-Dimensional Quadratic Finite Element for Duct Systems 7

2.1 Introduction 7

2.2 The Webster Horn Equation 8

2.3 Pipe Element Formulation 10

  2.3.1 Assembly of Elements 13

  2.3.2 Continuity Between Elements 15

2.4 Element Testing: The Eigenvalue Problem 16

  2.4.1 Finite Element Models 16

2.5 Application of the Pipe Element to Sound Transmission 18

  2.5.1 Transmission Loss of Damped Systems 19

  2.5.2 Sudden Area Changes 25

  2.5.3 Gradual Area Changes 27

  2.5.4 Helmholtz Resonators 32

  2.5.5 Sidebranch Resonator 34

  2.5.6 Transmission Loss Calculations for a Simple Expansion Chamber 37

2.6 Curved Pipe Sections 43

CHAPTER 3

One-Dimensional Element with Flexible Walls 44

3.1 Introduction 44

3.2 Webster Horn Equation with Flexible Walls 45

3.3 Flexible Walled Pipe Element 47

3.4 Element Testing 52

  3.4.1 Eigenvalue Models 52

  3.4.2 Standing Waves in a Tube 54

CHAPTER 4

A Simple Three-Dimensional Finite Element to Model Dipole and Quadrupole Mode Propagation in Ducts 63

4.1 Introduction 63

4.2 The Helmholtz Equation 64

4.3 3-D Hexahedral Element Formulation 66

  4.3.1 Assembly of Elements 73

  4.3.2 Continuity Between Elements 76

4.4 Element Testing: The Eigenvalue Problem 76

4.5 Transmission Loss of Damped Acoustic Systems with Special Consideration of Dipole and Qaudrupole Mode Effects 83

  4.5.1 Tapered Elements 86

  4.5.2 Dipole and Qaudrupole Mode Propagation 88

    4.5.2.1 Chambers 95

    4.5.2.2 Duct Bends 104

    4.5.2.3 Curved Duct Sections 107

    4.5.2.4 Junctions 111

CHAPTER 5

A Three-Dimensional HEX8 Finite Element with Flexible Boundaries 115

5.1 Introduction 115

5.2 3-D Hexahedral Element with Flexible Boundaries 116

5.3 Element Testing 124

 5.3.1 Eigenvalue Models 124

CHAPTER 6

The Hypercube Element 127

6.1 Introduction 127

6.2 The Hypercube Element 128

6.3 Modelling Dipole and Quadrupole Source Distributions 130

CHAPTER 7

Conclusions 142

REFERENCES 146

APPENDIX A 156

A.1 The Jacobi Method 156

A.2 LU Decomposition 164

List of Tables

2.1 Eigenvalues of a Closed Tube of Unit Length 18

2.2 Eigenvalue Model Prediction Errors 18

3.1 Eigenvalues of a Closed Tube of Unit Length with Mass-Controlled Flexible Walls 53

3.2 Eigenvalues of a Closed Tube of Unit Length with Stiffness-Controlled Flexible Walls 54

4.1 Axial Eigenvalues (k^2) of a Rectangular Duct Section. Comparison with Exact Eigenvalues and Those Calculated with 1-D Pipe Elements 78

4.2 Eigenvalues for a Circular Cylindrical Enclosure, 10 Radial Elements 82

4.3 Eigenvalue Model Prediction Errors 82

4.4 Radial and Diametral Modes in rad/s for Expansion Chamber; $r = 0.5$ m 85

4.5 Exact and Calculated Eigenvalues for a Straight Duct Section 93

5.1 Eigenvalues of a Closed Straight Duct Section of Unit Length with Mass-Controlled Flexible Walls 126

5.2 Eigenvalues of a Closed Straight Duct Section of Unit Length with Stiffness-Controlled Flexible Walls 126

List of Figures

2.1 Infinitesimal Fluid Element of Varying Cross-Sectional Area 8
2.2 Quadratic Variable Cross-Sectional Area Pipe Element 11
2.3 Unconstrained Pipe Elements 14
2.4 Global System of Connected Pipe Elements 14
2.5 5 Element Model of a Closed Tube 17
2.6 One-Dimensional Acoustic Enclosure 20
2.7 Reactive Muffler Model for Transmission Loss Calculations 23
2.8 Abrupt Area Change in a Pipe 25
2.9 Finite Element Model for Sudden Cross-Sectional Area Change in a Pipe (10 element model) 26
2.10 Exact and Approximate T.L. Values for a Sudden Area Change 27
2.11 Gradual Area Change in a Pipe (Tapered) 28
2.12 Finite Element Mesh for a Gradual Area Change in a Pipe (14 element model) 28
2.13 T.L. Values for Gradual Area Changes of Various Expansion Ratios 29
2.14 Exponential Horn Section 30
2.15 Finite Element Mesh for an Exponential Connector (14 element model) 30
2.16 T.L. Comparison Between Exp. Horn and Tapered Section 31
2.17 Helmholtz Resonator 32
2.18 Finite Element Model for a Helmholtz Resonator (15 element model) 33
2.19 T.L. Values for a Helmholtz Resonator 34
2.20 Closed-Tube Sidebranch Resonator 35

2.21 Finite Element Mesh of a Closed-Tube Sidebranch Resonator (26 element model) 36

2.22 T.L. Values for a Closed-Tube Sidebranch Resonator 36

2.23 Simple Expansion Chamber 37

2.24 Finite Element Mesh for a Simple Expansion Chamber (10 element model) ... 38

2.25 T.L. Values for a Reactive Muffler 38

2.26 Finite Element Mesh for an Expansion Chamber with Outlet Pipe Extended 0.6 Length of the Chamber (6 element model) 39

2.27 T.L. Values for Expansion Chamber with Outlet Pipe Extended 0.6 Length of the Chamber 40

2.28 Finite Element Mesh for an Expansion Chamber with Outlet Pipe Extended 0.5 Length of the Chamber (5 element model) 40

2.29 T.L Values for Expansion Chamber with Outlet Pipe Extended 0.5 Length of the Chamber 41

2.30 Finite Element Mesh for Expansion Chamber with Outlet Pipe Extended 0.4 Length of the Chamber (3 element model) 41

2.31 Finite Element Mesh for Expansion Chamber with Outlet Pipe Extended 0.4 Length of the Chamber (6 element model) 42

2.32 T.L. Values for Expansion Chamber with Outlet Pipe Extended 0.4 Length of the Chamber (3 and 6 element models) 42

3.1 Infinitesimal Fluid Element of Varying Cross-Sectional Area with Flexible Side Walls 45

3.2 Quadratic Variable Cross-Sectional Area Pipe Element with Flexible Side Walls 47

3.3 Tube with Forcing Piston at $x = 0$, Open end at $x = l$ 55

3.4 Standing Wave in a Rigid Walled Pipe; Piston at $x = 0$, Open at $x = l$;

$\omega = \pi c / 2l$ 56

3.5 Standing Wave in a Rigid Walled Pipe; Piston at $x = 0$, Open at $x = l$;

$\omega = 3\pi c / 2l$ 57

3.6 Standing Wave in a Rigid Walled Pipe; Piston at $x = 0$, Open at $x = l$;

$\omega = 5\pi c / 2l$ 57

3.7 Standing Wave in a Flexible Walled Pipe ($m_w = 10$); Piston at $x = 0$,

Open at $x = l$; $\omega = \pi c / 2l$ 58

3.8 Standing Wave in a Flexible Walled Pipe ($m_w = 10$); Piston at $x = 0$,

Open at $x = l$; $\omega = 3\pi c / 2l$ 58

3.9 Standing Wave in a Flexible Walled Pipe ($m_w = 10$); Piston at $x = 0$,

Open at $x = l$; $\omega = 5\pi c / 2l$ 59

3.10 Standing Wave in a Flexible Walled Pipe ($m_w = 1$); Piston at $x = 0$,

Open at $x = l$; $\omega = \pi c / 2l$ 60

3.11 Standing Wave in a Flexible Walled Pipe ($m_w = 1$); Piston at $x = 0$,

Open at $x = l$; $\omega = 3\pi c / 2l$ 60

3.12 Standing Wave in a Flexible Walled Pipe ($m_w = 1$); Piston at $x = 0$,

Open at $x = l$; $\omega = 5\pi c / 2l$ 61

3.13 Standing Wave in a Flexible Walled Pipe ($m_w = 0.01$); Piston at $x = 0$,

Open at $x = l$; $\omega = \pi c / 2l$ 61

3.14 Standing Wave in a Flexible Walled Pipe ($m_w = 0.01$); Piston at $x = 0$,

Open at $x = l$; $\omega = 3\pi c / 2l$ 62

3.15 Standing Wave in a Flexible Walled Pipe ($m_w = 0.01$); Piston at $x = 0$,

Open at $x = l$; $\omega = 5\pi c / 2l$ 62

4.1 Infinitesimal 3-D Fluid Element 64

4.2 Isoparametric HEX8 Element in Local and Global Coordinate Systems 66

4.3 HEX8 Element in Local Coordinate System 68
4.4 Unconstrained and Unconnected HEX8 Elements 74
4.5 Global System of Assembled HEX8 Elements 74
4.6 Rectangular Duct Section 77
4.7 Formation of Ring Segment 79
4.8 Ring Segment Cross-Section 79
4.9 10 HEX8 Elements Assembled in Ring Segment Form to Model a Cylindrical Enclosure 81
4.10 2-D Mesh of 10 Axisymmetric Ring Elements with 22 DOF 81
4.11 Axisymmetric Ring Element Mesh to Model a Cylindrical Expansion Chamber (66 DOF) 84
4.12 T.L. Results for a Cylindrical Expansion Chamber with Expansion Ratio = 10; One and Three-Dimensional Elements 84
4.13 Nodal Lines for Transverse Pressure Distributions in a Circular Duct, *m* Denotes Diametral Modes, *n* Denotes Radial Modes 85
4.14 T.L. Results for a Rectangular Expansion Chamber, Expansion Ratio = 10; One and Three Dimensional Elements 86
4.15 HEX8 Element Mesh Representing Sudden Area Changes in a Duct 87
4.16 Length of a Tapered HEX8 Element 88
4.17 T.L. Results for a Chamber with Various Taper Lengths 88
4.18 Location of Nodal Pressures for a Duct Cross-Section 90
4.19 Modes of Propagation for a Rectangular Section; the Plane wave, Dipole and Quadrupole Mode Pressure Distributions 91
4.20 Straight Duct Section; Unconstrained and Constrained (*) Pressure Nodes 93
4.21 Finite Element Model of Expansion Chamber; 12 HEX8 Elements 96
4.22 T.L. Values for an Expansion Chamber, Dipole Mode (1,0) Propagation 97
4.23 T.L. Values for an Expansion Chamber, Dipole Mode (0,1) Propagation 97

4.24 T.L. Values for an Expansion Chamber, Quadrupole Mode (1,1) Propagation 98
4.25 Finite Element Model of an Expansion Chamber, 14 HEX8 Elements 99
4.26 T.L. Values for an Expansion Chamber, Dipole Mode (1,0) Propagation 100
4.27 T.L. Values for an Expansion Chamber, Dipole Mode (1,0) Propagation 100
4.28 T.L. Values for an Expansion Chamber, Dipole Mode (0,1) Propagation 101
4.29 T.L. Values for an Expansion Chamber, Dipole Mode (0,1) Propagation 102
4.30 T.L. Values of an Expansion Chamber, Quadrupole Mode (1,1) Propagation 103
4.31 T.L. Values of an Expansion Chamber, Quadrupole Mode (1,1) Propagation 103
4.32 Finite Element Model of a 90° Duct Bend; 36 HEX8 Elements 104
4.33 T.L. Values for a 90° Duct Bend, Plane Wave Propagation 105
4.34 T.L. Values for a 90° Duct Bend, Dipole Mode (1,0) Propagation 106
4.35 T.L. Values for a 90° Duct Bend, Dipole Mode (0,1) Propagation 106
4.36 T.L. Values for a 90° Duct Bend, Quadrupole Mode (1,1) Propagation 107
4.37 Finite Element Model of a 90° Curved Duct Section; $R_1 = 0.30$ m, $R_2 = 0.45$ m; 36 HEX8 Elements 108
4.38 T.L. Values for a 90° Curved Duct Section, Plane Wave Propagation 109
4.39 T.L. Values for a 90° Curved Duct Section, Dipole Mode (1,0) Propagation 109
4.40 T.L. Values for a 90° Curved Duct Section, Dipole Mode (0,1) Propagation 110
4.41 T.L. Values for a 90° Curved Duct Section, Quadrupole Mode (1,1) Propagation 111
4.42 Finite Element Model of a Junction with 45° Sidebranch; 38 HEX8 Elements 112
4.43 T.L. Values for a Junction with 45° Sidebranch, Plane Wave Propagation 113

4.44 T.L. Values for a Junction with 45° Sidebranch, Dipole Mode (1,0) Propagation 113

4.45 T.L. Values for a Junction with 45° Sidebranch, Dipole Mode (0,1) Propagation 114

4.46 T.L. Values for a Junction with 45° Sidebranch, Quadrupole Mode (1,1) Propagation 114

5.1 HEX8 Element with Flexible Walls 116

5.2 Linear Isoparametric Surface Element in Local and Global Coordinate Systems 119

5.3 Closed Straight Duct Section with Flexible Side Walls and Rigid Ends 124

6.1 Elementary Source Distribution in a Duct 128

6.2 Hypercube Element (7 Assembled HEX8 Elements) 128

6.3 Surfaces of the Inner Cube Representing Axial and Transverse Sources in a Duct 129

6.4 Hypercube Element Representing a Sound Source in a Straight Duct Section 130

6.5 Axial Dipole (1,0) Source; Dipole (1,0) Prescribed at Outlet 131

6.6 Axial Quadrupole (1,1) Source; Quadrupole (1,1) Prescribed at Outlet 132

6.7 Axial Dipole (1,0) Source; Dipole (0,1) Prescribed at Outlet 132

6.8 Transverse Dipole (1,0) Source; Plane Wave Prescribed at Outlet 133

6.9 Transverse Dipole (0,1) Source; Plane Wave Prescribed at Outlet 134

6.10 Transverse Dipole (1,0) Source; Dipole (1,0) Prescribed at Outlet 134

6.11 Transverse Quadrupole (1,1) Source; Quadrupole (1,1) Prescribed at Outlet 135

6.12 Offset Source in a Straight Duct Section 136

6.13 Offset Axial Dipole (1,0) Source; Dipole (1,0) Prescribed at Outlet 136

6.14 Large Source in a Straight Duct Section 137

6.15 Large Axial Dipole (1,0) Source; Dipole (1,0) Prescribed at Outlet 138

6.16 Large Transverse Dipole (1,0) Source; Dipole (1,0) Prescribed at Outlet 138

6.17 Dipole (1,0) Prescribed to all Surfaces of the Inner Cube; Dipole (1,0) Prescribed at Outlet 139

6.18 Small Source in a Straight Duct Section 139

6.19 Dipole (1,0) Source; Dipole (1,0) Prescribed at Outlet 140

6.20 Quadrupole (1,1) Source; Quadrupole (1,1) Prescribed at Outlet 141

6.21 Small Dipole (1,0) Source (0.000001 m × 0.000001 m × 0.000001 m); Dipole (1,0) Prescribed at Outlet 141

CHAPTER 1
Introduction

Designers of ducted flow equipment such as air conditioning or ventilation systems and intake and exhaust systems need to consider acoustic behaviour as well as aerodynamic performance in the design and construction of the duct. These systems typically incur noise problems due to fans or duct configuration and there is a need to accurately predict noise generation and propagation within these systems. The sound field produced by noise sources in the duct system depends upon the geometry of the system, characteristics of the duct walls (flexible, rigid, lined) and the form of duct termination. Air flow through the system can also have the added effect of increasing or decreasing the speed at which sound waves travel through the system. Practical analytical solutions are only available for duct systems with very simple geometries and constraints. This leaves the engineer with only gross approximations to use when designing a duct system. Simple acoustic finite elements may be employed by the engineer to assist duct system design. Although finite elements are only a form of approximation, they provide much better accuracy than the rules of thumb available to the acoustics engineer and they are able to model any complex geometries.

The objective of this thesis was to present simple acoustic finite elements which could be easily implemented by engineers using current desktop computer technology. Two finite elements were used in this research; a one-dimensional element with quadratic pressure variation between nodes and a three-dimensional isoparametric hexahedral element with linear variations in pressure between nodes. These simple elements are sufficient to approximate low frequency duct systems, including the quadrupole mode. All elements and applicable equations are developed using Galerkin's method of weighted residuals, contrary to the use of variational principles in much of the literature. The propagation of sound through various duct components is considered for systems of no flow and low frequencies. Elements are formulated to model systems with both rigid walls and locally reacting flexible boundaries. As well, the propagation of plane wave modes and higher order modes up to the quadrupole mode have been considered. The higher order dipole and quadrupole modes cause bending and torsion in the walls of the

PAGINATION ERROR.	ERREUR DE PAGINATION.
TEXT COMPLETE.	LE TEXTE EST COMPLET.
NATIONAL LIBRARY OF CANADA.	BIBLIOTHEQUE NATIONALE DU CANADA.
CANADIAN THESES SERVICE.	SERVICE DES THESES CANADIENNES.

procedure can rapidly become very exhausting. For complicated non-uniform ducts with and without flow, numerical methods of solution must be employed.

A brief history of important developments in the use of finite elements to solve acoustic problems is presented here in a chronological order of development. This history is by no means complete but several significant works are presented here with particular reference to the duct and pipe acoustics discussed in this thesis. These works are fundamental references for an individual interested in acoustic finite elements.

The earliest research concerning the use of acoustic finite elements was work by Gladwell [57] in 1965. Energy variational principles were used which lead to the governing differential equations and boundary conditions. One-dimensional elements and two-dimensional square elements with cubic polynomial shape functions were considered, with the acoustic pressure and spatial derivatives as the nodal quantities. A coupled acoustic system consisting of an air column with piston at one end was modelled using 3 one-dimensional elements with resulting frequencies within 5% of the exact frequencies. Standing waves inside a square were approximated using 1 and 4 two-dimensional elements. The finite element approximation gave frequencies identical to those obtained by exact theory.

Craggs [24] used a three-dimensional cuboid element in 1971, with cubic Hermitian polynomial shape functions and acoustic velocity potential and spatial derivatives at the nodes. A Ritz variational method was used to formulate the element and the acoustics of a rectangular room were modelled. The first seven room modes were predicted to within 0.13% of exact solution using a one element model. This element is restricted to acoustic systems such as rooms or ducts with corners due to its non deformable cuboid shape. Later, Craggs [25, 26] employed simple tetrahedral elements with linear shape functions and acoustic pressure as the only nodal quantity to model irregular shaped enclosures. These elements were not as accurate as those used in earlier work [24, 57], but they did allow flexibility at modelling irregular shapes where extreme accuracy was not the governing criterion.

Young and Crocker [98] employed a rectangular cubic Hermitian element to model two-dimensional rectangular expansion chambers in 1975. Nodal parameters were the acoustic pressure and its spatial derivatives. Acoustic four-pole parameters were derived from the finite element models and used to predict the transmission loss of an expansion chamber with non-reflective impedance (ρc) at the ends. A finite element method for damped acoustic systems was developed by Craggs [27] to model axisymmetric reactive mufflers using simple, geometrically constrained linear isoparametric hexahedral elements with acoustic pressure as the nodal quantity. This isoparametric form of element was extremely flexible and could be used to model any geometry. The variational approach was used to develop the finite element approximations for a damped acoustic system, based on the concept of an adjoint system given earlier by Gladwell [58, 59] and Morse and Ingard [71]. This type of formulation allows a variety of forms of energy dissipation to be modelled and subsequently the work was continued by Craggs [28, 29] to include mufflers with dissipative liners.

Acoustic transmission in non-uniform ducts, including higher order modes in connecting straight ducts, was studied by Astley and Eversman [7] using finite elements with two-dimensional quadrilateral isoparametric formulation and acoustic pressure as the nodal quantity. The element was formulated using a Galerkin method rather than the traditional variational approach. Astley and Eversman [10] extended this work to include the effect of compressible mean flow in non-uniform ducts. The element was formulated with both acoustic pressure and velocity components as dependent variables and results of the work suggested that modal interactions are present for mean flow at high mach numbers.

The acoustic characteristics of duct bends with no flow were considered by Cabelli and Shepherd [19, 91] using two-dimensional quadratic isoparametric element models formulated in terms of acoustic pressure. Propagation of higher order cross modes was investigated and general predictions were made based on the outer and inner radii of the duct. Later, Cabelli [16] extended this work to include the effects of flow on the transmission and reflection characteristics of a duct bend. The irrotational compressible flow solution was obtained using six-noded triangular finite elements with the stream function and local density as nodal variables. Governing acoustic equations were approximated with eight-noded quadrilateral isoparametric elements in terms of velocity potential.

Simple one-dimensional finite elements were used by Craggs [31] to study the acoustic properties of pipe systems with restriction that the transverse dimensions of the element be small compared with the wavelength. The element was formulated using a variational approach with quadratic variation in pressure, the only nodal quantity. Eigenvalues of a closed tube of unit length were determined with a high degree of accuracy for only a few elements. Indications were that the element could be easily used to model pipe systems and pipes containing expansion chambers, the restriction being that frequencies are small enough so that the wavelength restriction holds, this being the case in many practical situations.

In the works presented to this point, only plane wave mode propagation has been considered using simple linear elements. Craggs [32] suggested higher order mode propagation up to the quadrupole mode for simple finite element models of duct networks using linear isoparametric hexahedral finite elements. The majority of the work presented in this thesis is an extension of this earlier research by Craggs.

In the earliest acoustics work with finite elements, rectangular elements were used to model problems with rectangular geometries. Typically, pressure or velocity potential were the nodal quantities and spatial derivatives were included. Cubic Hermitian elements were often employed giving very accurate results for restrictive rectangular geometries. This element was probably a favourite of early researchers. High accuracies were obtained using only a few elements, no small consideration as computer usage was probably quite expensive at the time.

Triangular or tetrahedral elements were initially used to model complex geometries and curved surfaces. The polynomial shape functions for these elements could be integrated analytically. Later, deformable isoparametric elements were used to model complex geometries but element integrations must be carried out numerically with this type of element due to the number of coordinate transformations between global and local domains.

Variational principles were used extensively in early finite element formulations. This was fine if an existing energy functional was available for the problem of interest. Recently, Galerkin's method of weighted residuals has become quite accepted for formulating acoustic finite elements as it is applicable to a more general problem set than variational methods; only a governing differential equation is needed for formulation. As well, it provides solutions identical to those provided by the Ritz variational method, for problems where an energy functional exists.

A one-dimensional finite element with quadratic pressure and area variation is formulated to approximate the Webster Horn equation by Galerkin's method of weighted residuals in Chapter 2. Element accuracy is tested by solving the acoustic eigenvalue problem for a rigid walled closed tube. The approximate equations governing the forced harmonic motion of a damped acoustic system are developed and then used in conjunction with a transmission loss expression to model pipe systems. Sudden area expansions, tapered sections, finite length exponential horns, Helmholtz resonators, sidebranches and expansion chambers are all considered. Advantages and limitations of one-dimensional acoustic theory are explored.

In Chapter 3, an element similar to the one developed in Chapter 2 is formulated except that the walls of the element are considered to be locally reacting, meaning that wall motion is either mass or stiffness controlled. Eigenvalues are determined for a closed tube with mass and stiffness controlled walls and comparison is made with the rigid walled case to demonstrate the effect of a locally reacting boundary on the natural frequencies of a system. Included are standing wave pressure distributions at the first three natural frequencies for a flexible walled open tube with forcing piston.

A three-dimensional linear isoparametric hexahedral finite element is developed with pressure as the nodal quantity in Chapter 4. The element is deformable and is able to model any geometry. The accuracy of the element is determined for two rigid walled cases: the eigenvalues are solved for a cylindrical enclosure, the eigenvalues are solved for a closed, straight duct section. Comparison is made between the one-dimensional element presented in Chapter 2 and the three-dimensional element to demonstrate the limitations of one-dimensional theory. Higher order modes such as the dipole and quadrupole modes are considered which cause bending and twisting of duct sections. Sound transmission and the effect of cut-off frequency on the propagation of higher order modes is demonstrated for various duct geometries including bends, curves and junctions.

A similar linear isoparametric hexahedral element is presented in Chapter 5, only that it has been formulated to include the effects of locally reacting boundaries that are either mass or stiffness controlled. The effects of a locally reacting boundary on the natural frequencies of a duct section are determined and comparison is made with the rigid walled case.

In Chapter 6, a hybrid element referred to as the *hypercube* is introduced which may be used to represent various dipole and quadrupole sources in ducts. The hypercube actually consists of seven HEX8 elements assembled to form a "cube within a cube" configuration. The advantage of this type of element is that it may be connected to a simple chain assembly of HEX8 elements, thus keeping with the goal of using simple element configurations to model low frequency duct acoustics. This element may be especially useful for modelling turbulent sources in ducts with flow.

Concluding comments and further potential research considerations are included in Chapter 7.

CHAPTER 2

A One-Dimensional Quadratic Finite Element for Duct Systems

2.1 Introduction

Finite elements are in common use now for studying the acoustic properties of duct systems. These elements are generally of the three-dimensional variety and may not be necessary for studying plane wave acoustics at low frequencies (one-dimensional theory). In this chapter, a simple one-dimensional quadratic acoustic finite element (pipe element) is developed for studying the acoustic properties of duct systems including various area discontinuities and branched systems, the only restriction being that the transverse dimensions of the element be small compared to the acoustic wavelength [71]. There has not been extensive previous research [31, 38, 57] into the application of one-dimensional acoustic finite elements but as will be shown later in the chapter, there are many practical, low frequency situations which arise where these elements may be used quite successfully.

Galerkin's method of weighted residuals is used to formulate the one-dimensional acoustic finite element discussed here which contrasts previous development of the pipe element by variational methods [31]. This method and other weighted residual methods provide an alternative to developing the finite element equations using Rayleigh-Ritz variational methods. While Ritz variational methods are commonly used to formulate finite element equations, they require an existing energy functional, thus limiting their application to specific problems where the functional is known. Alternatively, Galerkin's method may be applied to any differential equation, making the method more applicable to a larger set of problems than variational methods. Also, when Galerkin's method is applied to a differential equation with an energy functional, the solution is identical to the Rayleigh-Ritz solution [14].

All formulations presented in this Chapter are based on assumptions of systems with rigid (hard) walls and no flow. Following the goal of developing a simple element for the acoustics engineer, all transmission loss calculations made with finite element models were considered as part of an infinite transmission line (ρc termination). Other complex impedance terminations could be considered but the subsequent complexity was not warranted in this work. Computations with the pipe element were carried out on a 80386 personal computer using FORTRAN code.

Mathematical development of the Webster Horn equation is considered in the next section using a control volume formulation. This is followed by development of the corresponding finite element equations and eigenvalue testing of the element. The last sections concern the development of damped equations of motion which are used in conjunction with a transmission loss equation to model sudden area expansions, tapered sections, finite length exponential horns, Helmholtz resonators, sidebranches and reactive expansion chambers.

2.2 The Webster Horn Equation

The one-dimensional wave equation may be developed by considering an element of fluid under pressure which is fixed in space. Equations expressing Newton's second law of motion, the laws of the conservation of mass and the gas law are established and then combined to produce the 1-D wave equation.

An infinitesimal element of fluid of length *dx*, shown in Fig. 2.1, where the particle velocity, cross-sectional area at any x and fluid density are designated by u, A and ρ respectively. If the element is considered as a control volume, mass must be

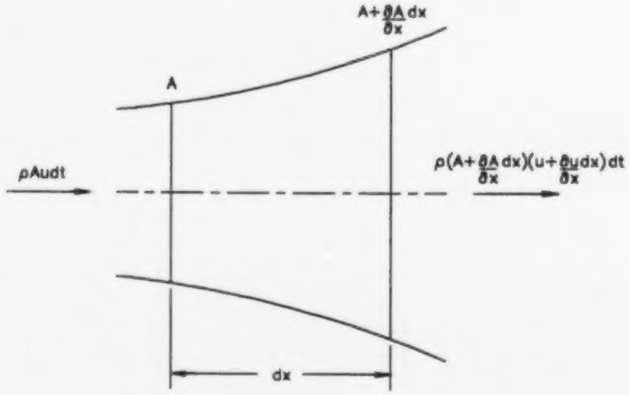
$A+\frac{\partial A}{\partial x}dx$
A
$\rho Audt$
$\rho(A+\frac{\partial A}{\partial x}dx)(u+\frac{\partial u}{\partial x}dx)dt$
dx

Figure 2.1: Infinitesimal Fluid Element of Varying Cross-Sectional Area

conserved and the mass change within the control volume is related to the inflow and outflow of fluid crossing the end faces of the element. This condition may be written as

$$\rho\left(A+\frac{\partial A}{\partial x}dx\right)\left(u+\frac{\partial u}{\partial x}dx\right)dt-\rho Audt+\frac{\partial \rho}{\partial t}Adxdt=0\,. \tag{2.1}$$

Simplification of Eq. (2.1) yields the linearized equation of mass conservation.

$$\rho A\frac{\partial u}{\partial x}+\rho u\frac{\partial A}{\partial x}+A\frac{\partial \rho}{\partial t}=0 \tag{2.2}$$

A linearized form of the momentum equation is also written as

$$-\frac{\partial p}{\partial x}=\rho\frac{\partial u}{\partial t} \tag{2.3}$$

and the acoustic pressure may be written as

$$\frac{\partial p}{\partial t}=\frac{\gamma p_0}{\rho}\frac{\partial \rho}{\partial t} \tag{2.4}$$

where γ is the ratio of the specific heats of the fluid. Eq. (2.4) is now substituted into Eq. (2.2) and the result is differentiated with respect to time. Thus,

$$A\frac{\partial^2 u}{\partial x\partial t}+\frac{\partial u}{\partial t}\frac{\partial A}{\partial x}+\frac{A}{\gamma p_0}\frac{\partial^2 p}{\partial t^2}=0\,. \tag{2.5}$$

The momentum equation may be differentiated with respect to *x*; the result being substituted into Eq. (2.5).

$$A\frac{\partial^2 p}{\partial x^2}+\frac{\partial p}{\partial x}\frac{\partial A}{\partial x}-\frac{\rho A}{\gamma p_0}\frac{\partial^2 p}{\partial t^2}=0 \tag{2.6}$$

The local speed of sound is defined as $c^2=\gamma p_0/\rho$, which is now substituted into Eq. (2.6), yielding the one-dimensional equation for acoustic waves travelling through a variable cross-sectional area wave guide at speed *c*,

$$\frac{\partial}{\partial x}\left(A\frac{\partial p}{\partial x}\right)-\frac{A}{c^2}\frac{\partial^2 p}{\partial t^2}=0. \tag{2.7}$$

If only harmonic motion is considered, the acoustic pressure has the form $p = pe^{j\omega t}$, where ω is the angular frequency and j is the complex operator. Substituting this into Eq. (2.7), the time derivative is eliminated thus resulting in the Webster Horn equation which represents one-dimensional sound waves in a pipe with varying cross-sectional area

$$\frac{\partial}{\partial x}\left(A\frac{\partial p}{\partial x}\right)+k^2Ap=0 \tag{2.8}$$

where k is the wavenumber, ω / c.

2.3 Pipe Element Formulation

A finite element which allows quadratic variation in both pressure and cross-sectional area throughout its length was chosen to approximate the Webster Horn equation. A quadratic element was chosen over a linear element as it provides better accuracy and fewer elements are required to model acoustic systems, increasing computational efficiency by reducing the number of pressure unknowns to be solved. The element, shown in Fig. 2.2, has three pressure degrees of freedom, at the ends and midway along the length of the element and will be referred to as the pipe element.

In a finite element approximation to the Webster Horn equation, pressure and area may be represented by quadratic interpolation polynomials

$$p=a_1+b_1\left(\frac{x}{l}\right)+c_1\left(\frac{x}{l}\right)^2 \tag{2.9}$$

$$A=a_2+b_2\left(\frac{x}{l}\right)+c_2\left(\frac{x}{l}\right)^2 \tag{2.10}$$

where a, b and c are constants representing pressures and cross-sectional areas at each element node.

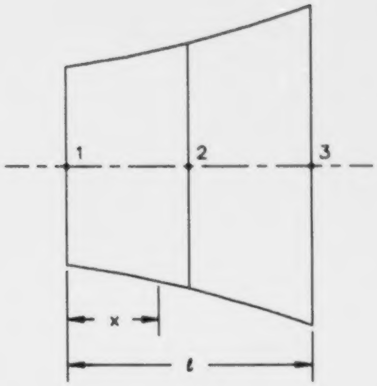

Figure 2.2: Quadratic Variable Cross-Section Pipe Element

After substitution of the nodal pressures into Eq. (2.9), the pressure polynomial is written as

$$p = p_1\left(1 - 3\frac{x}{l} + 2\frac{x^2}{l^2}\right) + p_2\left(4\frac{x}{l} - 4\frac{x^2}{l^2}\right) + p_3\left(-\frac{x}{l} + 2\frac{x^2}{l^2}\right). \tag{2.11}$$

Also, Eq. (2.11) may be written in matrix form

$$p = \{f\}^T\{p_e\} = \{p_e\}^T\{f\} \tag{2.12}$$

$$\{p_e\} = \begin{Bmatrix} p_1 \\ p_2 \\ p_3 \end{Bmatrix}$$

$$\{f\} = \begin{Bmatrix} \left(1 - 3\frac{x}{l} + 2\frac{x^2}{l^2}\right) \\ \left(4\frac{x}{l} - 4\frac{x^2}{l^2}\right) \\ \left(-\frac{x}{l} + 2\frac{x^2}{l^2}\right) \end{Bmatrix}$$

where $\{p_e\}$ is the vector containing the nodal acoustic pressures and $\{f\}$ is the vector containing the quadratic interpolation polynomials. The superscript T denotes the matrix has been transposed. In similar fashion, the cross-sectional area may be written as

$$A = A_1\left(1-3\frac{x}{l}+2\frac{x^2}{l^2}\right)+A_2\left(4\frac{x}{l}-4\frac{x^2}{l^2}\right)+A_3\left(-\frac{x}{l}+2\frac{x^2}{l^2}\right)$$

$$A = A_1+(4A_2-3A_1-A_3)\left(\frac{x}{l}\right)+(2A_1-4A_2+2A_3)\left(\frac{x^2}{l^2}\right). \tag{2.13}$$

Using Galerkin's method of weighted residuals, Eq. (2.12) is substituted into Eq. (2.8) and the residual, R, is written as [14]:

$$R=\frac{\partial}{\partial x}\left(A\{f_x'\}^T\right)\{p_e\}+k^2A\{f\}^T\{p_e\}, \tag{2.14}$$

where $\{f_x'\}$ denotes df/dx. Galerkin's equation is given as

$$\int_0^l \{f\}R\,dx=0 \tag{2.15}$$

and after substitution of the residual into Eq. (2.15), Galerkin's equation can be rewritten

$$\int_0^l\left(\{f\}\frac{\partial}{\partial x}\left(A\{f_x'\}^T\right)+k^2A\{f\}\{f\}^T\right)\{p_e\}\,dx=0. \tag{2.16}$$

The first term of Eq. (2.16) contains a matrix which is non-symmetric as the terms are not of the same order. It is integrated by parts with the result becoming

$$\int_0^l\left(A\{f_x'\}\{f_x'\}^T-k^2A\{f\}\{f\}^T\right)\{p_e\}\,dx=0 \tag{2.17}$$

with boundary conditions $A\partial p/\partial x=0$ at $x = 0$ and $x = l$ implying that there are no volume source terms present at these locations [31]. The relationship for cross-sectional area is now substituted into Eq. (2.17) and direct integration of the terms gives the finite element approximate equation of motion

$$\left([S]-k^2[P]\right)\{p\}=\{0\}, \tag{2.18}$$

where [S] and [P] represent the square, symmetric kinetic and potential energy matrices respectively. These matrices are given as:

$$[S]=\int_0^l \left(A\{f'_x\}\{f'_x\}^T\right)\{p_e\}dx$$

$$[S]=\alpha_1\begin{bmatrix}7 & -8 & 1\\ -8 & 16 & -8\\ 1 & -8 & 7\end{bmatrix}+\alpha_2\begin{bmatrix}3 & -4 & 1\\ -4 & 16 & -12\\ 1 & -12 & 11\end{bmatrix}+\alpha_3\begin{bmatrix}3 & -6 & 3\\ -6 & 32 & -26\\ 3 & -26 & 23\end{bmatrix}$$

$$\alpha_1=\frac{A_1}{3l},\ \alpha_2=\frac{(4A_2-3A_1-A_3)}{6l},\ \alpha_3=\frac{(2A_1-4A_2+2A_3)}{15l},$$

$$[P]=\int_0^l \left(A\{f\}\{f\}^T\right)\{p_e\}dx$$

$$[P]=\beta_1\begin{bmatrix}4 & 2 & -1\\ 2 & 16 & 2\\ -1 & 2 & 4\end{bmatrix}+\beta_2\begin{bmatrix}1 & 0 & -1\\ 0 & 16 & 4\\ -1 & 4 & 7\end{bmatrix}+\beta_3\begin{bmatrix}2 & -4 & -5\\ -4 & 64 & 24\\ -5 & 24 & 44\end{bmatrix}$$

$$\beta_1=\frac{A_1 l}{30},\ \beta_2=\frac{(4A_2-3A_1-A_3)l}{60},\ \beta_3=\frac{(2A_1-4A_2+2A_3)l}{420}$$

where all matrices have the dimensions 3×3. It is noted that for a pipe of uniform cross-sectional area ($A_1=A_2=A_3$), α_2, α_3, β_2 and β_3 all have values of zero.

2.3.1 Assembly of Elements

In Eq. (2.18), it is assumed that there are no volume source terms present meaning that the boundaries of the element are immobile. In this configuration, the element cannot be connected to another system. If volume sources Q_1 and Q_3 are present at the ends of the element, the inhomogeneous finite element equation becomes

$$\left([S]-k^2[P]\right)\{p_e\}=\rho\omega^2\begin{Bmatrix}Q_1\\Q_2\\Q_3\end{Bmatrix}. \tag{2.19}$$

The element assembly procedure is demonstrated by considering two pipe elements as shown in Fig. 2.3. In this configuration, the elements are unconstrained and have six pressure unknowns: p_1, p_2, p_3, p_4, p_5 and p_6 with volume sources: Q_1, Q_2, Q_3, Q_4, Q_5 and Q_6.

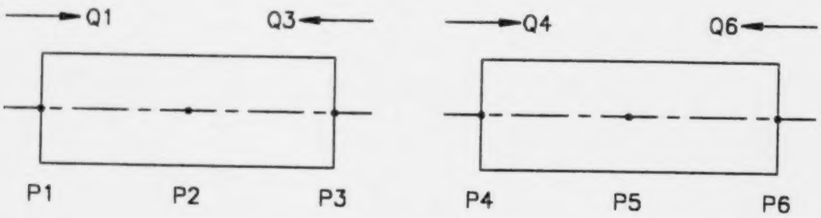

Figure 2.3: Unconstrained Pipe Elements

The elements may be joined at node 3 as shown in Fig. 2.4, and two conditions must be satisfied: $p_3=p_4=p_3^G$ and $\rho\omega^2Q_3+\rho\omega^2Q_4=0$. There are no external volume source terms introduced at the connection node as implied by the second equation shown above.

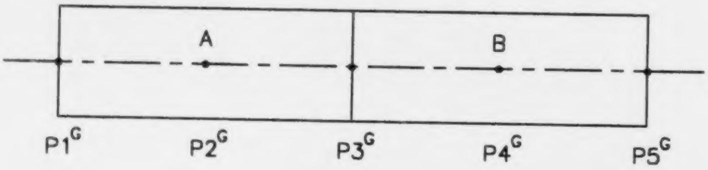

Figure 2.4: Global System of Connected Pipe Elements

The two element system with six degrees of freedom has now become a global system with five degrees of freedom with corresponding finite element equation given as

$$\left([S^G]-k^2[P^G]\right)\{p^G\}=\rho\omega^2\{Q^G\}, \tag{2.20}$$

with corresponding global kinetic and potential energy matrices

$$[S^G] = \begin{bmatrix} S_{11}^A & S_{12}^A & S_{13}^A & 0 & 0 \\ S_{21}^A & S_{22}^A & S_{23}^A & 0 & 0 \\ S_{31}^A & S_{32}^A & S_{33}^A + S_{11}^B & S_{12}^B & S_{13}^B \\ 0 & 0 & S_{21}^B & S_{22}^B & S_{23}^B \\ 0 & 0 & S_{31}^B & S_{32}^B & S_{33}^B \end{bmatrix}$$

$$[P^G] = \begin{bmatrix} P_{11}^A & P_{12}^A & P_{13}^A & 0 & 0 \\ P_{21}^A & P_{22}^A & P_{23}^A & 0 & 0 \\ P_{31}^A & P_{32}^A & P_{33}^A + P_{11}^B & P_{12}^B & P_{13}^B \\ 0 & 0 & P_{21}^B & P_{22}^B & P_{23}^B \\ 0 & 0 & P_{31}^B & P_{32}^B & P_{33}^B \end{bmatrix}$$

$$\{Q^G\} = \begin{Bmatrix} Q_1 \\ Q_2 \\ 0 \\ Q_4 \\ Q_5 \end{Bmatrix}$$

Individual element matrices can be assembled into a global system by overlaying them at the connecting nodes as demonstrated above. Many elements may be linked together using this procedure. It is common for the elements to be assembled together chain-like to form a system in one direction but the elements can also be connected to form branched systems as well.

2.3.2 Continuity Between Elements

A sufficient condition for the convergence of a finite element approximation is that continuity and completeness criteria [14] are satisfied. The continuity condition states that for second order differential equations such as the Webster Horn equation, only the dependent variable must be continuous across element boundaries. It is therefore sufficient to use a C^0 element (an element where only the dependent variable is continuous across element boundaries) in the finite element approximation as slope continuity is not required at the element boundaries. Only pressure continuity is required at the element boundaries. Completeness states that at least a linear polynomial should be used as a shape function when modelling a second order differential equation. The use of a quadratic polynomial satisfies this criterion. Both continuity and completeness have been satisfied in this finite element approximation assuring solution convergence. It should be noted that elements with both dependent variable and slope continuity (C^1) require fewer degrees of freedom upon assembly.

2.4 Element Testing: The Eigenvalue Problem

The accuracy of the pipe element was tested by predicting the natural frequencies of a closed tube with rigid walls containing a stationary medium. This test has been administered before with this element [31], but the results given here are a reassurance of the accuracy and convergence of the element. If the pressure perturbation modes in the x direction have the form [44]

$$p = A\cos\frac{n\pi x}{l}\sin\omega t,$$

then an exact solution for the eigenvalues, or natural frequencies, of Eq. (2.8) are given as

$$\left(\frac{\omega_n}{c}\right)^2 = \pi^2\left(\frac{n}{l}\right)^2, \tag{2.21}$$

where l is the length of the section and n is any integer denoting the mode number.

2.4.1 Finite Element Models

Finite element models with 5, 9 and 13 pipe elements were used to approximate the eigenvalues of a closed tube with a length of unity and cross-sectional area of 0.1 m^2. A model consisting of 5 elements is shown in Fig. 2.5 and is representative of the other finite element models. It has 11 pressure nodes or 11 degrees of freedom (DOF).

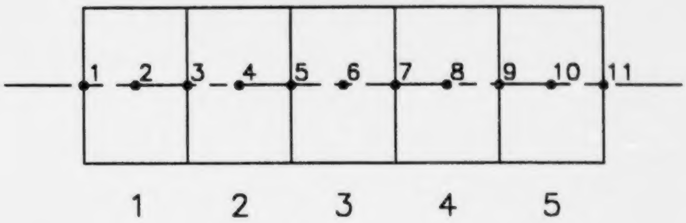

Figure 2.5: 5 Element Model of a Closed Tube

The exact eigenvalues of Eq. (2.22) and the eigenvalue approximations from the corresponding finite element models are shown in Table 2.1.

Results presented in Tables 2.1 and 2.2 demonstrate that a system of pipe elements is extremely accurate, even when only a few elements are used. The 5 element model with 11 DOF was accurate for the lower natural frequencies with a prediction error of 0.3% for the second natural frequency. The 9 element model with 19 DOF was quite accurate for the six modes presented here with a prediction error of 2.2% for the sixth natural frequency. A model with 13 elements and 27 DOF provided very accurate approximations to the first six natural frequencies having a prediction error of only 0.6% for the sixth natural frequency.

A Jacobi method eigenvalue routine [11, 82] was implemented in the finite element code for the eigenvalue approximations. This method will always provide absolute convergence to the eigenvalue solutions for real, symmetric matrices. The method is not as computationally efficient as some other eigenvalue routines but for the relatively small number of DOF in the finite element models presented here, computational times were acceptable. A complete listing of the Jacobi method and corresponding FORTRAN source code is given in the Appendix.

Table 2.1: Eigenvalues of a Closed Tube of Unit Length

Mode Number, *n*	Exact Eigenvalues	5 Elements	9 Elements	13 Elements
1	9.87	9.87	9.87	9.87
2	39.48	39.60	39.49	39.48
3	88.83	90.15	88.97	88.86
4	157.91	164.46	158.67	158.10
5	246.74	300.00	249.50	247.42
6	355.31	433.17	363.09	357.28

Table 2.2: Eigenvalue Model Prediction Errors

Mode Number, *n*	5 Elements % Error	9 Elements % Error	13 Elements % Error
1	0.0	0.0	0.0
2	0.3	0.03	0.0
3	1.5	0.2	0.03
4	4.2	0.5	0.1
5	21.6	1.1	0.3
6	21.9	2.2	0.6

2.5 Application of the Pipe Element to Sound Transmission

The transmission of sound energy in a duct can be reduced by absorbing part of the incident energy inside the duct using some sort of absorptive material. If the sound energy arrives at a discontinuity, some energy reflects back towards the source while a fraction of the sound energy will flow past the discontinuity. Reflective filters are most effective at low frequencies while absorptive filters are most effective at higher frequencies. The pipe element provides valid approximations only at the lower frequencies where only plane waves exist in the system. For this reason, only reflective systems will be modelled using the pipe element in this section.

Two common techniques are used to determine sound energy reduction in an acoustic system. The insertion loss technique compares the sound pressure levels at a specified point with and without filters present in the system while transmission loss (T.L.) gives the relationship between the energy in the incident wave at an inlet location and the transmitted wave at an outlet location. In much of the literature, a variety of reflective filters have been tested experimentally with much of the results presented in terms of T.L. In this section, many of these filters are modelled with the pipe element to demonstrate its diversity using T.L. calculations over a plane wave frequency range allowing easy comparison with the experimental T.L. results presented in the literature.

The T.L. equations are developed for a damped acoustic system and are implemented into the finite element equations in the following sections. Many reflective filters are modelled with the pipe element using T.L. calculations, demonstrating the application of the pipe element for approximating one-dimensional acoustic systems.

2.5.1 Transmission Loss of Damped Acoustic Systems

The approximate equations governing the forced harmonic motion of a damped acoustic system are developed using Galerkin's method of weighted residuals. A variational approach for studying damped vibration problems has been presented previously [59, 60, 71] based on the concept of an adjoint energy system which absorbs energy dissipated from the original system. An adjoint energy system need not be considered when developing the governing equations of motion using Galerkin's method but the resulting equations are identical to those developed using the variational approach and the adjoint energy system.

When damping exists in an acoustic system, both phase and amplitude are needed to completely describe the response. This has the effect of doubling the number of equations required to specify the response compared to the undamped case. Consider the one-dimensional enclosure shown in Fig. 2.6. The enclosure has velocity distribution $u = U \cos \omega t$ over surface A_1 at x_1 and reactive admittance $\zeta = U / p$ over A_2 at x_2.

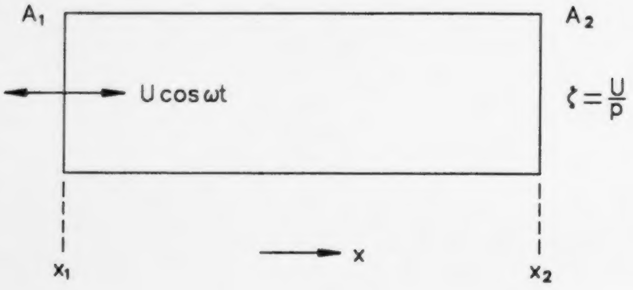

Figure 2.6: One-Dimensional Acoustic Enclosure

If there is no energy dissipation in the system, the approximate equations of motion may be obtained by applying Galerkin's method to the Webster Horn equation, Eq. (2.8), together with boundary conditions $\partial p / \partial x = j\rho\omega U$ on x_1, $\partial p / \partial x = -j\rho\omega\zeta p$ on x_2. The acoustic pressure may be represented by the following general approximation

$$p = [N]^T\{p_e\}, \tag{2.22}$$

where $[N]$ is a matrix containing the trial solutions, $\{p_e\}$ is a vector containing the nodal acoustic pressures and the superscript T denotes the transpose operation. Following Galerkin's method described earlier, Eq. (2.22) is substituted into Eq. (2.8) and the residual, R, is written as

$$R = \frac{\partial}{\partial x}\left(A[N_x']^T\right)\{p_e\} + k^2 A[N]^T\{p_e\}, \tag{2.23}$$

where $[N_x']$ denotes $\partial N / \partial x$. Galerkin's equation is now written as

$$\int_x [N] R dx = 0 \tag{2.24}$$

and upon substitution of Eq. (2.23) into Galerkin's equation, the result becomes

$$\int_x \left(\{N\} \frac{\partial}{\partial x}\left(A[N_x']^T\right) + k^2 [N][N]^T \right)\{p_e\} dx = 0. \tag{2.25}$$

The first term of Eq. (2.25) is integrated by parts and the boundary conditions are introduced, the result being the approximate governing equation of motion

$$\int_x A[N_x'][N_x']^T\{p_e\}dx - k^2\int_x A[N][N]^T\{p_e\}dx - \left([N]A[N_x']^T\{p_e\}\right)\Big|_{x_1+x_2} = 0. \quad (2.26)$$

Introduction of the real and imaginary parts of the response pressure, $p=(p_r+jp_i)e^{j\omega t}$; velocity, $U=(U_r+jU_i)e^{j\omega t}$; and admittance, $\zeta=(\zeta_r+j\zeta_i)e^{j\omega t}$ into Eq. (2.26) leads to a new equation of motion which describes the system

$$\begin{aligned}&[S]\{p_r\}+j[S]\{p_i\}-k^2[P]\{p_r\}-jk^2[P]\{p_i\}-j\rho\omega U_r\int_{x_1}[N]dx_1+\\&\rho\omega U_i\int_{x_1}[N]dx_1+j\rho\omega\zeta_r\int_{x_2}[N][N]^T\{p_r\}dx_2-\rho\omega\zeta_r\int_{x_2}[N][N]^T\{p_i\}dx_2-\\&-\rho\omega\zeta_i\int_{x_2}[N][N]^T\{p_r\}dx_2-j\rho\omega\zeta_i\int_{x_2}[N][N]^T\{p_i\}dx_2=0\end{aligned} \quad (2.27)$$

where the subscripts r and i denote the real and imaginary parts and j is the complex operator. As before, $[S]$ and $[P]$ represent the square, symmetric kinetic and potential energy matrices respectively. Collecting the real terms of Eq. (2.27), the resulting equation is of the form

$$\left([S]-k^2[P]-\rho\omega[C_i]\right)\{p_r\}-\rho\omega[C_r]\{p_i\}=\{Q_r\}. \quad (2.28)$$

Likewise, collecting the imaginary terms of Eq. (2.27) results in an equation of the form

$$\left([S]-k^2[P]-\rho\omega[C_i]\right)\{p_i\}+\rho\omega[C_r]\{p_r\}=\{Q_i\}. \quad (2.29)$$

If the real and imaginary response pressure vectors, $\{p_r\}$ and $\{p_i\}$, contain the input pressures p^1, the internal pressures p^S and the output pressures p^2, then the response pressure vectors may be written as

$$\{p_r\}=\begin{Bmatrix}p_r^1\\p_r^S\\p_r^2\end{Bmatrix},\ \{p_i\}=\begin{Bmatrix}p_i^1\\p_i^S\\p_i^2\end{Bmatrix},$$

the matrices $[C_r]$ and $[C_i]$ are given by

$$[C_r]=\begin{bmatrix}0 & 0 & 0\\ 0 & 0 & 0\\ 0 & 0 & \zeta_r D_{22}\end{bmatrix},\ [C_i]=\begin{bmatrix}0 & 0 & 0\\ 0 & 0 & 0\\ 0 & 0 & \zeta_i D_{22}\end{bmatrix},$$

and the real and imaginary source vectors, $\{Q_r\}$ and $\{Q_i\}$ are

$$\{Q_r\}=\rho\omega\begin{Bmatrix}-D_{11}U_i\\ 0\\ 0\end{Bmatrix},\ \{Q_i\}=\rho\omega\begin{Bmatrix}+D_{11}U_r\\ 0\\ 0\end{Bmatrix}.$$

Here D_{11} is a coupling matrix linking the nodal pressures at the input boundary; similarly, D_{22} is a coupling matrix linking the nodal pressures at the output boundary. As a matter of convenience, Eq. (2.28) and Eq. (2.29) are combined into single matrix form

$$\begin{bmatrix}[S]-k^2[P]-\rho\omega[C_i] & -\rho\omega[C_r]\\ +\rho\omega[C_r] & [S]-k^2[P]-\rho\omega[C_i]\end{bmatrix}\begin{Bmatrix}p_r\\ p_i\end{Bmatrix}=\begin{Bmatrix}Q_r\\ Q_i\end{Bmatrix}. \qquad (2.30)$$

It is worth noting that all terms in Eq. (2.30) are real quantities and for a given source, standard algorithms such as Gauss elimination or LU decomposition and back substitution may be employed to solve the system of simultaneous linear equations. A complete description of the LU method and corresponding FORTRAN source code is given in the Appendix.

The study of transmission loss is an ideal concept for analyzing the acoustic behaviour of various systems. Transmission loss is defined as the ratio, in decibels (dB), of the power of an incident acoustic wave to the power of a transmitted acoustic wave thus giving an indication of the pressure losses for a particular acoustic system. It is therefore an ideal quantity for analytical computations; the transmission loss equations are developed from Eq. (2.30). Consider the reactive muffler element shown in Fig. 2.7. The usual assumptions regarding the transmission loss calculations for the muffler element are as follows: the muffler element is inserted into an infinite transmission line (ρc termination), the system is excited by plane progressive wave input and there are no reflections of the transmitted and reflected waves because of the previous assumption. At the muffler input, a plane wave, $p^+e^{j\omega t}$, provides system excitation and the wave reflected back by the muffler is given by $p^- e^{j\omega t}$. The wave transmitted down the line from the muffler is given by $p_t e^{j\omega t}$.

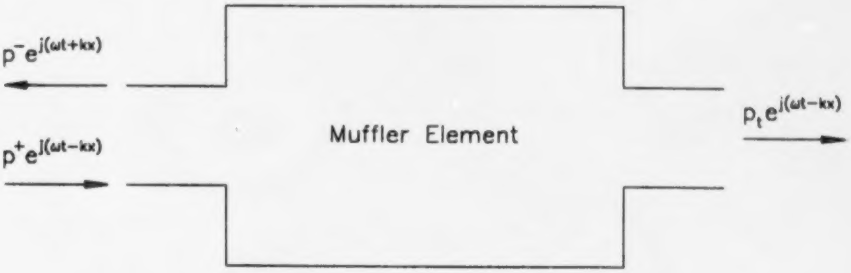

Figure 2.7: Reactive Muffler Model for Transmission Loss Calculations

Total acoustic pressure at the muffler input is $p=(p^+ + p^-)e^{j\omega t}$; the particle velocity on the muffler input surface is $U=(1/\rho c)(p^+ - p^-)e^{j\omega t}$; the normal acoustic admittance is taken as entirely real and is given by $\zeta_r = 1/\rho c$. System excitation is provided by a velocity source given by the incident pressure wave $p^+/\rho c$ (assumed entirely real). Therefore, the real and imaginary velocity vectors are $U_r = p_r^+/\rho c - p_r^-/\rho c$ and $U_i = p_i^-/\rho c$ respectively. These quantities may be substituted into Eq. (2.30) resulting in a new set of equations. The response vectors are now given as

$$\{p_r\} = \begin{Bmatrix} p_r^+ + p_r^- \\ p_r^S \\ p_r^2 \end{Bmatrix}, \quad \{p_i\} = \begin{Bmatrix} p_i^+ + p_i^- \\ p_i^S \\ p_i^2 \end{Bmatrix},$$

and the source vectors have now become

$$\{Q_r\} = k\begin{Bmatrix} D_{11}p_i^- \\ 0 \\ 0 \end{Bmatrix}, \quad \{Q_i\} = k\begin{Bmatrix} D_{11}\left(p_r^+ - p_r^-\right) \\ 0 \\ 0 \end{Bmatrix}.$$

In this form, the unknown quantities, p^-, are on the right-hand side of Eq. (2.30) and the known quantities, p^+, are on the left. For convenience, Eq. (2.30) is rearranged so that only unknown quantities are present on the left side

$$\begin{bmatrix} [S]-k^2[P] & -\rho\omega\left[C_r^\bullet\right] \\ +\rho\omega\left[C_r^\bullet\right] & [S]-k^2[P] \end{bmatrix} \begin{Bmatrix} p_r^\bullet \\ p_i^\bullet \end{Bmatrix} = \begin{Bmatrix} Q_r^\bullet \\ Q_i^\bullet \end{Bmatrix}. \tag{2.31}$$

The pressure vectors can now be written as

$$\left\{p_r^\bullet\right\} = \begin{Bmatrix} p_r^- \\ p_r^S \\ p_r^2 \end{Bmatrix}, \ \left\{p_i^\bullet\right\} = \begin{Bmatrix} p_i^- \\ p_i^S \\ p_i^2 \end{Bmatrix},$$

the matrix $\left[C_r^\bullet\right]$ is given as

$$\left[C_r^\bullet\right] = \begin{bmatrix} (1/\rho c)D_{11} & 0 & 0 \\ 0 & 0 & 0 \\ 0 & 0 & (1/\rho c)D_{22} \end{bmatrix},$$

and the source vectors are now written as

$$Q_r^\bullet = -\left([S'] - k^2[P']\right)p_r^+,$$

$$Q_i^\bullet = \begin{Bmatrix} kD_{11}p_r^+ \\ 0 \\ 0 \end{Bmatrix},$$

where the matrix $\left([S'] - k^2[P']\right)$ represents columns of $\left([S] - k^2[P]\right)$ corresponding to the input nodes.

For a system in which the incident pressure vector has values of unity, the transmission loss at the output nodes may be calculated from the following equation

$$T.L. = -10\log_{10}\left(p_r^2 + p_i^2\right). \tag{2.32}$$

If inlet and outlet cross-sectional areas are not equivalent, Eq. (2.32) must be modified as follows

$$T.L. = -10\log_{10}\left(\left(p_r^2 + p_i^2\right)\frac{A_o}{A_i}\right) \tag{2.33}$$

to allow for the difference in cross-sectional areas. Here A_o is the outlet cross-sectional area and A_i is the inlet cross-sectional area.

2.5.2 Sudden Area Changes

This section considers the situation in which the cross-sectional area of the pipe abruptly changes as shown in Fig. 2.8. A transmitted wave travels down the pipe while another wave is reflected back from the discontinuity towards the source. The boundary conditions of pressure continuity and mass conservation are satisfied at the discontinuity.

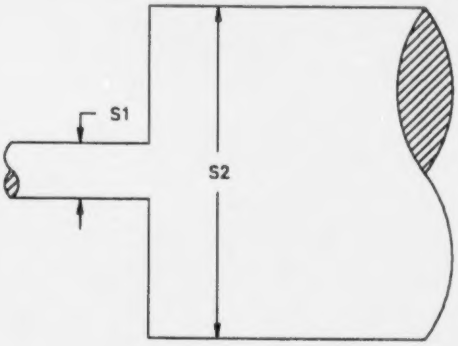

Figure 2.8: Abrupt Area Change in a Pipe

Since some sound is reflected at the discontinuity and not all the sound power is transmitted, the transmission loss equation for the case of a sudden area change in a pipe [44] is given as

$$T.L. = 10\log_{10}\left(\frac{(S_1+S_2)^2}{4S_1S_2}\right). \tag{2.34}$$

The transmission loss is symmetric in S_1 and S_2, meaning the transmission loss is the same whether the sound is incident at S_1 or S_2. It is assumed that the transmitted and reflected waves are plane waves but in the immediate region of the discontinuity, there is a departure of the plane wave front. In practice, this condition is not of great concern and transmission loss values calculated with Eq. (2.34) are satisfactory [37].

A sudden change in pipe cross-sectional area can be easily represented by the pipe element. Consider the finite element mesh shown in Fig. 2.9. The mesh consists of 10 pipe elements with 21 DOF. This model was assumed to be part of an infinite transmission line and a plane wave with incident pressure values of unity was input form the left at S_1. Application of this condition to Eq. (2.31) involves replacing the coupling matrices D_{11} and D_{22} with the respective input and output cross-sectional areas for the chamber. A plane wave with incident pressure values of unity was input into the chamber, allowing the use of Eq. (2.33) for the calculation of transmission loss values. The cross-sectional areas were 0.001 m² and 0.01 m² respectively.

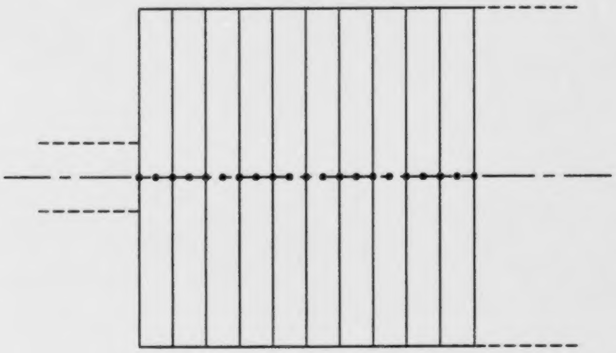

Figure 2.9: Finite Element Mesh for Sudden Cross-Sectional Area Change in a Pipe (10 element model)

Approximate transmission loss values were calculated with Eq. (2.33) up to a frequency of 500 Hz. These values compare well with the exact transmission loss value of 4.8073 dB calculated with Eq. (2.34) as shown in Fig. 2.10.

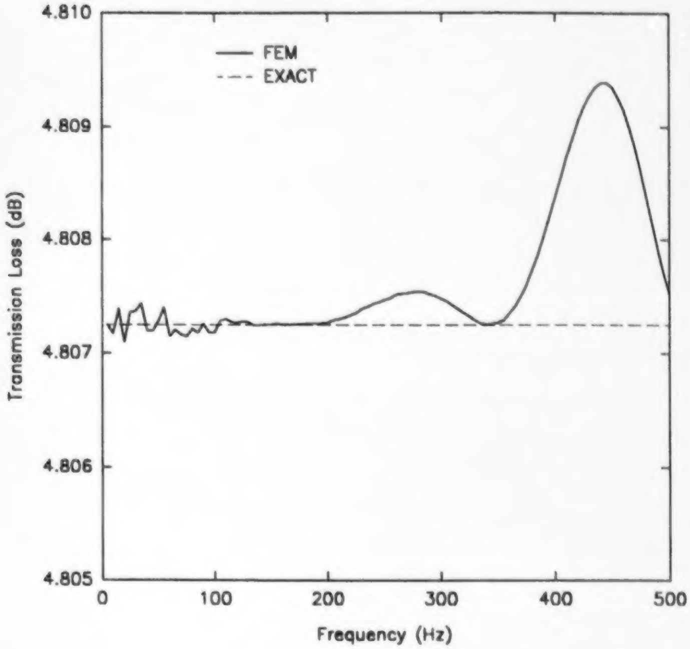

Figure 2.10: Exact and Approximate T.L. Values for a Sudden Area Change

The approximate transmission loss values determined with the pipe element are very accurate at the lower frequencies and even in the region around 400 Hz, the transmission loss values differ from the exact value by only 0.05%. At higher frequencies, the error increases because the one-dimensional model does not allow for transverse wave motion. A simple area change can reduce sound transmission in a pipe but most effective reflective filters make use of more than one area change.

2.5.3 Gradual Area Changes

The pipe element has been formulated to model one-dimensional systems with varying cross-sectional areas and is particularly useful for approximating systems with tapered and exponential horn shaped sections. Consider the tapered section shown in Fig. 2.11 of section length l with cross-sectional areas S_1 and S_2. This section is easily modelled with a mesh of pipe elements as shown in Fig. 2.12. The mesh consists of 10 elements in the tapered region and 2 elements each in the inlet and outlet regions of the section with a combined total of 29 DOF. The length of the tapered region was 0.5 m with an inlet cross-sectional area of 0.01 m^2 and expansion ratios of 25 and 50. For the transmission loss calculations, the model was assumed to be part of an infinite transmission line.

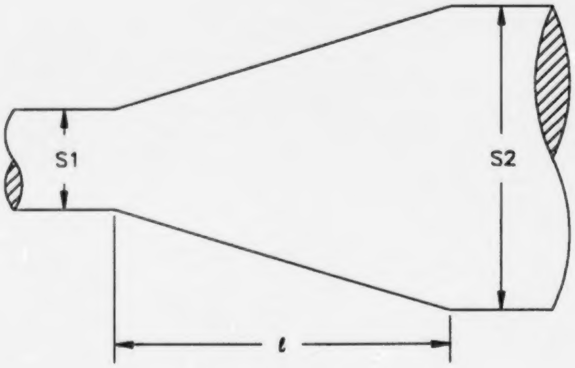

Figure 2.11: Gradual Area Change in a Pipe (Tapered)

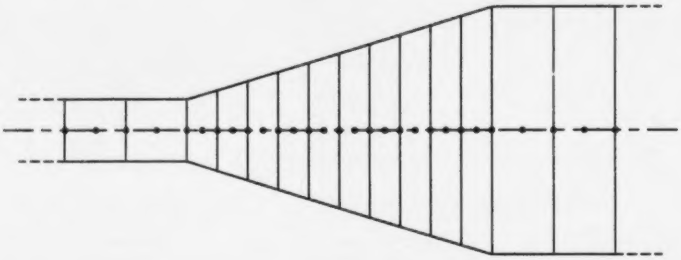

Figure 2.12: Finite Element Mesh for a Gradual Area Change in a Pipe (14 element model)

Calculated transmission loss values up to 500 Hz for the two expansion ratios are presented in Fig. 2.13 and are in exact agreement with measured T.L. values for a similar system [13].

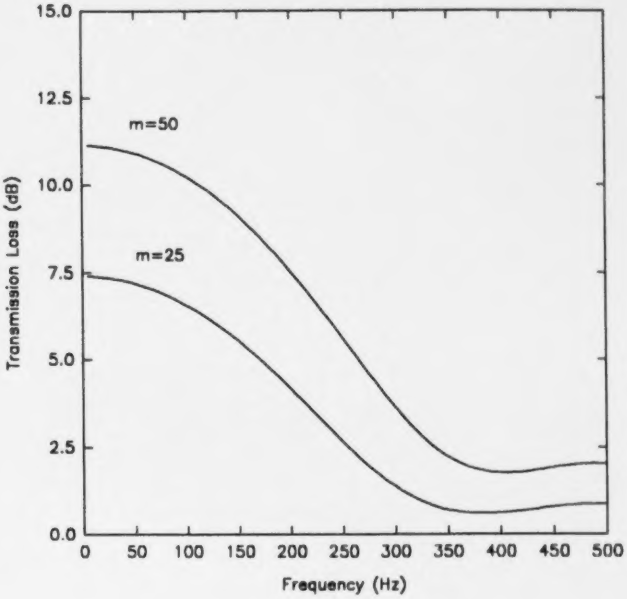

Figure 2.13: T.L. Values For Gradual Area Changes of Various Expansion Ratios

Exponential horns may also be modelled with a system of pipe elements. Due to the complexities of the mouth and throat impedances for exponential horns, the results presented here consider the horn to be a part of an infinite transmission line as an exponential connector, allowing a ρc termination (infinite transmission line) to be applied at the mouth and throat of the horn. This restriction allows the transmission loss values of the horn to be compared with a tapered section of similar dimensions.

Consider the exponential horn shown in Fig. 2.14. The cross-sectional area at the mouth of the horn is denoted by S_m with corresponding throat cross-sectional area denoted by S_t. The length of the horn region is denoted by l.

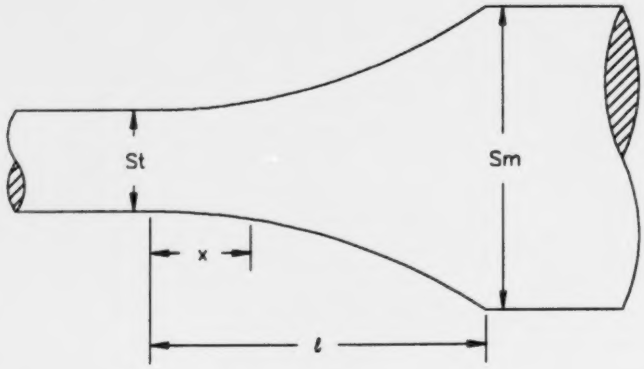

Figure 2.14: Exponential Horn Section

The cross-sectional area of the exponential horn is governed by the following equation:

$$S = S_t e^{\alpha x} \tag{2.35}$$

where α is the flare constant of the horn and x is the distance from the throat. If the length of the horn is less than 1/4 wavelength, it may be treated as an area discontinuity [13] and thus may be modelled by finite elements using the ρc termination. A finite element model of an exponential connector is shown in Fig. 2.15. The model consists of 14 pipe elements with 29 DOF. The length of the horn was 0.5 m with throat cross-sectional area 0.01 m^2 and mouth cross-sectional area 0.2 m^2. The flare constant was 5.99465 m^{-1}.

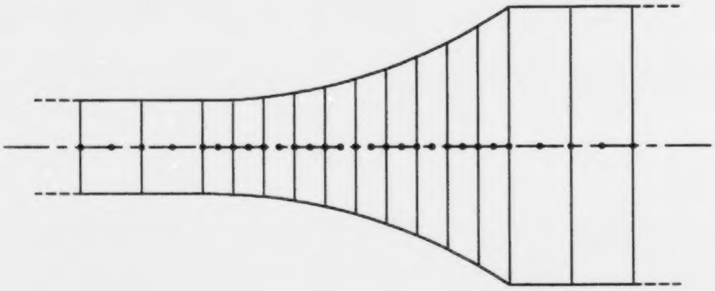

Figure 2.15: Finite Element Mesh for an Exponential Connector (14 element model)

Transmission loss values are presented in Fig. 2.16 for an exponential connector and a tapered region of similar dimensions. Examination of the results shows that for lower frequencies, the exponential connector does indeed behave as a simple area discontinuity. At about 170 Hz, this approximation does not apply and the T.L. values begin to differ due to the ρc termination used in the finite element approximation. At very high frequencies, the mouth impedance becomes resistive again and is approximately equal to that of a plane wave in a tube (ρc termination).

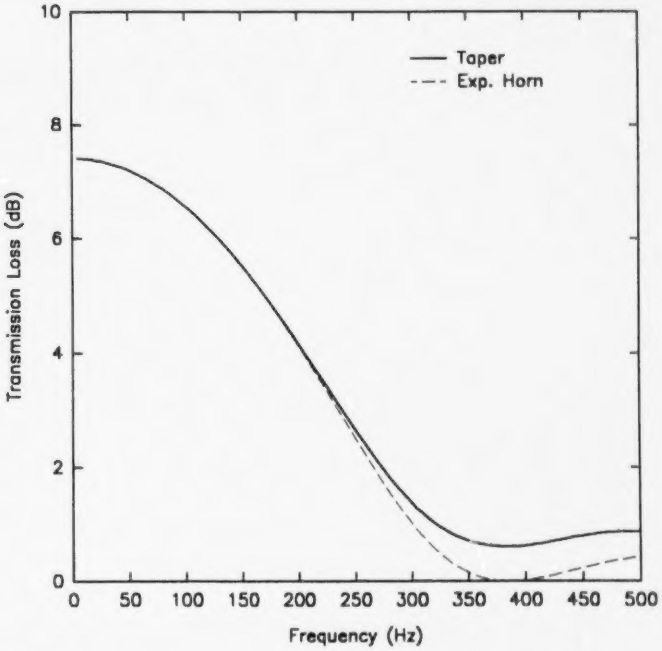

Figure 2.16: T.L. Comparison Between Exp. Horn and Tapered Section

As demonstrated above, tapered sections and exponential horn sections can be successfully modelled with the pipe element. For the exponential horn, impedance terms can become very complicated and vary with frequency. Therefore, the selected case of an exponential connector was modelled because it allowed the use of the prescribed infinite transmission line assumption.

2.5.4 Helmholtz Resonators

A Helmholtz resonator, or commonly referred to as the volume resonator, eliminates an undesired frequency component from an acoustic system. It is depicted in Fig. 2.17. Resonator volume is represented by V, the cross-sectional area and length of the neck are represented by A and l respectively, S denotes the cross-sectional area of the duct and P_i, P_r, P_t denote the incident, reflected and transmitted pressure waves.

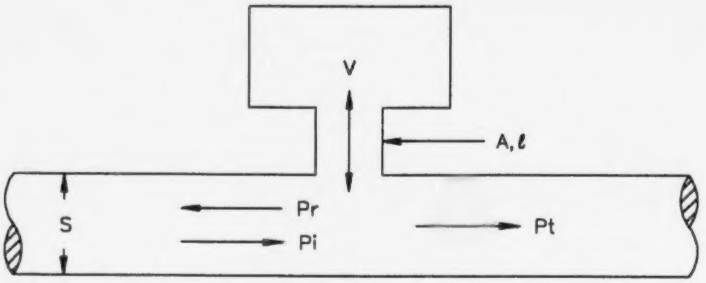

Figure 2.17: Helmholtz Resonator

The resonator behaves like a spring-mass system where the neck of the chamber behaves like a mass and the chamber volume behaves like a spring. A pressure wave is incident upon the resonator, the mass of fluid in the neck is forced, causing the chamber volume to oscillate. Some of the energy of the incident pressure wave is absorbed while the remaining energy either reflects back towards the source or transmits down the duct. The equation which describes the spring-mass behaviour of the neck and volume of the resonator has the form of a harmonic oscillator

$$\ddot{x}+\frac{c^2A}{Vl}x=0 \tag{2.36}$$

where c is the speed of sound. Subsequently, the frequency of the resonator (Hz) can be written as

$$f_r=\frac{c}{2\pi}\sqrt{\frac{A}{Vl}} \tag{3.37}$$

and the wavelength of the pressure wave is assumed to be larger than the dimensions of the resonator. Also, in most practical situations, there is an end effect on the effective mass length of the neck which must be considered. At the resonator frequency, transmission loss is infinite [37] which is an ideal situation to be modelled by a mesh of pipe elements.

A pipe element mesh representing a Helmholtz resonator and duct section is shown in Fig. 2.18. The mesh consists of 15 pipe elements with 33 DOF. The duct section is part of an infinite transmission line with a cross-sectional area of 0.01 m^2. Resonator volume was 0.006 m^3, neck length was 0.05 m with a cross-sectional area of 0.005 m^2.

Notice that the pipe element may be assembled to model junctions such as the location where the resonator neck is connected to the duct. At this junction, the pressure is a simple scalar quantity so it does not accurately represent acoustic pressure at this point. One such case is when the junction is connected to the duct at a specific angle other than 90°; this is not taken into account by a mesh of pipe elements. This will be explained in detail in Chapter 4.

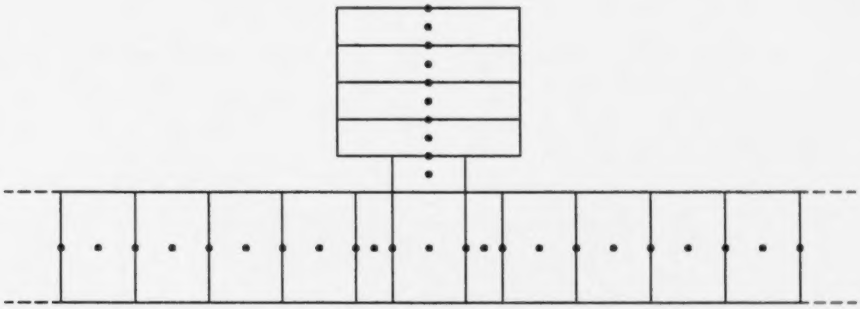

Figure 2.18: Finite Element Mesh for a Helmholtz Resonator (15 element model)

Transmission loss values are presented in Fig. 2.19 for the Helmholtz resonator of consideration. Examination of the results shows that T.L. becomes infinite at a frequency of 205 Hz which compares well to the actual transmission loss value of 210 Hz calculated with Eq. (3.37). Discrepancy between the values is likely due to the sampling frequency interval of 5 Hz used in the finite element calculations.

A simple Helmholtz resonator can be successfully modelled using the pipe element. The fine element mesh presented in Fig. 2.18 is generally unnecessary for most practical purposes; only in regions where discontinuities are present should the element mesh be fine. Three-dimensional elements are needed to model resonators with more complicated configurations.

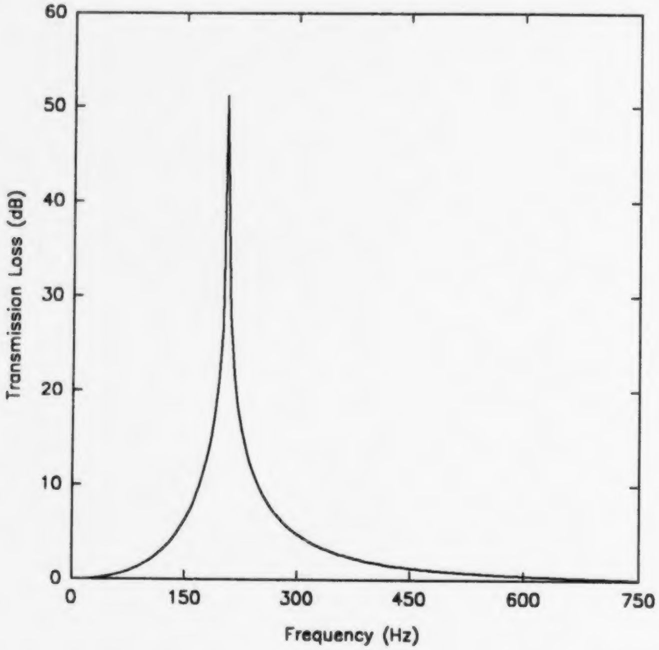

Figure 2.19: T.L. Values for a Helmholtz Resonator

2.5.5 Sidebranch Resonator

Just as the pipe element was able to model a Helmholtz resonator, it also can be used to model a sidebranch resonator such as the one shown in Fig. 2.20. A sidebranch resonator eliminates sound propagation at very narrow frequencies for particular intervals and serves a similar function as the Helmholtz resonator described earlier. Notation is similar to that used for the Helmholtz resonator except here l is the length of the sidebranch and P_b is the branch pressure.

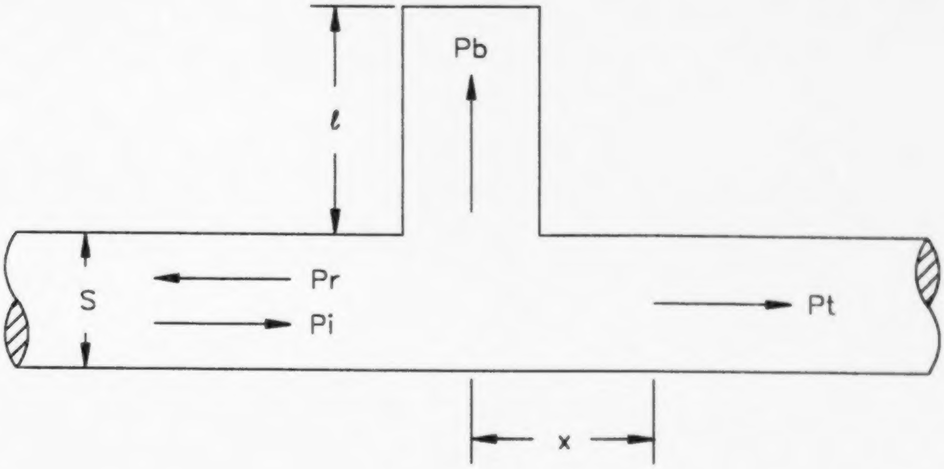

Figure 2.20: Closed-Tube Sidebranch Resonator

The impedance relationship for the sidebranch has the form [96]

$$Z_b = j\rho c \frac{\cos kl}{\sin kl} \tag{3.38}$$

which becomes zero when $kl = n\pi/2$ (n=1,2,3,...). Therefore, the sidebranch length can be determined for maximum T.L. using the quarter wavelength formula $l = nc/4f$ for a particular frequency. The cross-sectional area of the sidebranch is irrelevant pertaining to T.L., only the length of the branch is important.

A finite element mesh representing a closed-tube sidebranch resonator is shown in Fig. 2.21 consisting of 26 pipe elements and 45 DOF. The cross-sectional area of the duct was 0.01 m² and the length of the sidebranch was 0.25 m.

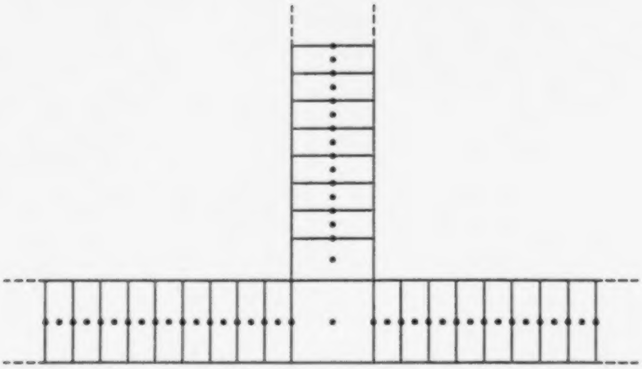

Figure 2.21: Finite Element Mesh of a Closed-Tube Sidebranch Resonator (26 element model)

Transmission loss values are presented in Fig. 2.22 for this particular sidebranch resonator and the T.L. becomes infinite at 343 Hz which is in exact accordance with the frequency predicted by Eq. (3.38).

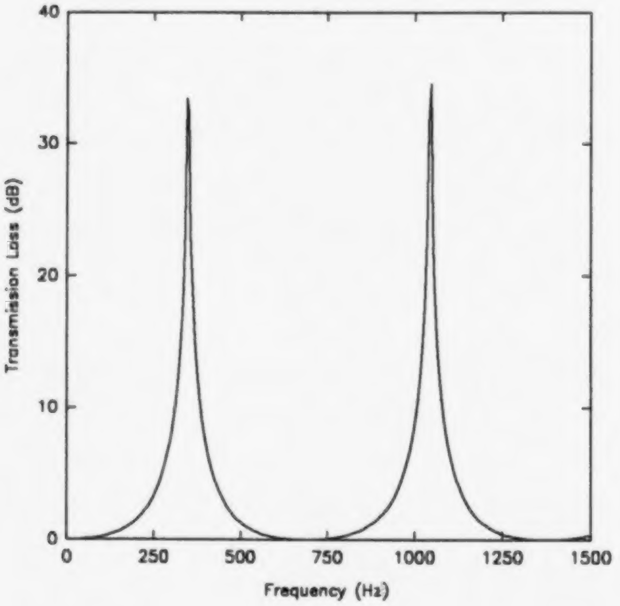

Figure 2.22: T.L. Values for a Closed-Tube Sidebranch Resonator

2.5.6 Transmission Loss Calculations for a Simple Expansion Chamber

A simple expansion chamber may be represented as shown in Fig. 2.8. At the inlet to the chamber are the incident and reflected pressure waves and at the chamber outlet is the transmitted pressure wave.

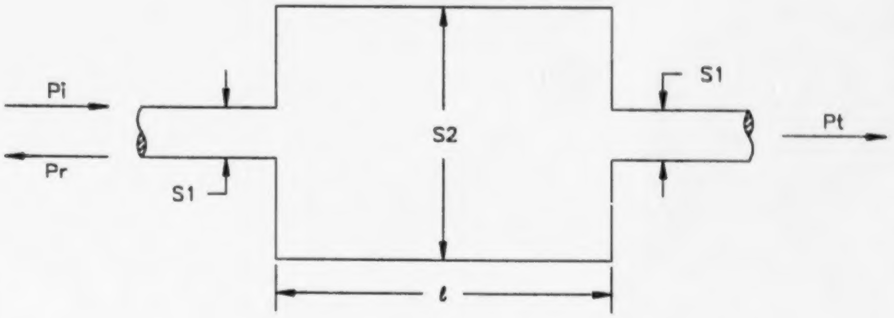

Figure 2.23: Simple Expansion Chamber

The length of the chamber is represented by l; inlet and outlet cross-sectional areas are equal in this case and are denoted by S_1; the chamber cross-sectional area is denoted by S_2. The expansion ratio of the chamber may be written as $m = S_2 / S_1$. Assuming plane wave input and output from the chamber (one-dimensional theory), the equation for the transmission loss (dB) of the chamber is given as:

$$T.L. = 10\log_{10}\left(1+\frac{1}{4}\left(m-\frac{1}{m}\right)^2 \sin^2 kl\right), \tag{2.39}$$

which is the exact equation for the transmission loss of a reactive muffler. Consider the finite element mesh shown in Fig. 2.24. The model consisted of 10 one-dimensional elements with a total of 21 DOF.

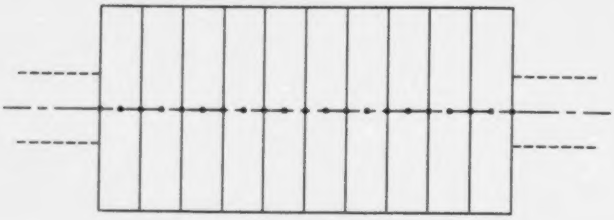

Figure 2.24: Finite Element Mesh for a Simple Expansion Chamber (10 element model)

This model was assumed to be part of an infinite transmission line (ρc impedance termination), meaning no waves will be reflected from the ends of the chamber.

Transmission loss results for various expansion ratios are shown in Fig. 2.25. Comparison of the finite element transmission loss results calculated with Eq. (2.32) and exact transmission loss results calculated with Eq. (2.39) show no discernible differences. Values for which the transmission loss becomes zero are given by $kl = n\pi$ (where n = 0, 1, 2, ...). Values for which transmission loss is a maximum occur when $l = n\lambda / 4$ (where n = 1, 3, 5, ...). Here k is the wavenumber ω / c and λ is the acoustic wavelength.

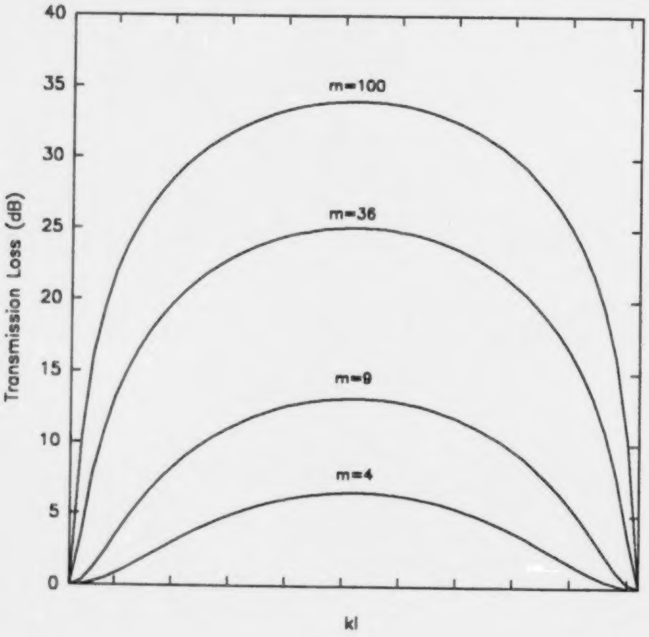

Figure 2.25: T.L. Values for a Reactive Muffler

The one-dimensional pipe element has proven to be extremely accurate in approximating acoustic systems and the finite element transmission loss equations have also proven to be accurate in calculating the transmission loss of a reactive muffler. For completeness, a variety of expansion chambers are now modelled with pipe elements to further demonstrate their application.

Expansion chambers with inward extending inlet and outlet pipes may be modelled using a mesh of pipe elements. Transmission losses can vary considerably for various inward extending pipe configurations and attenuation can be increased substantially because the part of the chamber between the end of the extended pipe and the chamber sidewall acts as a sidebranch resonator. When the frequency is such that the length of the intrusion corresponds to a quarter wavelength $\lambda / 4$, or odd multiples of, then the extended pipe is at a node point and very little sound is transmitted [27]. High transmission losses occur whenever the length of the extended pipe is $l_{in} = (\lambda / 4) \times n$, n=1, 2, 3,...

The following finite element models of expansion chambers with extended inlet or outlet pipes and their corresponding T.L. curves further demonstrate the diverse application of the pipe element. These results compare identically to transmission losses calculated for similar expansion chambers using three-dimensional finite elements [27].

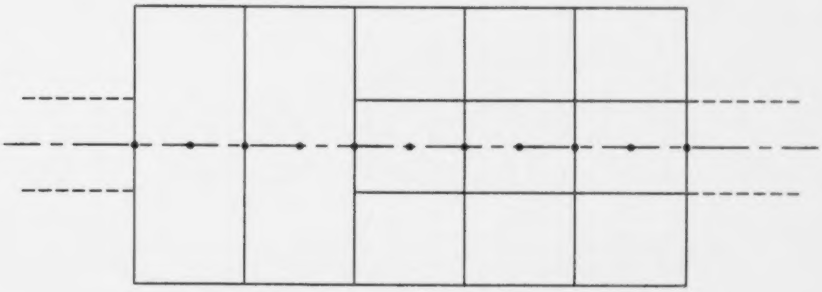

Figure 2.26: Finite Element Mesh for an Expansion Chamber with Outlet Pipe Extended 0.6 Length of the Chamber (6 element model)

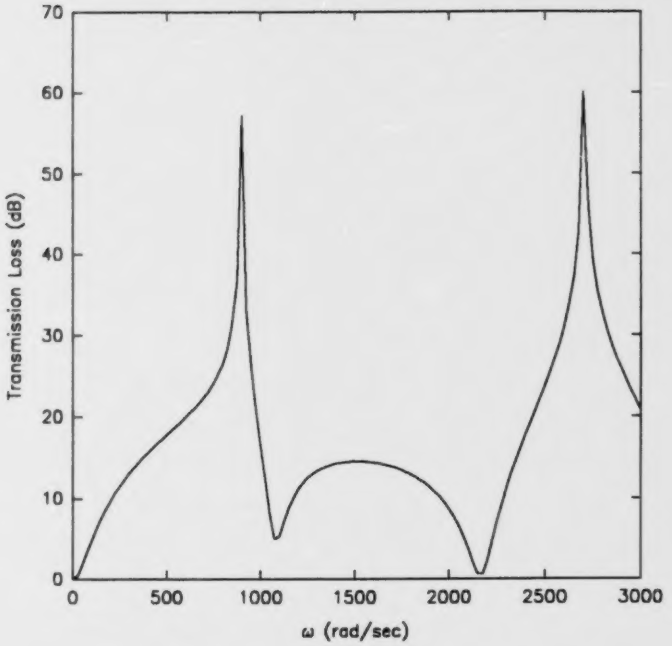

Figure 2.27: T.L. Values for Expansion Chamber with Outlet Pipe Extended 0.6 Length of the Chamber

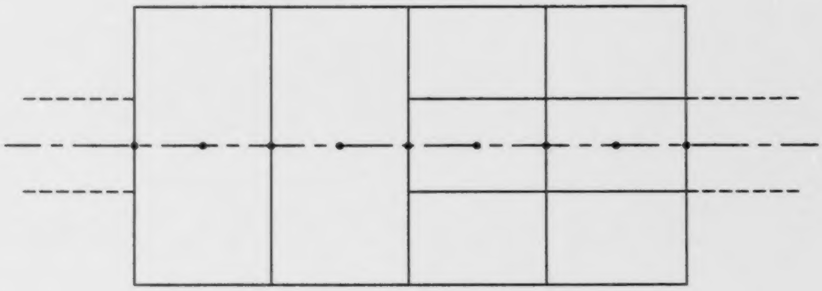

Figure 2.28: Finite Element Mesh for an Expansion Chamber with Outlet Pipe Extended 0.5 Length of the Chamber (5 element model)

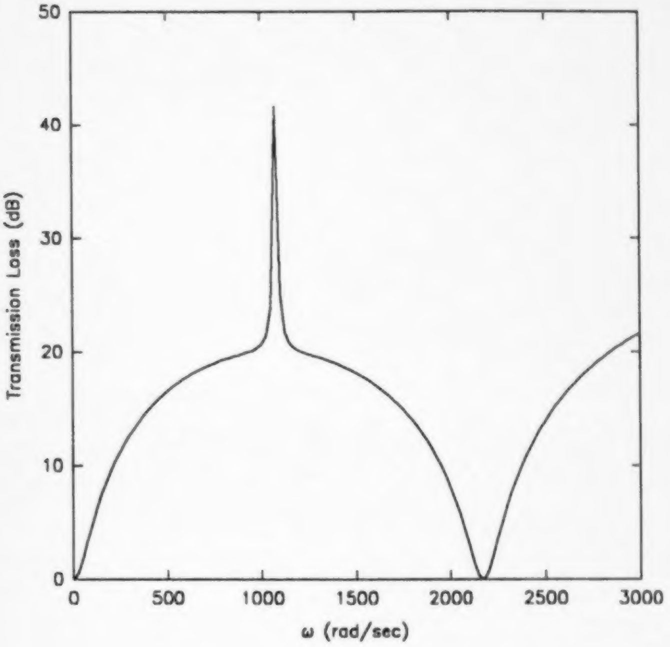

Figure 2.29: T.L. Values for Expansion Chamber with Outlet Pipe Extended 0.5 Length of the Chamber

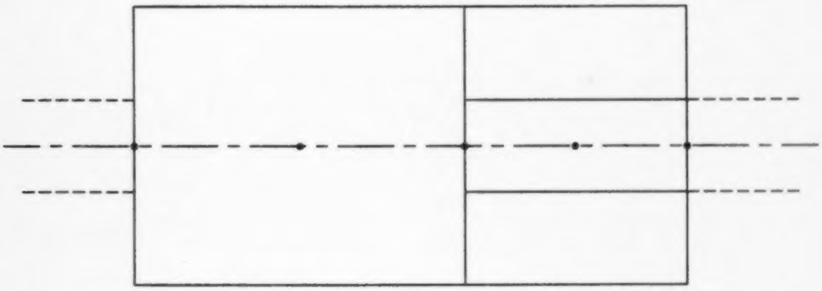

Figure 2.30: Finite Element Mesh for Expansion Chamber with Outlet Pipe Extended 0.4 Length of the Chamber (3 element model)

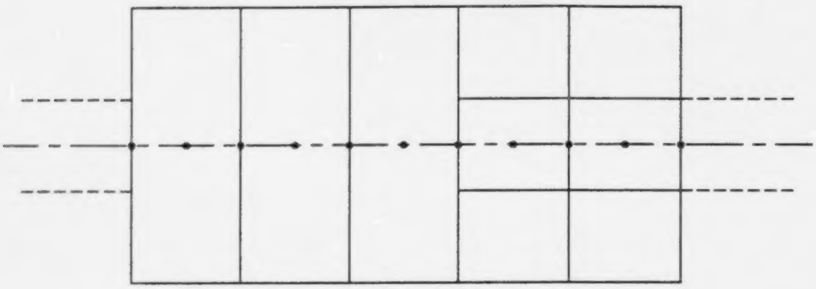

Figure 2.31: Finite Element Mesh for Expansion Chamber with Outlet Pipe Extended 0.4 Length of the Chamber (6 element model)

The transmission loss calculations of Fig. 2.32 represent the finite element models of Figures 2.30 and 2.31. The purpose of this comparison was to demonstrate the accuracy improvement of the finite element approximation as the number of elements is increased.

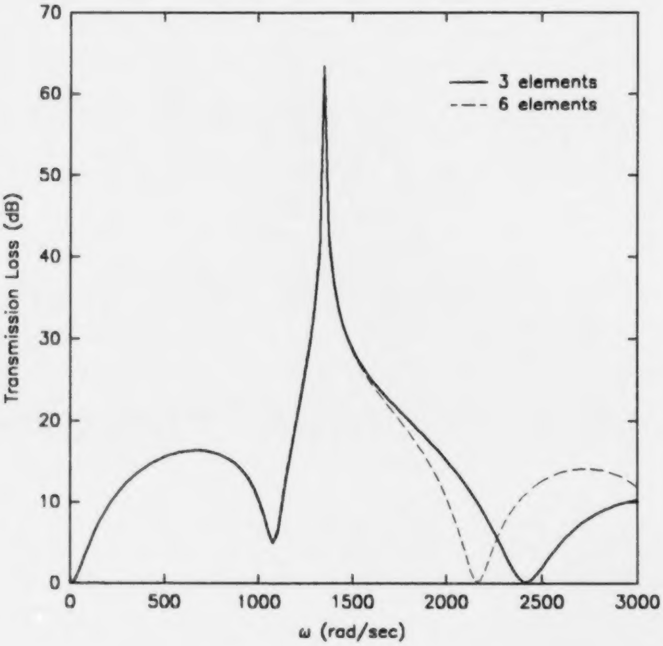

Figure 2.32: T.L. Values for Expansion Chamber with Outlet Pipe Extended 0.4 Length of the Chamber (3 and 6 element models)

2.6 Curved Pipe Sections

The pipe element may be used to approximate duct and pipe systems where plane wave theory applies; these are systems where the acoustic wavelength is such that it is much greater than the transverse dimensions of the element. Narrow curved pipe sections may be considered as being straight for long wave propagation [84, 86, 87, 88]. Therefore, the pipe element may be used to model curved pipe sections if the aforementioned conditions apply.

CHAPTER 3
One-Dimensional Element with Flexible Walls

3.1 Introduction

In this chapter, a one-dimensional finite element is developed which is suitable for approximating pipe systems where the pipe walls are flexible, not rigid. The pipe walls are considered to be *locally reacting*, meaning that the motion of one portion of the pipe wall is dependent only on the acoustic pressure incident on that portion of the wall and is independent of the motion of all other surrounding wall portions. No expansive wave motion is produced along the pipe by the wave motion inside.

The interaction between sound waves and a locally reacting surface is defined by specifying its acoustic impedance (or admittance) as a function of frequency. For the work considered here, the surface impedance is assumed to be either mass controlled or stiffness controlled. This is an extension of previous research [26], where three-dimensional acoustic finite elements were used to model irregular enclosures with flexible boundaries. As well, the assumption of locally reacting flexible walls is necessary from the point of view of analytical tractability [71].

A flexible walled pipe element is a natural extension of the pipe element described in Chapter 2. That element was shown to be extremely useful in modelling duct and piping systems where low frequencies were involved, particularly for reactive muffler systems. The assumption that the pipe walls were rigid (infinite transverse impedance) does not necessarily apply to most practical situations; walls of finite thickness are generally compliant in nature and the transverse impedance is finite. Thus, the development of a flexible walled pipe element would be useful for simple low frequency approximations of practical duct and piping systems.

In this chapter, the one-dimensional wave equation is formulated which allows for flexible boundaries. Using Galerkin's method of weighted residuals, a flexible walled pipe element is composed by similar process as the pipe element of Chapter 2. The effects of mass controlled and stiffness controlled wall motion are considered by determining the eigenvalues of a closed tube. As well, the effects of wall motion on the standing waves in an open tube are considered.

3.2 Webster Horn Equation with Flexible Walls

A one-dimensional wave equation may be developed for systems with flexible walls by considering an element of fluid fixed in space acted on by pressure forces. Equations expressing Newton's second law of motion, mass conservation and the gas law are established and then used in combination to produce a wave equation suitable for pipe systems with flexible walls.

An infinitesimal fluid element of length dx is shown in Fig. 3.1, where u is the particle velocity of the fluid, A the cross-sectional area, ρ the fluid density and v the wall velocity normal to the surface of the element. If the element is considered as a control volume, mass must be conserved and the mass change within the control volume is related to the inflow and outflow of fluid crossing the end faces of the element. This may be written as

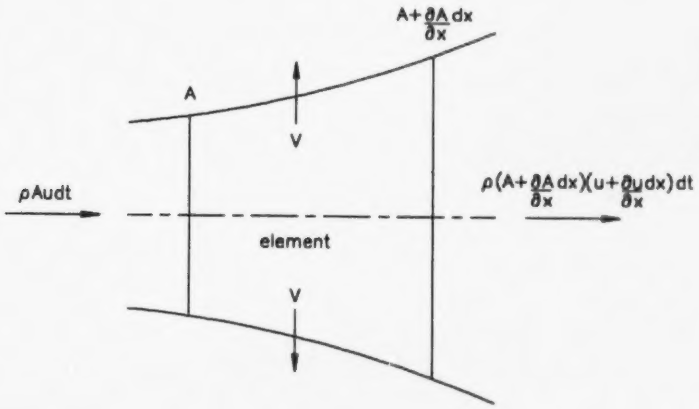
$A+\frac{\partial A}{\partial x}dx$
A
V
$\rho Audt$
$\rho(A+\frac{\partial A}{\partial x}dx)(u+\frac{\partial u}{\partial x}dx)dt$
element
V

Figure 3.1: Infinitesimal Fluid Element of Varying Cross-Sectional Area with Flexible Side Walls

$$\rho\left(A+\frac{\partial A}{\partial x}\right)\left(u+\frac{\partial u}{\partial x}\right)dt-\rho Audt+\frac{\partial \rho}{\partial t}Adxdt+\rho vr_p dxdt=0 \qquad (3.1)$$

where r_p is the radial perimeter of the element. Simplification of Eq. (3.1) yields

$$\rho A\frac{\partial u}{\partial x}+\rho u\frac{\partial A}{\partial x}+\frac{\partial \rho}{\partial t}A+\rho v r_p=0 \tag{3.2}$$

which is the linearized equation of mass conservation. Wall velocity normal to the surface of the element can be expressed as the ratio of the acoustic pressure and the acoustic impedance of the surface $(v = p / Z_w)$. Therefore, Eq. (3.2) can be rewritten as

$$\rho A\frac{\partial u}{\partial x}+\rho u\frac{\partial A}{\partial x}+\frac{\partial \rho}{\partial t}A+\rho\frac{r_p}{Z_w}p=0. \tag{3.3}$$

A linearized form of the momentum equation is given as

$$-\frac{\partial p}{\partial x}=\rho\frac{\partial u}{\partial t} \tag{3.4}$$

and the acoustic pressure may be written as

$$\frac{\partial p}{\partial t}=\frac{\gamma p_0}{\rho}\frac{\partial \rho}{\partial t} \tag{3.5}$$

where γ is the ratio of specific fluid heats. Eq. (3.5) is now substituted into Eq. (3.3) and the result is differentiated with respect to time, yielding

$$A\frac{\partial^2 u}{\partial x\partial t}+\frac{\partial u}{\partial t}\frac{\partial A}{\partial x}+\frac{A}{\gamma p_0}\frac{\partial^2 p}{\partial t^2}+\frac{r_p}{Z_w}\frac{\partial p}{\partial t}=0. \tag{3.6}$$

The momentum equation may be differentiated with respect to x; the result being substituted into Eq. (3.6).

$$-\frac{\gamma p_0}{\rho}A\frac{\partial^2 p}{\partial x^2}-\frac{\gamma p_0}{\rho}\frac{\partial p}{\partial x}\frac{\partial A}{\partial x}+A\frac{\partial^2 p}{\partial t^2}+\gamma p_0\frac{r_p}{Z_w}\frac{\partial p}{\partial t}=0 \tag{3.7}$$

The local speed of sound is defined as $c^2=\gamma p_0/\rho$, which is now substituted into Eq. (3.7), yielding the one-dimensional equation for acoustic waves travelling through a wave guide with variable cross-sectional area and flexible walls

$$A\frac{\partial^2 p}{\partial x^2}+\frac{\partial p}{\partial x}\frac{\partial A}{\partial x}-\frac{A}{c^2}\frac{\partial^2 p}{\partial t^2}-\rho\frac{r_p}{Z_w}\frac{\partial p}{\partial t}=0. \tag{3.8}$$

If only harmonic motion is considered, the acoustic pressure has the form $p = pe^{j\omega t}$, where ω is the angular frequency and j is the complex operator. Upon substitution of harmonic acoustic pressure into Eq. (3.8), the time derivative is eliminated thus yielding the Webster Horn equation for one-dimensional waves in pipes of varying cross-sectional area with flexible walls

$$\frac{\partial}{\partial x}\left(A\frac{\partial p}{\partial x}\right)+k^2Ap+j\rho\omega\frac{r_p}{Z_w}p=0, \tag{3.9}$$

where k is the wavenumber, ω/c.

3.3 Flexible Walled Pipe Element

A one-dimensional finite element which allows quadratic variation in pressure, cross-sectional area and radial perimeter was chosen to approximate Eq. (3.9). The element, shown in Fig. 3.2, has three pressure degrees of freedom, at the ends of the element and midway along its length as was the case with the pipe element described earlier. This element will be referred to as the flex-wall pipe element and is formulated using Galerkin's method of weighted residuals by procedure similar to that which was presented in Section 2.3.

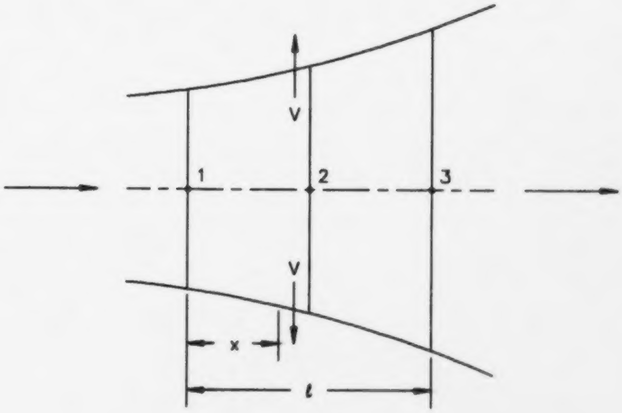

Figure 3.2: Quadratic Variable Cross-Section Pipe Element with Flexible Side Walls

For the finite element approximation to Eq. (3.9), pressure, cross-sectional area and radial perimeter may be represented by the following quadratic interpolation polynomials

$$p = a_1 + b_1\left(\frac{x}{l}\right) + c_1\left(\frac{x}{l}\right)^2 \tag{3.10}$$

$$A = a_2 + b_2\left(\frac{x}{l}\right) + c_2\left(\frac{x}{l}\right)^2 \tag{3.11}$$

$$r_p = a_3 + b_3\left(\frac{x}{l}\right) + c_3\left(\frac{x}{l}\right)^2 \tag{3.12}$$

where *a*, *b* and *c* are constants representing pressures, cross-sectional areas and radial perimeters at each element node. After substitution of the nodal pressures into Eq. (3.10), the pressure polynomial is written as

$$p = p_1\left(1 - 3\frac{x}{l} + 2\frac{x^2}{l^2}\right) + p_2\left(4\frac{x}{l} - 4\frac{x^2}{l^2}\right) + p_3\left(-\frac{x}{l} + 2\frac{x^2}{l^2}\right). \tag{3.13}$$

Also, Eq. (3.13) may be written in matrix form

$$p = \{f\}^T\{p_e\} = \{p_e\}^T\{f\} \tag{3.14}$$

$$\{p_e\} = \begin{Bmatrix} p_1 \\ p_2 \\ p_3 \end{Bmatrix}$$

$$\{f\} = \begin{Bmatrix} \left(1 - 3\frac{x}{l} + 2\frac{x^2}{l^2}\right) \\ \left(4\frac{x}{l} - 4\frac{x^2}{l^2}\right) \\ \left(-\frac{x}{l} + 2\frac{x^2}{l^2}\right) \end{Bmatrix}$$

where $\{p_e\}$ is the vector containing the nodal acoustic pressures and $\{f\}$ is the vector containing the quadratic interpolation polynomials. The superscript T denotes a matrix transpose. In similar fashion, the cross-sectional area and radial perimeter may by written as

$$A = A_1\left(1-3\frac{x}{l}+2\frac{x^2}{l^2}\right)+A_2\left(4\frac{x}{l}-4\frac{x^2}{l^2}\right)+A_3\left(-\frac{x}{l}+2\frac{x^2}{l^2}\right)$$

$$A = A_1+\left(4A_2-3A_1-A_3\right)\left(\frac{x}{l}\right)+\left(2A_1-4A_2+2A_3\right)\left(\frac{x^2}{l^2}\right) \tag{3.15}$$

$$r_p = r_{p_1}\left(1-3\frac{x}{l}+2\frac{x^2}{l^2}\right)+r_{p_2}\left(4\frac{x}{l}-4\frac{x^2}{l^2}\right)+r_{p_3}\left(-\frac{x}{l}+2\frac{x^2}{l^2}\right)$$

$$r_p = r_{p_1}+\left(4r_{p_2}-3r_{p_1}-r_{p_3}\right)\left(\frac{x}{l}\right)+\left(2r_{p_1}-4r_{p_2}+2r_{p_3}\right)\left(\frac{x^2}{l^2}\right). \tag{3.16}$$

Using Galerkin's method of weighted residuals, Eq. (3.14) is substituted into Eq. (3.9) and the residual, R, is obtained

$$R=\frac{\partial}{\partial x}\left(A\{f_x'\}^T\right)\{p_e\}+k^2A\{f\}^T\{p_e\}+j\rho\omega\frac{r_p}{Z_w}\{f\}^T\{p_e\} \tag{3.17}$$

where $\{f_x'\}$ denotes $\partial f/\partial x$. Galerkin's equation is given as

$$\int_0^l \{f\}R\,dx=0 \tag{3.18}$$

and after substitution of the residual into Eq. (3.18), Galerkin's equation can be rewritten as

$$\int_0^l\left(\{f\}\frac{\partial}{\partial x}\left(A\{f_x'\}^T\right)+k^2A\{f\}\{f\}^T+j\rho\omega\frac{r_p}{Z_w}\{f\}\{f\}^T\right)\{p_e\}\,dx=0. \tag{3.19}$$

Notice that the first term of Eq. (3.19) contains a matrix which is non-symmetric as the terms are not of the same order. It is integrated by parts with the result becoming

$$\int_0^l \left(A\{f'_x\}\{f'_x\}^T - k^2 A\{f\}\{f\}^T - j\rho\omega \frac{r_p}{Z_w}\{f\}\{f\}^T \right)\{p_e\}\,dx = 0 \qquad (3.20)$$

with boundary conditions $A\partial p / \partial x = 0$ at $x = 0$ and $x = l$ implying that there are no volume source terms present at these locations. The relationships for cross-sectional area and radial perimeter are now substituted into Eq. (3.20) and direct integration of the terms gives the approximation of Eq. (3.9) for one flex-wall pipe element

$$\left([S] - k^2[P] - j\rho \frac{\omega}{Z_w}[A] \right)\{p_e\} = \{0\}, \qquad (3.21)$$

where $[S]$ and $[P]$ represent the kinetic and potential energy matrices respectively and are square, symmetric. The square, symmetric matrix $[A]$ is similar in composition as the potential energy matrix. These matrices are given as

$$[S] = \int_0^l \left(A\{f'_x\}\{f'_x\}^T \right)\{p_e\}\,dx$$

$$[S] = \alpha_1 \begin{bmatrix} 7 & -8 & 1 \\ -8 & 16 & -8 \\ 1 & -8 & 7 \end{bmatrix} + \alpha_2 \begin{bmatrix} 3 & -4 & 1 \\ -4 & 16 & -12 \\ 1 & -12 & 11 \end{bmatrix} + \alpha_3 \begin{bmatrix} 3 & -6 & 3 \\ -6 & 32 & -26 \\ 3 & -26 & 23 \end{bmatrix}$$

$$\alpha_1 = \frac{A_1}{3l}, \quad \alpha_2 = \frac{(4A_2 - 3A_1 - A_3)}{6l}, \quad \alpha_3 = \frac{(2A_1 - 4A_2 + 2A_3)}{15l}$$

$$[P] = \int_0^l \left(A\{f\}\{f\}^T \right)\{p_e\}\,dx$$

$$[P] = \beta_1 \begin{bmatrix} 4 & 2 & -1 \\ 2 & 16 & 2 \\ -1 & 2 & 4 \end{bmatrix} + \beta_2 \begin{bmatrix} 1 & 0 & -1 \\ 0 & 16 & 4 \\ -1 & 4 & 7 \end{bmatrix} + \beta_3 \begin{bmatrix} 2 & -4 & -5 \\ -4 & 64 & 24 \\ -5 & 24 & 44 \end{bmatrix}$$

$$\beta_1 = \frac{A_1 l}{30}, \quad \beta_2 = \frac{(4A_2 - 3A_1 - A_3)l}{60}, \quad \beta_3 = \frac{(2A_1 - 4A_2 + 2A_3)l}{420}$$

$$[A]=\int_0^l \left(\{f\}\{f\}^T\right)\{p_e\}dx$$

$$[A]=\chi_1\begin{bmatrix}4 & 2 & -1\\ 2 & 16 & 2\\ -1 & 2 & 4\end{bmatrix}+\chi_2\begin{bmatrix}1 & 0 & -1\\ 0 & 16 & 4\\ -1 & 4 & 7\end{bmatrix}+\chi_3\begin{bmatrix}2 & -4 & -5\\ -4 & 64 & 24\\ -5 & 24 & 44\end{bmatrix}$$

$$\chi_1=\frac{r_{p_1}l}{30},\ \chi_2=\frac{\left(4r_{p_2}-3r_{p_1}-r_{p_3}\right)l}{60},\ \chi_3=\frac{\left(2r_{p_1}-4r_{p_2}+2r_{p_3}\right)l}{420}$$

where all matrices presented here have the dimensions 3×3.

Consider the case where the wall motion of the pipe is either mass controlled or stiffness controlled. If wall motion is mass controlled, the wall velocity can be written as [26]

$$v=\frac{jp}{\omega m_w} \tag{3.22}$$

where m_w is the generalised wall mass. Making use of the relationship $v=p/Z_w$, Eq. (3.22) can be written in terms of the wall impedance

$$Z_w=\frac{\omega m_w}{j}. \tag{3.23}$$

Substituting this expression into Eq. (3.21) gives the equation of motion as

$$\left(\left([S]+\frac{\rho}{m_w}[A]\right)-k^2[P]\right)\{p_e\}=\{0\}. \tag{3.24}$$

Notice that for a mass controlled wall, terms are added to the kinetic energy matrix. This has the effect of increasing the natural frequencies of the system.

Alternatively, consider the case where wall motion is stiffness controlled. The wall velocity can be represented by [26]

$$v=-j\frac{\omega p}{c^2k_w} \tag{3.25}$$

where k_w is the generalised wall stiffness. Again, Eq. (3.25) can be written in terms of wall impedance

$$Z_w = -\frac{c^2 k_w}{j\omega}. \tag{3.26}$$

This result is now substituted into Eq. (3.21) and the resulting equation of motion becomes

$$\left([S] - k^2\left([P] + \frac{\rho}{k_w}[A]\right)\right)\{p_e\} = \{0\}. \tag{3.27}$$

For the stiffness controlled wall, terms are added to the potential energy matrix. This has the effect of reducing the natural frequencies of the system. Examining Eqs. (3.24) and (3.27), it can be seen that if either the mass or stiffness is increased indefinitely, (the generalised mass or stiffness terms are increasing), the added terms to the kinetic and potential energy matrices become zero corresponding to the limiting rigid wall condition.

The flex-wall pipe element is assembled using the same method as the pipe element. This procedure is described in Section 2.3.1. Continuity and convergence conditions are both satisfied for this element by the arguments presented in Section 2.3.2.

3.4 Element Testing

The effects of a flexible boundary on the frequencies of a one-dimensional system are demonstrated here by two methods. First, the eigenvalues of a closed tube with flexible walls are determined and compared with the rigid case; second, the effects of flexible walls on standing waves in a tube are demonstrated. Cases where wall motion is mass controlled and stiffness controlled are considered. The results presented here are entirely numerical. No experimental results exist in the literature for one-dimensional systems with flexible walls using the locally reacting assumption but the results presented here do agree with conclusions presented in earlier research [26].

3.4.1 Eigenvalue Models

Finite element models consisting of 13 flex-wall pipe elements with 27 DOF were used to approximate the eigenvalues of a closed tube of unit length with various generalised wall masses. These results are presented in Table 3.1. For comparison purposes, eigenvalues for the rigid walled closed tube of Section 2.4.1 are included as well.

Table 3.1: Eigenvalues of a Closed Tube of Unit Length with Mass-Controlled Flexible Walls

Mode Number, n	Rigid Walled	Flex-Wall $m_w = 0.01$	Flex-Wall $m_w = 1$	Flex-Wall $m_w = 10$	Flex-Wall $m_w = 10000$
1	9.87	1366.28	23.43	11.23	9.87
2	39.48	1395.89	53.05	40.84	39.48
3	88.86	1445.27	102.42	90.22	88.86
4	158.10	1514.50	171.66	159.45	158.10
5	247.42	1603.83	260.98	248.78	247.42
6	357.28	1713.69	370.84	358.63	357.28

The results presented in Table 3.1 demonstrate that a mass controlled boundary increases the natural frequencies of the system. For cases where the mass is increased indefinitely ($m_w = 10000$), the additional terms of Eq. (3.24) approach zero and the eigenvalues approach the limiting, rigid walled case. Generally, the eigenvalues for generalised wall masses of $m_w = 1$ and $m_w = 10$ display the expected characteristics where the natural frequencies of the closed tube are increased by the mass controlled wall, increasing as the generalised wall mass decreases. A mass controlled flexible wall has greater effect on the lower natural frequencies than the higher ones; the lower natural frequencies differ from the rigid case in larger proportion than do the higher frequencies. This may be explained by considering that for low frequencies where the wavelength is much longer than the transverse dimensions of the tube, wave motion is along the axis. As frequencies increase, some transverse wave motion develops which is unaffected by the flexible boundary due to the assumption of locally reacting surfaces.

Eigenvalues for the same closed tube with stiffness controlled flexible walls with various generalised wall stiffnesses were calculated as well with the results being presented in Table 3.2.

Table 3.2: Eigenvalues of a Closed Tube of Unit Length with Stiffness Controlled Flexible Walls

Mode Number, n	Rigid Walled	Flex-Wall $k_w = 0.01$	Flex-Wall $k_w = 1$	Flex-Wall $k_w = 10$	Flex-Wall $k_w = 10000$
1	9.87	0.014	1.26	5.87	9.86
2	39.48	0.058	5.05	23.47	39.46
3	88.86	0.13	11.36	52.84	88.86
4	158.10	0.23	20.24	94.15	158.31
5	247.42	0.36	31.76	147.74	248.43
6	357.28	0.53	46.08	214.30	360.35

Results presented in Table 3.2 indicate that a stiffness controlled boundary affects the natural frequencies of a system in a way opposite to the effects provided by the mass controlled boundary. For cases where the stiffness is increased indefinitely, the additional terms added to the potential energy matrix approach zero and the eigenvalues approach the limiting, rigid wall condition. As wall stiffness increases, the natural frequencies of the system increase as well, converging on the rigid wall case.

3.4.2 Standing Waves in a Tube

Pressure distributions for standing waves in a tube are presented here to further demonstrate the effects of a flexible boundary on the natural frequencies of one-dimensional systems. Only the case where the tube wall is mass controlled is considered. The pressure distributions are determined for a tube with generalised wall masses of $m_w = 10$, $m_w = 1$ and $m_w = 0.01$. As well, the distributions are also included for the rigid walled case for comparison purposes.

To approximate the standing waves in a tube using one-dimensional finite elements, the system requires some means of forcing. An oscillating piston positioned at $x = 0$ produces the required forcing by introducing a volume source to the system as depicted in Fig. 3.3. At $x = l$, the end of the tube is open introducing a zero pressure boundary condition. The natural frequencies of this tube can be determined if the acoustic pressure is assumed to have the form

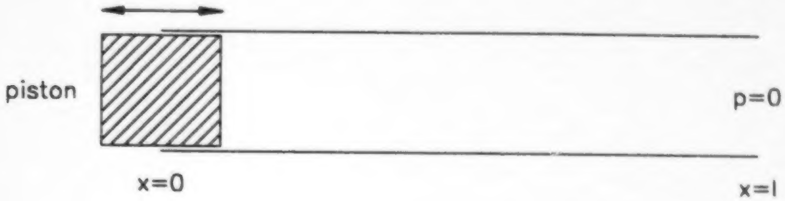

Figure 3.3: Tube with Forcing Piston at $x = 0$, Open End at $x = l$

$$p(x) = (A\cos kx + B\sin kx)e^{j\omega t}. \tag{3.28}$$

The particle velocity at the face of the piston is represented by $u = Ue^{j\omega t}$. Acoustic pressure and particle velocity are related by Eq. (3.4). Substituting the pressure and velocity terms into Eq. (3.4), and introducing the zero pressure boundary condition at $x = l$, leads to the equation for the pressure distribution of the tube

$$p(x) = -j\rho cU\frac{\sin kx}{\cos kl}e^{j\omega t}. \tag{3.29}$$

The pressure distribution of the tube becomes infinite when $\cos kl = 0$, meaning the corresponding natural frequencies are represented by Eq. (3.30)

$$\omega_n = \frac{(2n-1)\pi c}{2l} \tag{3.30}$$

where (n=1, 2, 3,...).

A finite element mesh consisting of 20 pipe elements with 41 DOF was used to model the standing wave pressure distribution in a rigid walled open tube with an oscillating piston at one end. Only the first three natural frequencies given by Eq. (3.30) were considered. Pressures were plotted for each node point along the entire length of the tube. The pressure distributions for each of the first three natural frequencies are presented in Figures 3.4, 3.5 and 3.6. Notice that the dotted line represents the centreline of the tube. The results are identical to those obtained by plotting the real part of Eq. (3.29). These results for a rigid walled tube will be used as a reference to further demonstrate the effects of a flexible walled tube on the natural frequencies.

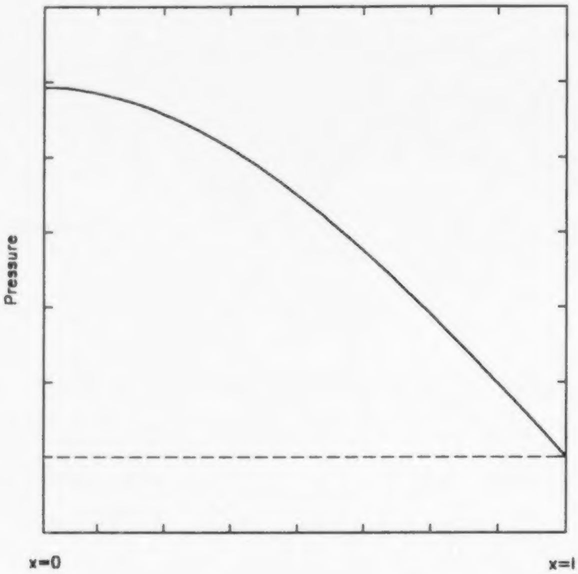

Figure 3.4: Standing Wave in a Rigid Walled Pipe; Piston at $x = 0$, Open at $x = l$; $\omega = \pi c / 2l$

A similar tube with a mass controlled flexible wall is now modelled with a mesh of flex-wall pipe elements. The flexible wall has a generalised mass of value m_w = 10. Pressure distributions for the first three natural frequencies determined form Eq. (3.30) are presented in Figures (3.7), (3.8) and (3.9). Comparison with the rigid walled results presented earlier demonstrate that even for a generalised mass of 10, the flexible walled tube appears nearly rigid and pressure distributions are nearly identical to the rigid case. This is not unexpected as inspection of the eigenvalues given in Table 3.1 confirms that for m_w = 10, the tube wall is becoming quite rigid.

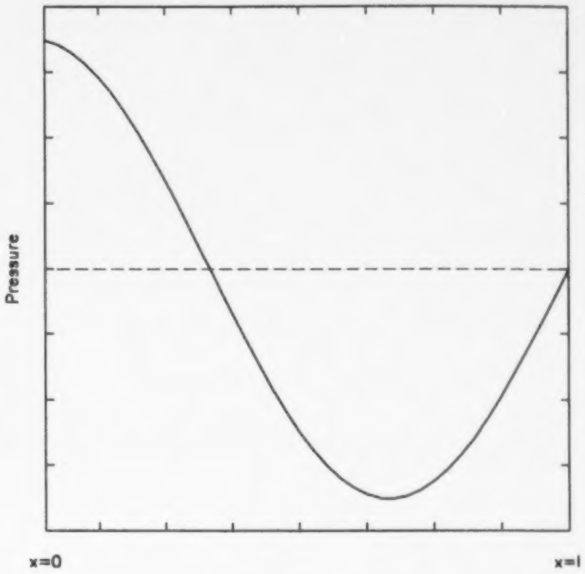

Figure 3.5: Standing Wave in a Rigid Walled Pipe; Piston at $x = 0$, Open at $x = l$; $\omega = 3\pi c / 2l$

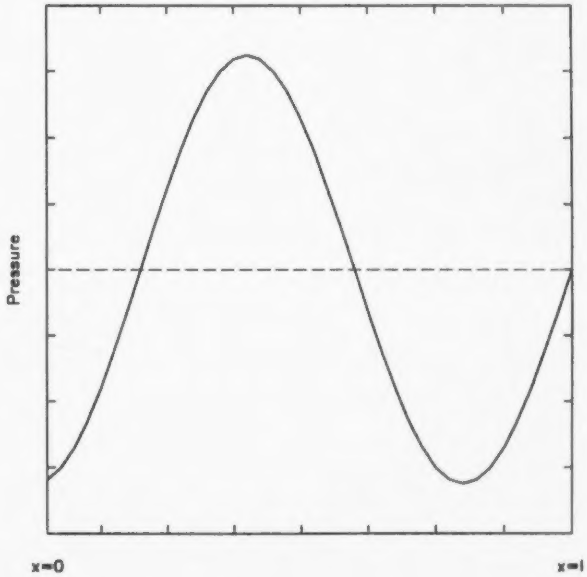

Figure 3.6: Standing Wave in a Rigid Walled Pipe; Piston at $x = 0$, Open at $x = l$; $\omega = 5\pi c / 2l$

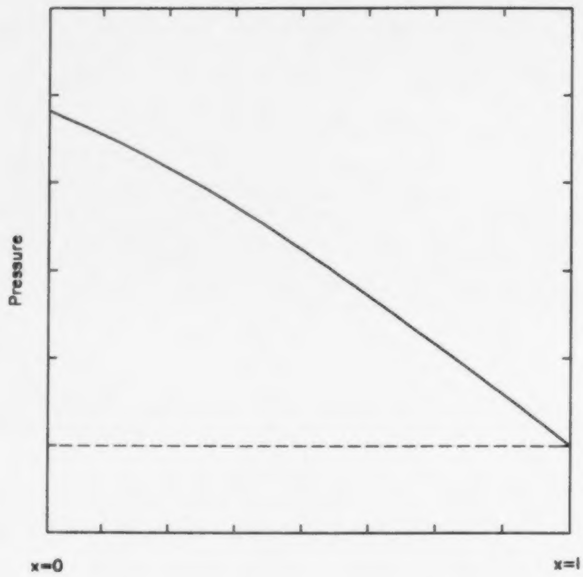

Figure 3.7: Standing Wave in a Flexible Walled Pipe (m_w = 10); Piston at $x = 0$, Open at $x = l$; $\omega = \pi c / 2l$

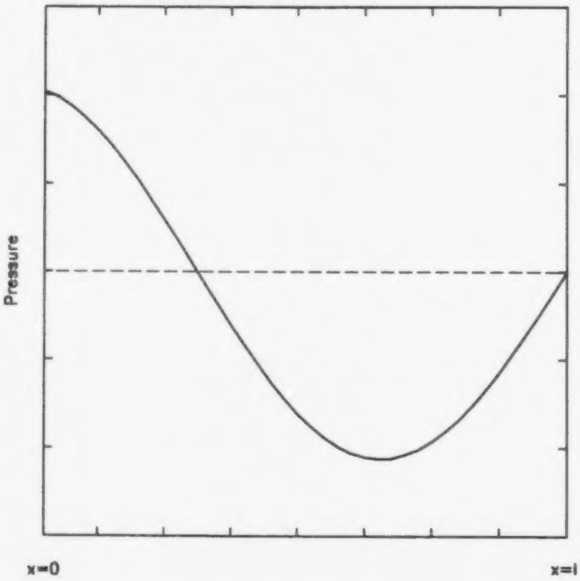

Figure 3.8: Standing Wave in a Flexible Walled Pipe (m_w = 10); Piston at $x = 0$, Open at $x = l$; $\omega = 3\pi c / 2l$

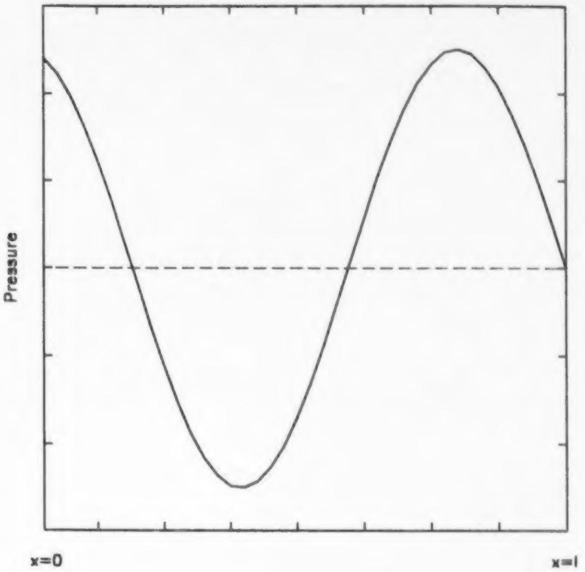

Figure 3.9: Standing Wave in a Flexible Walled Pipe (m_w = 10); Piston at $x = 0$, Open at $x = l$; $\omega = 5\pi c / 2l$

Flexible walled tubes with generalised masses of m_w = 1 and m_w = 0.01 were also considered with pressure distributions for the first three natural frequencies of Eq. (3.30) presented in Figures 3.10 - 3.15. For the case where m_w = 1, pressure distributions are out of phase as compared with the rigid walled case. This result is not unexpected as the eigenvalues for the closed tube given in Table 3.1 demonstrate the significant effect a flexible boundary has on the natural frequencies of a system. Clearly, for the case where m_w = 0.01, all energy has essentially been absorbed by the pipe walls and there is minimal pressure distribution along the length of the pipe. The pipe is acting as an effective Helmholtz resonator.

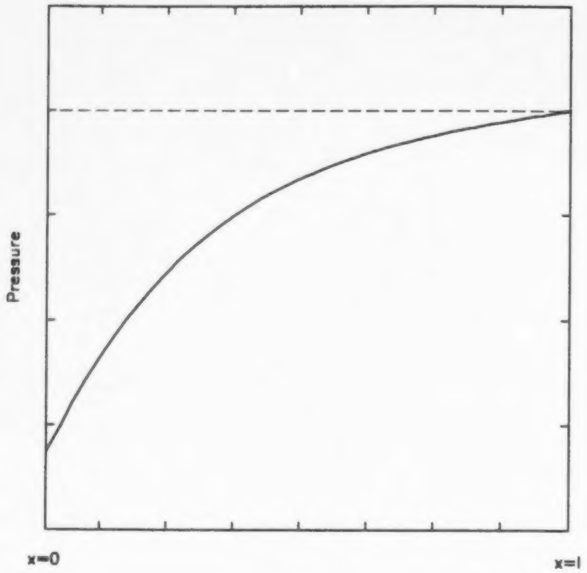

Figure 3.10: Standing Wave in a Flexible Walled Pipe ($m_w = 1$); Piston at $x = 0$, Open at $x = l$; $\omega = \pi c / 2l$

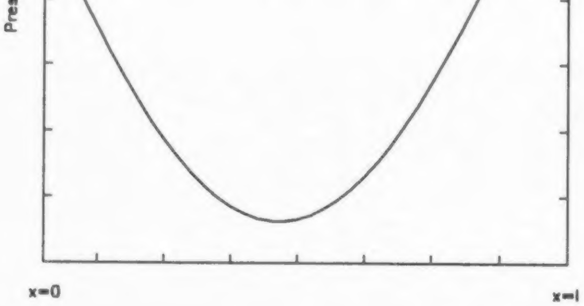

Figure 3.11: Standing Wave in a Flexible Walled Pipe ($m_w = 1$); Piston at $x = 0$, Open at $x = l$; $\omega = 3\pi c / 2l$

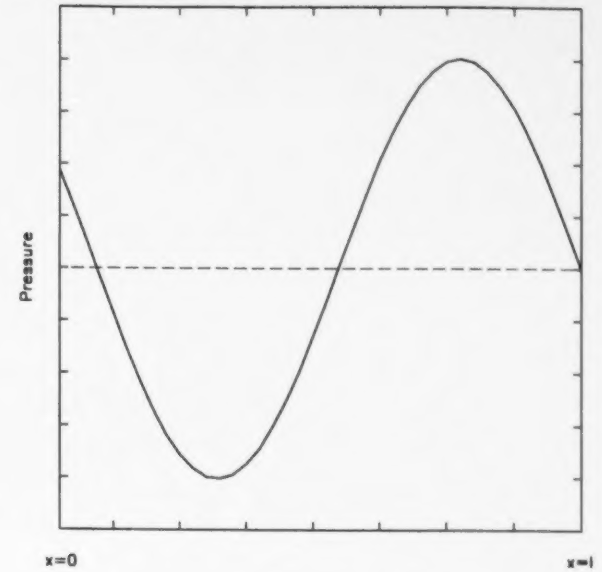

Figure 3.12: Standing Wave in a Flexible Walled Pipe ($m_w = 1$); Piston at $x = 0$, Open at $x = l$; $\omega = 5\pi c / 2l$

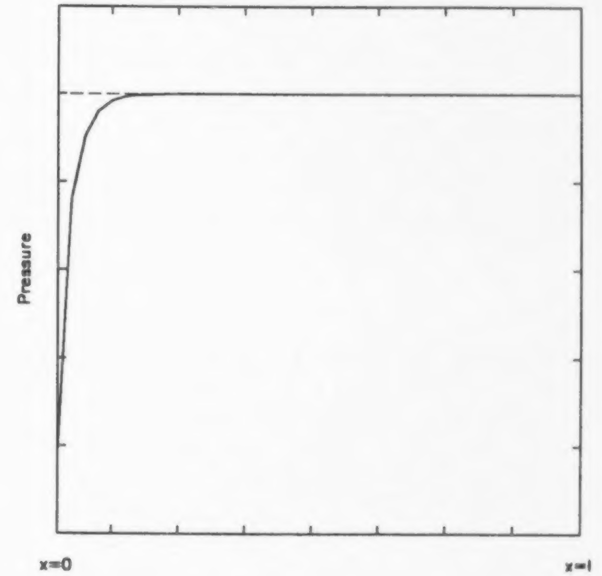

Figure 3.13: Standing Wave in a Flexible Walled Pipe ($m_w = 0.01$); Piston at $x = 0$, Open at $x = l$; $\omega = \pi c / 2l$

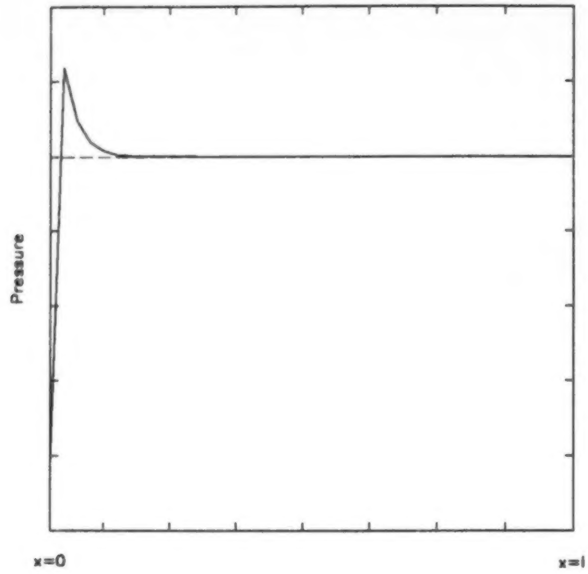

Figure 3.14: Standing Wave in a Flexible Walled Pipe ($m_w = 0.01$); Piston at $x = 0$, Open at $x = l$; $\omega = 3\pi c / 2l$

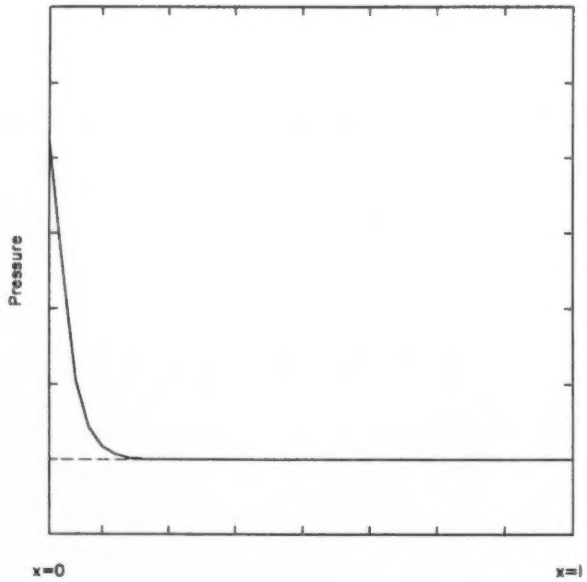

Figure 3.15: Standing Wave in a Flexible Walled Pipe ($m_w = 0.01$); Piston at $x = 0$, Open at $x = l$; $\omega = 5\pi c / 2l$

CHAPTER 4

A Simple Three-Dimensional Finite Element to Model Dipole and Quadrupole Mode Propagation in Ducts

4.1 Introduction

Higher order three-dimensional finite elements with quadratic or even cubic pressure variations are commonly used to study the acoustics of duct systems. The added complexities of these higher order elements are generally not necessary for low frequency duct acoustics where the frequencies of excitation and duct section dimensions are such that lower modes of transmission dominate the response and a simpler element mesh may be sufficient. It is the objective of this chapter to demonstrate that chain-assembled three-dimensional finite elements may be used to successfully model low frequency duct acoustics including significant 3-D effects such as higher order mode cut-off frequencies. Also, the limitations of plane wave theory will be discussed.

A three-dimensional linear isoparametric hexahedral finite element is formulated with acoustic pressure as the only nodal quantity using Galerkin's method of weighted residuals and will be referred to subsequently as the HEX8 element. The HEX8 element is deformable and is able to easily model any duct geometries. The accuracy of the element is shown for two rigid walled cases with stationary flow: a closed, straight duct section and a cylindrical enclosure.

On any one face of the HEX8 element, there are only four degrees of freedom, thus only four modes of propagation are allowed [32]. This makes the HEX8 element an ideal choice for modelling higher order modes such as the dipole and quadrupole modes which cause bending and torsional twisting of the duct walls. Sound transmission and the effect of cut-off frequencies on the propagation of higher modes is demonstrated for various duct geometries including chambers, bends, curves and junctions.

All formulations presented in this chapter are based on assumptions of systems with rigid (acoustically hard) walls and stationary flow. Following the goal of developing simple elements for the acoustics engineer, all finite element models were considered as part of an infinite transmission line (ρc termination). Other complex impedance terminations could be considered but the subsequent complexity was not warranted in this work. Computations with the HEX8 element were carried out on an IBM RS/6000 320H workstation using FORTRAN source code.

Mathematical development of the 3-D Helmholtz equation is considered in the next section based on a control volume formulation. This is followed by formulation of the corresponding finite element equations and eigenvalue testing of the element. The remaining sections concern the propagation of higher order dipole and quadrupole modes using the damped transmission loss equations developed in Chapter 2.

4.2 The Helmholtz Equation

The three-dimensional wave equation may be developed by considering a 3-D element of fluid fixed in space acted upon by uniform ambient pressure. Equations expressing the laws of conservation of mass, momentum equations and pressure-density relationships are established and then combined to formulate the 3-D wave equation in rectangular coordinates.

An infinitesimal element of fluid is shown in Fig. 4.1, where *u*, *v* and *w* represent fluid particle velocities in their respective coordinates, *p* is the acoustic pressure and ρ is the fluid density.

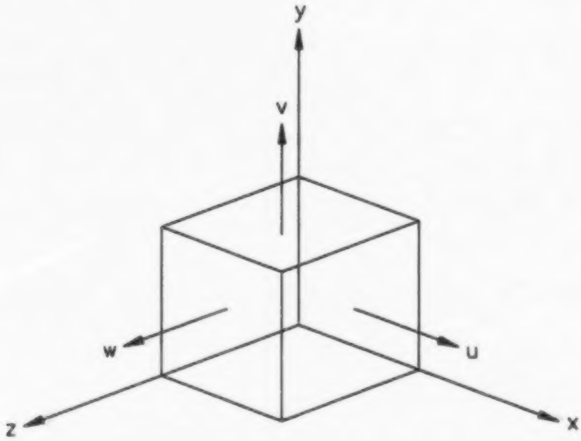

Figure 4.1: Infinitesimal 3-D Fluid Element

If the element is considered as a control volume, mass must be conserved and the linearized equation of mass conservation is given as

$$\rho\left(\frac{\partial u}{\partial x}+\frac{\partial v}{\partial y}+\frac{\partial w}{\partial z}\right)=-\frac{\partial \rho}{\partial t}. \tag{4.1}$$

The linearized momentum equations in the x, y and z coordinates are written as

$$-\frac{\partial p}{\partial x}=\rho\frac{\partial u}{\partial t},\quad -\frac{\partial p}{\partial y}=\rho\frac{\partial v}{\partial t},\quad -\frac{\partial p}{\partial z}=\rho\frac{\partial w}{\partial t}$$

and the pressure-density relationship is given by the following equation

$$\frac{\partial p}{\partial t}=c^2\frac{\partial \rho}{\partial t} \tag{4.2}$$

which is the same as Eq. (2.4) where c is the local speed of sound of the fluid medium. Substitution of Eq. (4.2) into Eq. (4.1) produces an equation of the form

$$\rho\left(\frac{\partial u}{\partial x}+\frac{\partial v}{\partial y}+\frac{\partial w}{\partial z}\right)=-\frac{1}{c^2}\frac{\partial p}{\partial t} \tag{4.3}$$

which can be differentiated with respect to time becoming

$$\rho\left(\frac{\partial^2 u}{\partial x\partial t}+\frac{\partial^2 v}{\partial y\partial t}+\frac{\partial^2 w}{\partial z\partial t}\right)=-\frac{1}{c^2}\frac{\partial^2 p}{\partial t^2}. \tag{4.4}$$

The linearized momentum equations may be used to eliminate the particle velocities from Eq. (4.4), resulting in the 3-D wave equation in rectangular coordinates

$$\left(\frac{\partial^2 p}{\partial x^2}+\frac{\partial^2 p}{\partial y^2}+\frac{\partial^2 p}{\partial z^2}\right)-\frac{1}{c^2}\frac{\partial^2 p}{\partial t^2}=0. \tag{4.5}$$

If only harmonic motion is considered, the acoustic pressure has the form $p = pe^{j\omega t}$ where ω is the radian frequency. Upon substitution of the pressure term into the wave equation, the time derivative is eliminated thus yielding the Helmholtz equation in 3-D rectangular coordinates

$$\frac{\partial^2 p}{\partial x^2}+\frac{\partial^2 p}{\partial y^2}+\frac{\partial^2 p}{\partial z^2}+k^2 p=0 \qquad (4.6)$$

where k is the wavenumber ω / c.

4.3 3-D Hexahedral Element Formulation

A three-dimensional isoparametric hexahedral finite element which allows linear variations in pressure between its node points was chosen to approximate the Helmholtz equation. The HEX8 element was formulated using Galerkin's method of weighted residuals but because of the added degrees of freedom and the extra two dimensions, it is not practical to evaluate all of the terms analytically as was done with the pipe element. Numerical integration procedures are used to formulate the element allowing greater flexibility in implementing the HEX8 element.

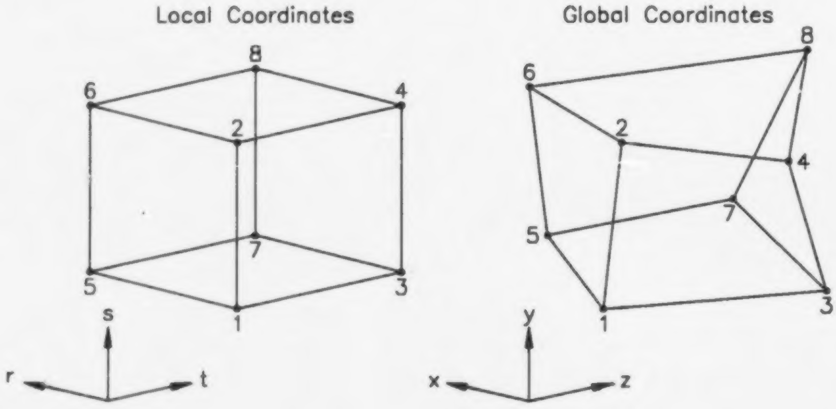

Figure 4.2: Isoparametric HEX8 Element in Local and Global Coordinate Systems

The HEX8 element is shown in Fig. 4.2 in its local (r, s, t) and global (x, y, z) coordinate systems. In its local coordinate system, the element remains a fixed cube with nodal coordinates varying between the values -1 and +1. In its global coordinate system, the element may be deformed into almost any shape, the restriction being that all interior angles of the element be smaller than 180°. As will be demonstrated later in this Chapter, the HEX8 element is easily distorted into many configurations allowing the modelling of many complex geometries.

In a finite element approximation to the Helmholtz equation, the linear pressure distribution between the nodes of the element may be represented by simple polynomials [14]

$$p = a_1 + a_2 r + a_3 s + a_4 t + a_5 rs + a_6 rt + a_7 st + a_8 rst \tag{4.7}$$

or in matrix form

$$p = \{F\}^T \{\alpha\} \tag{4.8}$$

where

$$\{F\}^T = \{1 \quad r \quad s \quad t \quad rs \quad rt \quad st \quad rst\}$$

and

$$\{\alpha\} = \begin{Bmatrix} a_1 \\ a_2 \\ a_3 \\ a_4 \\ a_5 \\ a_6 \\ a_7 \\ a_8 \end{Bmatrix}$$

where the superscript T denotes a matrix transform. The pressure is expressed in terms of generalised coordinates $a_1 \cdots a_8$ which govern the contribution of each of the terms of the simple polynomial. These may be related to the acoustic pressures at the individual node points of the element by inserting boundary values for each nodal pressure. Boundary values for the eight node points of the HEX8 element in its local coordinates are shown in Fig. 4.3.

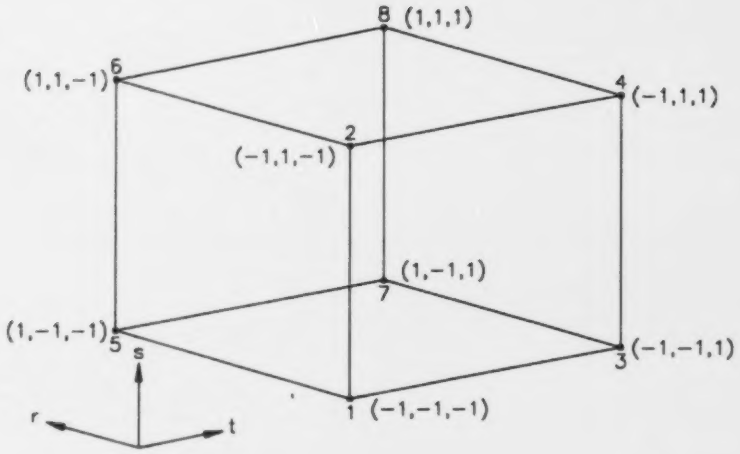

Figure 4.3: HEX8 Element in the Local Coordinate System

Insertion of the boundary values for each nodal pressure results in a system of eight equations and eight unknowns which can be expressed in matrix form as

$$\{p_e\} = [T]\{\alpha\} \text{ or } \{\alpha\} = [T^{-1}]\{p_e\},$$

where the transformation matrix is

$$[T] = \begin{bmatrix} 1 & -1 & -1 & -1 & 1 & 1 & 1 & -1 \\ 1 & -1 & 1 & -1 & -1 & 1 & -1 & 1 \\ 1 & -1 & -1 & 1 & 1 & -1 & -1 & 1 \\ 1 & -1 & 1 & 1 & -1 & -1 & 1 & -1 \\ 1 & 1 & -1 & -1 & -1 & -1 & 1 & 1 \\ 1 & 1 & 1 & -1 & 1 & -1 & -1 & -1 \\ 1 & 1 & -1 & 1 & -1 & 1 & -1 & -1 \\ 1 & 1 & 1 & 1 & 1 & 1 & 1 & 1 \end{bmatrix}$$

The pressure at any point (*r, s, t*) within the element can now be written in terms of the nodal pressures

$$p = \{F\}^T[T^{-1}]\{p_e\}. \tag{4.9}$$

The use of simple polynomials rather than shape functions means the transformation matrix must be inverted but this need only be done once with the result stored in computer memory and used as needed. This should not be considered as a disadvantage to using simple polynomials rather than shape functions as the computer code for an element formed by polynomials has a much more generalised form than the code for an element formed by shape functions. This allows the computer code to be easily modified to accommodate other higher order elements.

The polynomials which govern the variation in pressure may be used to govern the variation in geometry. This is the basis of an isoparametric finite element and allows the geometry of the element to be distorted. Therefore, the regular geometry in the local coordinate system is transformed to a distorted geometry in the global coordinate system by the following transformations

$$x = \{F\}^T\left[T^{-1}\right]\{x_e\}$$

$$y = \{F\}^T\left[T^{-1}\right]\{y_e\}$$

$$z = \{F\}^T\left[T^{-1}\right]\{z_e\}$$

where $\{x_e\}$, $\{y_e\}$ and $\{z_e\}$ are vectors containing the x, y and z coordinates at the element node points. The relationship between the local and global coordinates may be determined by applying the rules of partial differentiation. Using the chain rule, we have

$$\frac{\partial}{\partial r} = \frac{\partial x}{\partial r}\frac{\partial}{\partial x} + \frac{\partial y}{\partial r}\frac{\partial}{\partial y} + \frac{\partial z}{\partial r}\frac{\partial}{\partial z}$$

$$\frac{\partial}{\partial s} = \frac{\partial x}{\partial s}\frac{\partial}{\partial x} + \frac{\partial y}{\partial s}\frac{\partial}{\partial y} + \frac{\partial z}{\partial s}\frac{\partial}{\partial z}$$

$$\frac{\partial}{\partial t} = \frac{\partial x}{\partial t}\frac{\partial}{\partial x} + \frac{\partial y}{\partial t}\frac{\partial}{\partial y} + \frac{\partial z}{\partial t}\frac{\partial}{\partial z}.$$

In matrix form, this may be written as

$$\begin{Bmatrix} \frac{\partial}{\partial r} \\ \frac{\partial}{\partial s} \\ \frac{\partial}{\partial t} \end{Bmatrix} = \begin{bmatrix} \frac{\partial x}{\partial r} & \frac{\partial y}{\partial r} & \frac{\partial z}{\partial r} \\ \frac{\partial x}{\partial s} & \frac{\partial y}{\partial s} & \frac{\partial z}{\partial s} \\ \frac{\partial x}{\partial t} & \frac{\partial y}{\partial t} & \frac{\partial z}{\partial t} \end{bmatrix} \begin{Bmatrix} \frac{\partial}{\partial x} \\ \frac{\partial}{\partial y} \\ \frac{\partial}{\partial z} \end{Bmatrix}$$

$$\begin{Bmatrix} \frac{\partial}{\partial r} \\ \frac{\partial}{\partial s} \\ \frac{\partial}{\partial t} \end{Bmatrix} = [J] \begin{Bmatrix} \frac{\partial}{\partial x} \\ \frac{\partial}{\partial y} \\ \frac{\partial}{\partial z} \end{Bmatrix}$$

where the Jacobian matrix is written as

$$[J] = \begin{bmatrix} \frac{\partial x}{\partial r} & \frac{\partial y}{\partial r} & \frac{\partial z}{\partial r} \\ \frac{\partial x}{\partial s} & \frac{\partial y}{\partial s} & \frac{\partial z}{\partial s} \\ \frac{\partial x}{\partial t} & \frac{\partial y}{\partial t} & \frac{\partial z}{\partial t} \end{bmatrix}$$

relating the global coordinate derivatives to the local coordinate derivatives. This may be rewritten in the following form

$$\begin{Bmatrix} \frac{\partial}{\partial x} \\ \frac{\partial}{\partial y} \\ \frac{\partial}{\partial z} \end{Bmatrix} = \left[J^{-1}\right] \begin{Bmatrix} \frac{\partial}{\partial r} \\ \frac{\partial}{\partial s} \\ \frac{\partial}{\partial t} \end{Bmatrix}$$

implying that the inverse of $[J]$ exists. The inverse exists provided that there is a unique (one-to-one) correspondence between the global and local element coordinates [11]. Only in situations where the element has been extremely distorted does the uniqueness condition between the coordinate systems fail. This occurs when an interior angle in the element has become 180° or greater. Transformation of the coordinate systems is given by

$$dx\,dy\,dz = \|J\|\,dr\,ds\,dt$$

where $\|J\|$ denotes the absolute value of the determinant of the Jacobian [11].

The finite element approximations to the Helmholtz equation may be formulated using Galerkin's method of weighted residuals. Upon substitution for pressure in the Helmholtz equation, the residual R, may be written as

$$R = \{F_x''\}^T[T^{-1}]\{p_e\} + \{F_y''\}^T[T^{-1}]\{p_e\} + \{F_z''\}^T[T^{-1}]\{p_e\} + k^2\{F\}^T[T^{-1}]\{p_e\} \quad (4.10)$$

where the vector $\{F_x''\}$ denotes $\partial^2 F/\partial x^2$, $\{F_y''\}$ denotes $\partial^2 F/\partial y^2$ and $\{F_z''\}$ denotes $\partial^2 F/\partial z^2$. Galerkin's equation is written in the usual form

$$\iiint \{f\}\,R\,dx\,dy\,dz = 0 \quad (4.11)$$

where

$$\{f\} = [T^{-1}]^T\{F\}$$

and after substitution of the residual into Galerkin's equation, the result becomes

$$\iiint\Big([T^{-1}]^T\{F\}\{F_x''\}^T[T^{-1}] + [T^{-1}]^T\{F\}\{F_y''\}^T[T^{-1}] + [T^{-1}]^T\{F\}\{F_z''\}^T[T^{-1}] + \\ + k^2[T^{-1}]^T\{F\}\{F\}^T[T^{-1}]\Big)\{p_e\}\,dx\,dy\,dz = 0$$

In this form, the matrices in the first three terms are null and non-symmetric. Green's first theorem states:

$$\int_V \{F\}\{F_n''\}^T dV = \int_S \{F\}\left\{\frac{\partial F}{\partial n}\right\} dS - \int_V \{F_n'\}\{F_n'\}^T dV$$

and by making use of this theorem, Galerkin's equation may now be written in a form with symmetric matrices

$$\iiint\left(\left[T^{-1}\right]^T\{F'_x\}\{F'_x\}^T\left[T^{-1}\right]+\left[T^{-1}\right]^T\{F'_y\}\{F'_y\}^T\left[T^{-1}\right]+\left[T^{-1}\right]^T\{F'_z\}\{F'_z\}^T\left[T^{-1}\right]-\right.$$
$$\left.-k^2\left[T^{-1}\right]^T\{F\}\{F\}^T\left[T^{-1}\right]\right)\{p_e\}\,dx\,dy\,dz=0$$

with boundary condition $\partial p/\partial\bar{n}=0$ on the surface of the element where $\bar{n}$ is a vector in the direction of the outward normal.

The Jacobian may now be introduced to transform from the global x, y, z coordinates to the local r, s, t coordinates

$$\int_{-1}^{+1}\int_{-1}^{+1}\int_{-1}^{+1}\left(\left[T^{-1}\right]^T[G]^T\left[J^{-1}\right]^T\left[J^{-1}\right][G]\left[T^{-1}\right]\|J\|\right)\{p_e\}\,dr\,ds\,dt-$$
$$-k^2\int_{-1}^{+1}\int_{-1}^{+1}\int_{-1}^{+1}\left(\left[T^{-1}\right]^T\{F\}\{F\}^T\left[T^{-1}\right]\|J\|\right)\{p_e\}\,dr\,ds\,dt=0$$

making note that

$$[G]=\begin{Bmatrix}\left\{\dfrac{\partial F}{\partial r}\right\}^T\\ \left\{\dfrac{\partial F}{\partial s}\right\}^T\\ \left\{\dfrac{\partial F}{\partial t}\right\}^T\end{Bmatrix}$$

Here, $[G]$ is a 3×8 matrix. Galerkin's equation may be separated into two parts, the kinetic and potential energy matrices respectively

$$[S]=\int_{-1}^{+1}\int_{-1}^{+1}\int_{-1}^{+1}\left(\left[T^{-1}\right]^T[G]^T\left[J^{-1}\right]^T\left[J^{-1}\right][G]\left[T^{-1}\right]\|J\|\right)\{p_e\}\,dr\,ds\,dt \tag{4.12}$$

$$[P]=\int_{-1}^{+1}\int_{-1}^{+1}\int_{-1}^{+1}\left(\left[T^{-1}\right]^T\{F\}\{F\}^T\left[T^{-1}\right]\|J\|\right)\{p_e\}\,dr\,ds\,dt \tag{4.13}$$

where $[S]$ and $[P]$ are square, symmetric and 8×8 in size. Notice that all integrations are between the limits -1 to $+1$, conforming with standard limits of numerical integration schemes such as the Gauss quadrature technique [11]. The approximate finite element equation of motion can now be written as

$$([S]-k^2[P])\{p\}=\{0\}. \tag{4.14}$$

4.3.1 Assembly Of Elements

It is assumed in Eq. (4.14) that there are no volume source terms present meaning that the boundaries of the HEX8 element are immobile. In this configuration, the element cannot be connected to another system. If volume sources are present at the nodes of the element, the inhomogeneous form of the finite element equation becomes

$$([S]-k^2[P])\{p_e\}=\rho\omega^2\{Q_e\}. \tag{4.15}$$

The assembly procedure for the HEX8 element is demonstrated by considering the two finite elements shown in Fig. 4.4. In this configuration, the elements are unconstrained and have a total of sixteen pressure unknowns and sixteen volume sources. The elements may be connected at nodes 5, 6, 7, 8 and 9, 10, 11, 12 as shown in Fig. 4.5; the following conditions must be satisfied

$$p_5=p_9=p_5^G,\ p_6=p_{10}=p_6^G,\ p_7=p_{11}=p_7^G,\ p_8=p_{12}=p_8^G$$

$$\rho\omega^2\begin{Bmatrix}Q_5\\Q_6\\Q_7\\Q_8\end{Bmatrix}+\rho\omega^2\begin{Bmatrix}Q_9\\Q_{10}\\Q_{11}\\Q_{12}\end{Bmatrix}=0.$$

There are no volume source terms introduced at the connection nodes as implied by the second equation.

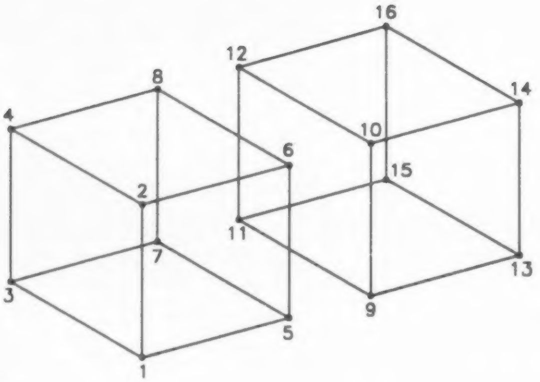
16
12
14
8
4
10
6
15
2
11
7
13
3
9
5
1

Figure 4.4: Unconstrained and Unconnected HEX8 Elements

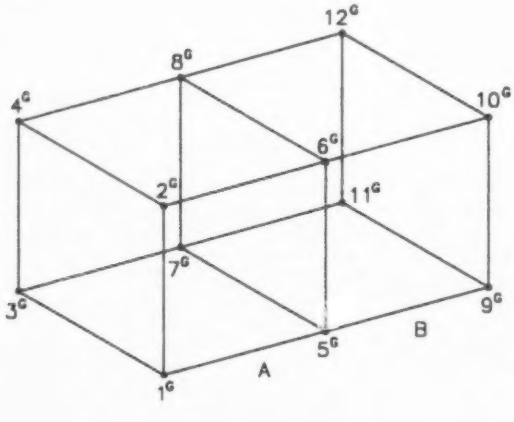
12^G
8^G
4^G
10^G
6^G
2^G
11^G
7^G
3^G
9^G
B
5^G
A
1^G

Figure 4.5: Global System of Assembled HEX8 Elements

The two element system, with sixteen degrees of freedom, shown in Fig. 4.4 has become the global system shown in Fig. 4.5. The global system now has twelve degrees of freedom with corresponding equation of motion

$$\left(\left[S^G\right]-k^2\left[P^G\right]\right)\left\{p^G\right\}=\rho\omega^2\left\{Q^G\right\} \tag{4.16}$$

where the global kinetic energy matrix is

$$\left[S^G\right]=\begin{bmatrix} S^A_{11} & \cdots & S^A_{15} & S^A_{16} & S^A_{17} & S^A_{18} & \cdots & 0 \\ \vdots & \ddots & \vdots & \vdots & \vdots & \vdots & ⋰ & \vdots \\ S^A_{51} & \cdots & S^A_{55}+S^B_{11} & S^A_{56}+S^B_{12} & S^A_{57}+S^B_{13} & S^A_{58}+S^B_{14} & \cdots & S^B_{18} \\ S^A_{61} & \cdots & S^A_{65}+S^B_{21} & S^A_{66}+S^B_{22} & S^A_{67}+S^B_{23} & S^A_{68}+S^B_{24} & \cdots & S^B_{28} \\ S^A_{71} & \cdots & S^A_{75}+S^B_{31} & S^A_{76}+S^B_{32} & S^A_{77}+S^B_{33} & S^A_{78}+S^B_{34} & \cdots & S^B_{38} \\ S^A_{81} & \cdots & S^A_{85}+S^B_{41} & S^A_{86}+S^B_{42} & S^A_{87}+S^B_{43} & S^A_{88}+S^B_{44} & \cdots & S^B_{48} \\ \vdots & ⋰ & \vdots & \vdots & \vdots & \vdots & \ddots & \vdots \\ 0 & \cdots & S^B_{81} & S^B_{82} & S^B_{83} & S^B_{84} & \cdots & S^B_{88} \end{bmatrix}$$

the global potential energy matrix is

$$\left[P^G\right]=\begin{bmatrix} P^A_{11} & \cdots & P^A_{15} & P^A_{16} & P^A_{17} & P^A_{18} & \cdots & 0 \\ \vdots & \ddots & \vdots & \vdots & \vdots & \vdots & ⋰ & \vdots \\ P^A_{51} & \cdots & P^A_{55}+P^B_{11} & P^A_{56}+P^B_{12} & P^A_{57}+P^B_{13} & P^A_{58}+P^B_{14} & \cdots & P^B_{18} \\ P^A_{61} & \cdots & P^A_{65}+P^B_{21} & P^A_{66}+P^B_{22} & P^A_{67}+P^B_{23} & P^A_{68}+P^B_{24} & \cdots & P^B_{28} \\ P^A_{71} & \cdots & P^A_{75}+P^B_{31} & P^A_{76}+P^B_{32} & P^A_{77}+P^B_{33} & P^A_{78}+P^B_{34} & \cdots & P^B_{38} \\ P^A_{81} & \cdots & P^A_{85}+P^B_{41} & P^A_{86}+P^B_{42} & P^A_{87}+P^B_{43} & P^A_{88}+P^B_{44} & \cdots & P^B_{48} \\ \vdots & ⋰ & \vdots & \vdots & \vdots & \vdots & \ddots & \vdots \\ 0 & \cdots & P^B_{81} & P^B_{82} & P^B_{83} & P^B_{84} & \cdots & P^B_{88} \end{bmatrix}$$

along with the corresponding global volume source vector

$$\left\{Q^G\right\}=\begin{Bmatrix} Q_1 \\ \vdots \\ 0 \\ 0 \\ 0 \\ 0 \\ \vdots \\ Q_{12} \end{Bmatrix}$$

Individual element matrices can be assembled together into a global system by overlaying them at the connecting nodes as demonstrated above. Many elements may be connected together into almost any imaginable shape and configuration using this procedure. On must only consider the practical limitations of computer memory size.

4.3.2 Continuity Between Elements

Sufficient conditions that assure the convergence of a finite element approximation are that certain continuity and completeness criteria [14] are satisfied. The continuity condition states that for second order differential equations such as the Helmholtz equation, only the dependent variable must be continuous across element boundaries. The HEX8 element discussed here has C^0 continuity, meaning that only the independent pressure variable p is continuous across the element boundaries. Completeness states that at least a linear polynomial should be used when modelling a second order differential equation. The use of a linear polynomial satisfies this criterion. Both continuity and completeness have been satisfied in the finite element approximation of the Helmholtz equation, assuring solution convergence.

4.4 Element Testing: The Eigenvalue Problem

The accuracy of the HEX8 element was tested by predicting the natural frequencies of a rectangular duct section with rigid walls containing a stationary medium. If the pressure perturbation modes have the form [44]

$$p = A\cos\left(\frac{l\pi x}{l_x}\right)\cos\left(\frac{m\pi y}{l_y}\right)\cos\left(\frac{n\pi z}{l_z}\right) \tag{4.17}$$

then an exact solution for the eigenvalues of the Helmholtz equation in terms of the wavenumber k, is

$$k^2 = \pi^2\left[\left(\frac{l}{l_x}\right)^2 + \left(\frac{m}{l_y}\right)^2 + \left(\frac{n}{l_z}\right)^2\right] \tag{4.18}$$

where l, m and n are any integers and l_x, l_y and l_z represent the dimensions of the enclosure as shown in Fig. 4.6.

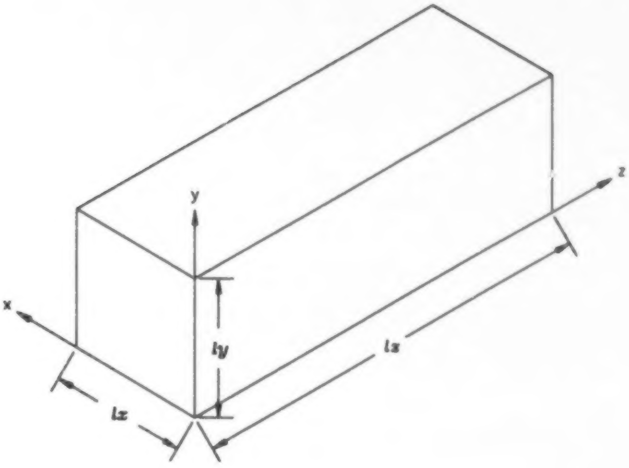

Figure 4.6: Rectangular Duct Section

Finite element models consisting of 40 HEX8 elements with 164 DOF and 80 HEX8 elements with 324 DOF were used to approximate the axial eigenvalues of a rectangular duct section with dimensions 0.1 m × 0.1 m × 1.0 m with the results being presented in Table 4.1. The elements were just chained together to form the duct section by the method described in Section 4.3.1, thus the flexibility of the system was increased only in the axial direction. For comparison purposes, the axial eigenvalues of this duct section were also approximated using 13 pipe elements with 27 DOF.

Results presented in Table 4.1 clearly demonstrate that for essentially one-dimensional systems such as the duct section considered here, the one-dimensional pipe element has distinct advantages over the three-dimensional HEX8 element. A pipe element model with 27 DOF approximates the sixth axial natural frequency with a prediction error of 0.55% while HEX8 element models with 164 DOF and 324 DOF approximate the sixth longitudinal natural frequency with prediction errors of 1.86% and 0.46% respectively. There are significant reductions in computational time and core memory requirements by employing the pipe element to model simple one-dimensional systems rather than using HEX8 elements. The pipe element employs a quadratic pressure formulation which allows the use of fewer elements and thus fewer degrees of freedom when modelling an acoustic system. Of course, one must remember that the pipe element is restricted to plane wave acoustics for simple geometries. Higher order mode effects or three-dimensional wave motions cannot be modelled with the pipe element. Higher order three-dimensional elements such as the quadratic HEX20 element or cubic HEX32 element could be utilised rather than the HEX8 element but the added complexity of using such elements is not warranted for low frequency acoustic systems.

Table 4.1: Axial Eigenvalues (k^2) of a Rectangular Duct Section. Comparison with Exact Eigenvalues and Those Calculated with 1-D Pipe Elements

Mode Number, *n*	Exact Eigenvalues	13 Pipe Elements	40 HEX8 Elements	80 HEX8 Elements
1	9.87	9.87	9.87	9.87
2	39.48	39.48	39.56	39.50
3	88.83	88.86	89.24	88.93
4	157.91	158.10	159.22	158.23
5	246.74	247.42	249.93	247.23
6	355.31	357.28	361.93	356.95

A significant benefit of using the isoparametric HEX8 element is that it may be distorted into almost any shape, allowing the modelling of many intricate geometries. To demonstrate the accuracy of the element in a deformed configuration, the eigenvalues were determined for a circular, cylindrical enclosure with rigid walls and stationary flow. For this model, the 8 DOF HEX8 element was converted to a 4 DOF axisymmetric ring element by a series of geometric and nodal pressure constraints. In this procedure, a typical HEX8 element (refer to Fig. 4.2) is constrained into the ring segment shown in Fig. 4.7 by the following geometric constraints.

$$x_1 = x_2 = x_3 = x_4 = 0$$

$$x_5 = r_1 \sin\phi,\ \ x_6 = r_2 \sin\phi,\ \ x_7 = r_3 \sin\phi,\ \ x_8 = r_4 \sin\phi$$

$$y_1 = r_1,\ \ y_2 = r_2,\ \ y_3 = r_3,\ \ y_4 = r_4$$

$$y_5 = r_1 \cos\phi,\ \ y_6 = r_2 \cos\phi,\ \ y_7 = r_3 \cos\phi,\ \ y_8 = r_4 \cos\phi$$

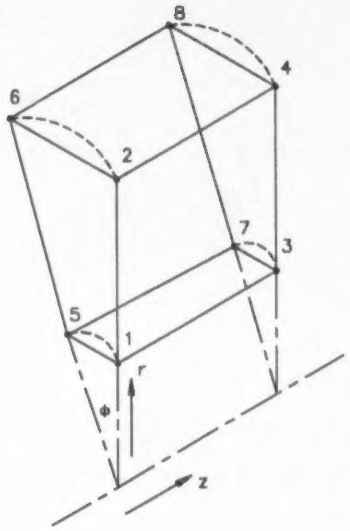

Figure 4.7: Formation of Ring Segment

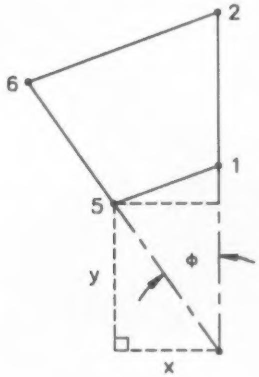

Figure 4.8: Ring Segment Cross-Section

These constraints may be better visualised if one considers the cross-section of a ring segment shown in Fig. 4.8. Further constraints may be applied to the nodal pressures

$$p_5 = p_1,\; p_6 = p_2,\; p_7 = p_3,\; p_8 = p_4$$

which completes the series of geometric and pressure constraints applied to the HEX8 element. The HEX8 element now exists as a two-dimensional, 4 DOF axisymmetric ring element suitable for modelling cylindrical enclosures.

For circular ducts, the wave equation can be separated to give the following equation for pressure variation in the radial direction

$$\frac{\partial^2 p}{\partial r^2}+\frac{1}{r}\frac{\partial p}{\partial r}+\left(k^2-\frac{m^2}{r^2}\right)p=0 \tag{4.19}$$

where k is the wavenumber, m a constant and r is the radius of the duct. Using the relationship $x=kr$, Eq. (4.19) can be transformed into the Bessel equation [47] assuming $k\neq 0$

$$\frac{\partial^2 p}{\partial x^2}+\frac{1}{x}\frac{\partial p}{\partial x}+\left(1-\frac{m^2}{x^2}\right)p=0. \tag{4.20}$$

From the Bessel equation, the radial dependence of acoustic pressure in a circular duct has the form

$$p=AJ_m(kr),\ (k\neq 0) \tag{4.21}$$

where J_m is a Bessel function of the first kind of order m and A is a constant. At the wall of the duct, the boundary condition is such that the normal component of the velocity approaches zero

$$v=BJ'_m(kr)=0,\ (k\neq 0) \tag{4.22}$$

where B is a constant. For each value of m, this condition is fulfilled resulting in a series of wave numbers, $k_{m,n}$ associated with each solution of Eq. (4.20).

The accuracy of the constraint procedure was tested by calculating the eigenvalues in the radial direction for a cylindrical enclosure with radius 0.1 m. Ten HEX8 elements were assembled radially outward from the centreline of the enclosure in ring segment form as shown in Fig. 4.9. Pressure constraints were applied to the nodes resulting in a two-dimensional mesh of ten axisymmetric ring elements with 22 DOF as shown in Fig. 4.10.

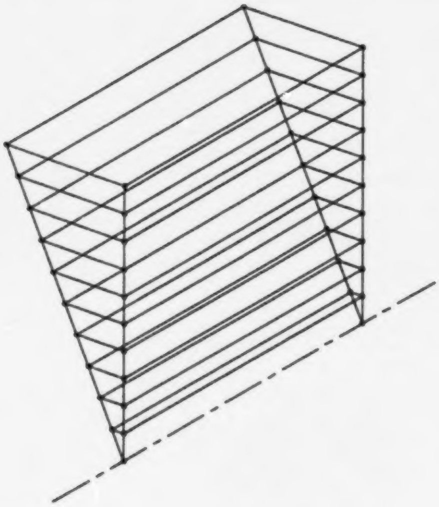

Figure 4.9: 10 HEX8 Elements Assembled in Ring Segment Form to Model a Cylindrical Enclosure

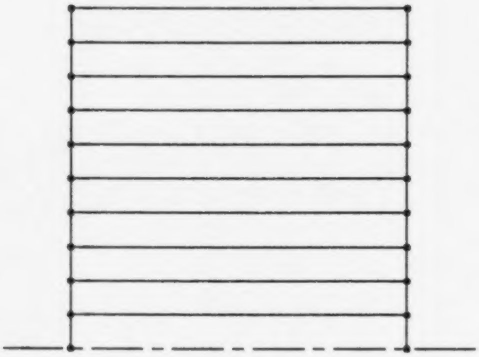

Figure 4.10: 2-D Mesh of 10 Axisymmetric Ring Elements with 22 DOF

Eigenvalues for the first four modes in the radial direction for various angles ϕ along with the exact eigenvalues are given in Table 4.2.

Table 4.2: Eigenvalues for a Circular Cylindrical Enclosure, 10 Radial Elements

Mode	Exact Solution $J_0(kr)=0$	$\phi=6^\circ$	$\phi=10^\circ$	$\phi=20^\circ$	$\phi=30^\circ$
1,0	3.83	3.85	3.86	3.91	3.98
2,0	7.02	7.14	7.16	7.24	7.38
3,0	10.17	10.56	10.58	10.72	10.91
4,0	13.32	14.20	14.24	14.40	14.68

Table 4.3: Eigenvalue Model Prediction Errors

Mode	$\phi=6^\circ$ % Error	$\phi=10^\circ$ % Error	$\phi=20^\circ$ % Error	$\phi=30^\circ$ % Error
1,0	0.53	0.78	2.00	3.93
2,0	1.75	2.00	3.21	5.19
3,0	3.77	4.03	5.33	7.29
4,0	6.59	6.85	8.11	10.20

Eigenvalue results presented in Table 4.2 indicate that decreasing ϕ improves the accuracy of the finite element mesh but it should be noted that too small a value of ϕ produced numerical errors. The accuracy of the eigenvalues may also be improved by increasing the number of elements in the radial direction. These results demonstrate that the HEX8 element can be easily distorted to model complicated geometries while retaining an acceptable degree of accuracy. Higher order finite elements such as the HEX20 or HEX32 elements would provide much improved accuracy for modelling a cylindrical enclosure but the purpose of using the HEX8 element in this case was to illustrate that the simple HEX8 element may be used to model complex geometries with much success. Later, this fact will be illustrated further as the simple HEX8 element is used to model many complicated duct configurations.

4.5 Transmission Loss of Damped Acoustic Systems with Special Consideration of Dipole and Qaudrupole Mode Effects

Even at low frequencies, three-dimensional wave effects in a duct may generate higher order modes and if these modes are not attenuated sufficiently, they alter the acoustics of the duct considerably. The plane wave theory presented in Chapter 2 does not allow for the onset of higher order modes, thus its use should be limited to providing an initial generalisation of the low frequency response of the duct. Subsequent calculations with three-dimensional elements should then be undertaken to determine the higher order mode effects present in the system. Three-dimensional effects are a primary source of discrepancy between measured values of acoustic response and that predicted by plane wave theory at higher frequencies [71] and their presence cannot be neglected.

In keeping with the goal of providing uncomplicated finite element methods for the acoustics engineer, the simple three-dimensional HEX8 element will now be implemented throughout this section to model higher order modes present in various duct configurations, concentrating on the effects of dipole and quadrupole modes. First, a comparison of the pipe element and HEX8 element must be made to demonstrate the limitations of plane wave theory. A simple cylindrical expansion chamber with expansion ratio = 10 was modelled using a network of 10 pipe elements with 21 DOF and using 50 HEX8 elements constrained by the procedure outlined in Section 4.4 to form a mesh of axisymmetric ring elements with 66 DOF as shown in Fig. 4.11. The chamber was part of an infinite transmission line (ρc termination) with plane wave input. The equations of Section 2.5.1 were used to calculate the transmission loss of the chamber.

Transmission loss results for the chamber over a 10000 rad/s frequency range are presented in Fig. 4.12. They clearly illustrate the onset of higher order modes at approximately 1500 rad/s for the three-dimensional model, indicating the failure of plane wave theory. Ensuing higher order modes dominate the remainder of the frequency range. These higher order modes appear as radial and diametral pressure distributions as indicated in Fig. 4.13; their wavenumbers $k_{m,n}$ appear in Table 4.4 as solutions of $J_m(k_{m,n}r) = 0$.

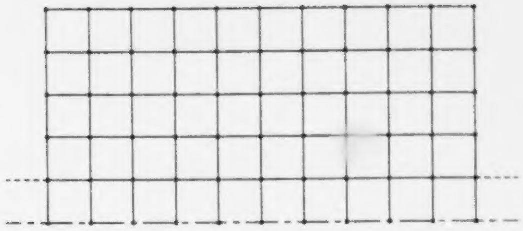

Figure 4.11: Axisymmetric Ring Element Mesh to Model Cylindrical Expansion Chamber (66 DOF)

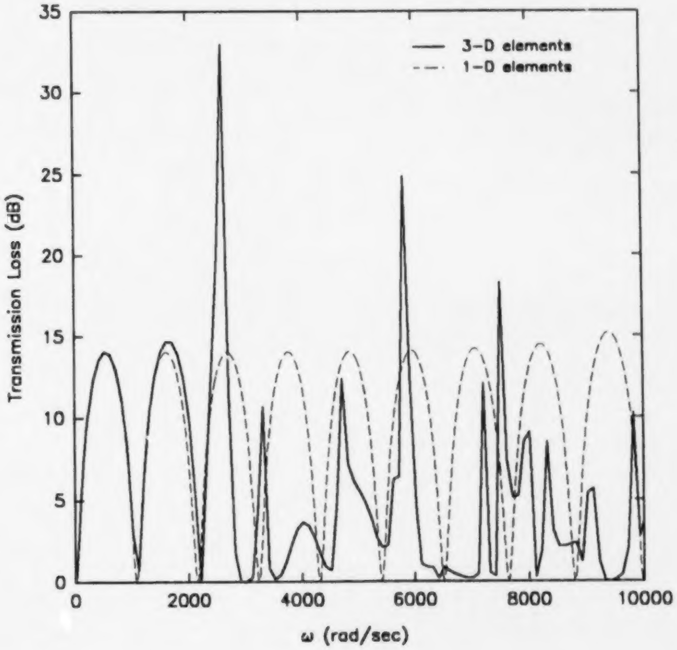

Figure 4.12: Transmission Loss Results for a Cylindrical Expansion Chamber with Expansion Ratio = 10; One and Three-Dimensional Elements

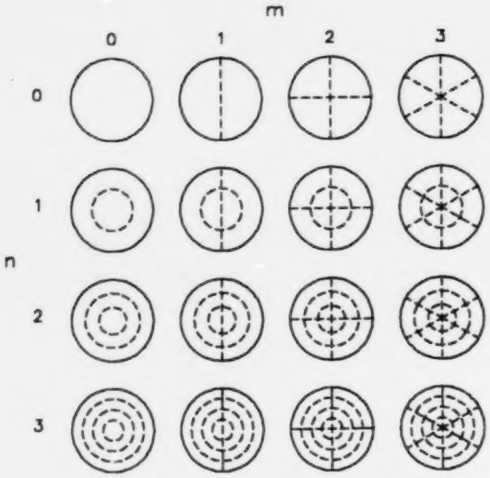

Figure 4.13: Nodal Lines for Transverse Pressure Distributions in a Circular Duct, *m* Denotes Diametral Modes, *n* Denotes Radial Modes

Table 4.4: Radial and Diametral Modes in rad/s for Expansion Chamber $r = 0.5$ m

		m			
		0	1	2	3
	0	0	1262.24	2092.30	2881.20
n	1	2627.38	3656.38	4603.06	5501.72
	2	4815.72	5858.44	6839.42	7786.10
	3	6976.62	8033.06	9034.62	10008.74

A courser mesh of axisymmetric ring elements would provide acceptable accuracies. A mesh with three elements in the radial direction rather than the five used here would provide similar results. A similar rectangular expansion chamber with expansion ratio = 10 was also modelled using 10 pipe elements and 10 HEX8 elements. In this case, the HEX8 elements were not distributed transversely, they were only assembled axially. Transmission loss results for the chamber are shown in Fig. 4.14 and indicate that a simple configuration of HEX8 elements assembled axially can be used to model plane wave effects in a duct. The difference between the two TL curves is present because the pipe element has quadratic pressure variations between the nodes while the HEX8 element only has linear pressure variations between nodes, thus the pipe element provides improved accuracy in the axial direction for similar mesh sizes. It should be noted here that the pipe element is restricted to simple one-dimensional systems where offsets, bends and junctions do not exist. Thus, chain-assembled HEX8 elements have a much greater degree of application.

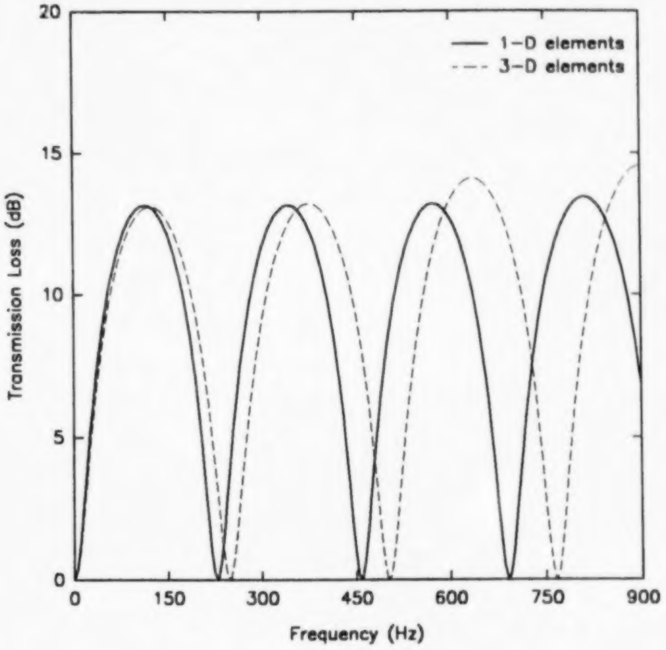

Figure 4.14: Transmission Loss Results for a Rectangular Expansion Chamber, Expansion Ratio = 10; One and Three-Dimensional Elements

4.5.1 Tapered Elements

With respect to computational efficiency, it is beneficial to try to limit the global degrees of freedom of an element mesh representing a duct. Therefore, an element mesh consisting of simply chained HEX8 elements is the desired configuration. In many duct networks, there may appear sudden area expansions, contractions or chambers. A simple HEX8 element is sufficient to model these discontinuities for low frequencies where the wavelength of the acoustic wave is much longer than the transverse dimensions of the duct and transverse wave motion in the region of the discontinuity can be assumed to be negligible.

It would then be ideal to use a single HEX8 element to model an area discontinuity. Consider the element mesh shown in Fig. 4.15, which represents a sudden area expansion and contraction in a duct. At the area discontinuities, a single HEX8 element has been deformed (flattened out) to model the sudden area expansion and contraction. Dimensions for the 0.15 m × 0.45 m × 0.75 m chamber region are given in Fig. 4.16, along with the taper length, *l*, of the deformed element. Reducing the taper length of the element effectively flattens it out. Transmission loss results are given in Fig. 4.17 for this chamber with taper lengths of 0.001 m and 0.00001 m respectively and show no discernible differences, indicating that the HEX8 element may be tapered to model area discontinuities. There are limits as to how much the element may be tapered; a taper length of zero causes interior angles within the element to be 180°, causing singularities to appear in the Jacobian matrix. The element may be tapered to a length of almost zero, within the numerical precision of the computer.

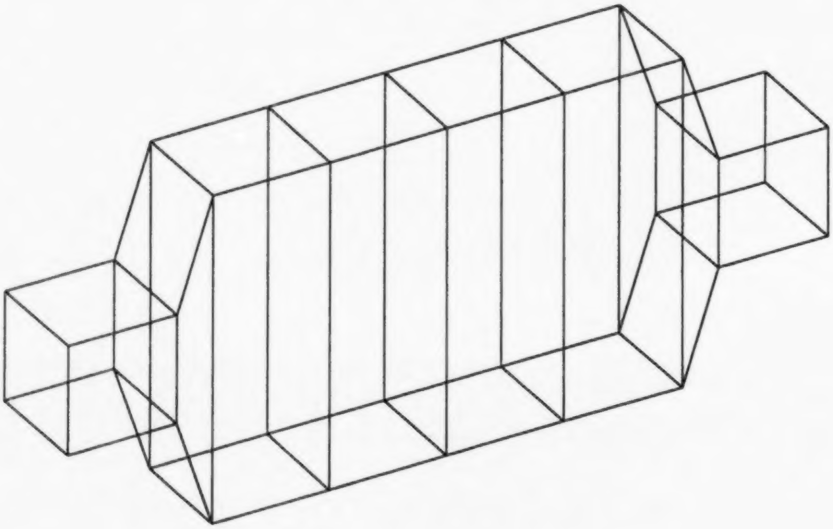

Figure 4.15: HEX8 Element Mesh Representing Sudden Area Changes in a Duct

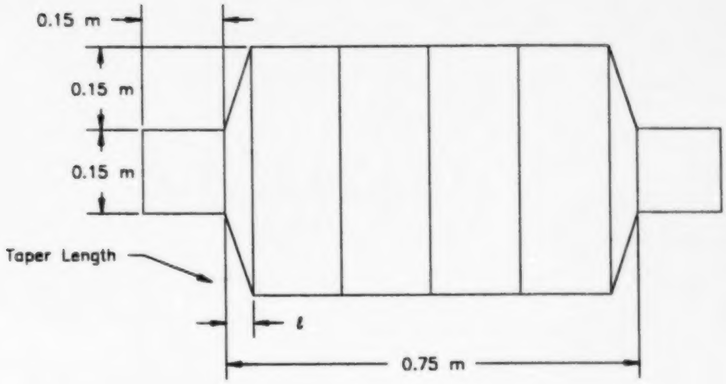

Figure 4.16: Length of a Tapered HEX8 Element

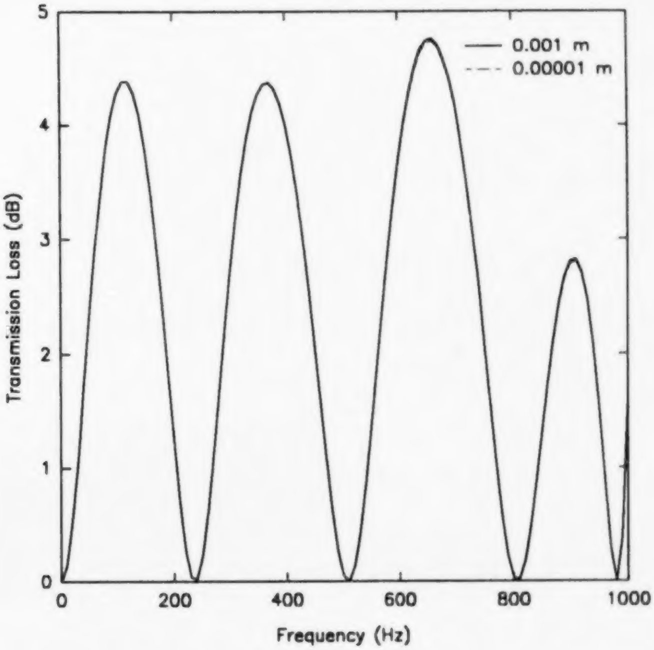

Figure 4.17: Transmission Loss Results for a Chamber with Various Taper Lengths

4.5.2 Dipole and Quadrupole Mode Propagation

In duct acoustics at low frequencies, most of the energy is transmitted with the plane wave mode or fundamental wave. As frequencies are increased, however, some of the higher order transverse modes become excited and are also propagated, and these additional modes must also be considered. Therefore, in addition to the fundamental wave travelling in the axial direction having wavefronts which are uniform across the duct section, there are waves reflecting from the duct walls as they proceed through the duct, for which the pressure distribution is not uniform across the duct [71]. In this section, the simple HEX8 element formulated earlier will be adapted to model significant higher order acoustic mode effects using a technique introduced in earlier research work [32]. Here, the method is extended to include the effects of dipole and quadrupole modes on duct sections including chambers, bends, curves and junctions. These modes are significant as they cause bending and twisting forces in duct walls at low frequencies and therefore cannot be neglected.

Each acoustic mode has a cut-off frequency and for driving frequencies above this frequency, the mode will propagate along the duct with usually very little attenuation; for driving frequencies less than the cut-off frequency, attenuation is very large and the mode will not propagate as a wave. At frequencies below the cut-off frequency of the lowest higher mode, only the plane wave mode propagates, all other modes are strongly attenuated.

If one recalls the HEX8 element shown in Fig. 4.2, the element can be said to have four pressure unknowns at each of its faces and the pressure vector at any surface can be expressed as a linear combination of four pressure distributions [32]

$$\{p\} = a\begin{Bmatrix}1\\1\\1\\1\end{Bmatrix} + b\begin{Bmatrix}-1\\1\\-1\\1\end{Bmatrix} + c\begin{Bmatrix}1\\1\\-1\\-1\end{Bmatrix} + d\begin{Bmatrix}-1\\1\\1\\-1\end{Bmatrix}$$

where a, b, c and d are constants. The first vector corresponds to the plane wave mode which has a cut-off frequency of zero. The second and third vectors correspond to dipole modes which have cut-off frequencies given by $\lambda_c = \pi/L_x$, $\lambda_c = \pi/L_y$, where L_x and L_y represent the transverse dimensions of the duct in the x and y directions as shown in Fig. 4.18. The fourth vector represents a quadrupole mode which has an exact cut-off frequency given by [32]

$$\lambda_c = \pi\sqrt{(1/L_x)^2 + (1/L_y)^2}. \qquad (4.23)$$

These modes are shown in Fig. 4.19 in a form representing their respective pressure distributions as they would appear in a duct cross-section. In a finite element configuration where HEX8 elements have been assembled axially in a duct section, only four pressure nodes are present at any point in the duct cross-section, allowing only four modes of propagation; the plane wave mode, the dipole two modes and the quadrupole mode. As such, the HEX8 element is the simplest one for modelling dipole and quadrupole mode effects in ducts, keeping with the original goals of this thesis to provide simple finite element methods for the acoustics engineer to study low frequency duct acoustics.

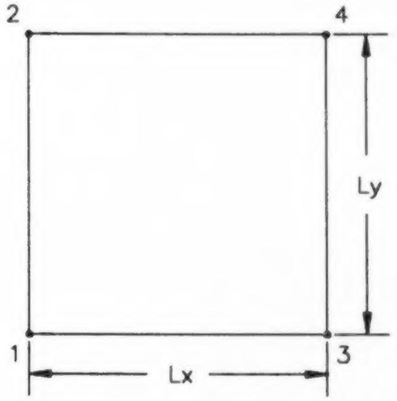

Figure 4.18: Location of Nodal Pressures for a Duct Cross-Section.

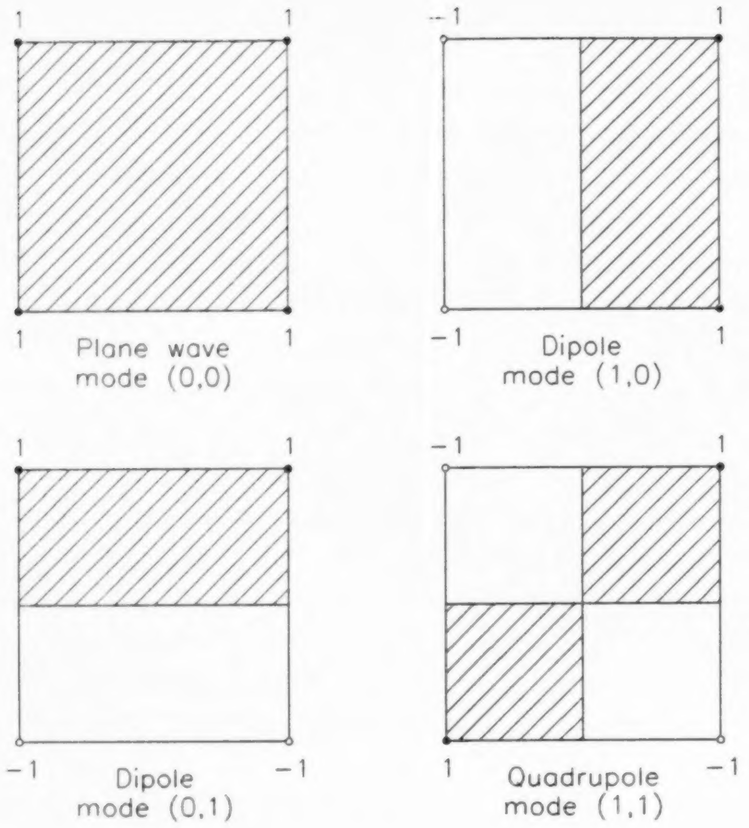

Figure 4.19: Modes of Propagation for a Rectangular Section: the Plane Wave, Dipole and Quadrupole Mode Pressure Distributions.

The higher order dipole and quadrupole modes can be considered as multipole sources (point volume velocity sources), each an array of simple sources of equal amplitudes but with equal or opposite phases. These are the relevant point multipole sources of order because aerodynamic sound can be described in terms of equivalent source distributions of dipole and quadrupole order [64].

The dipole sources shown in Fig. 4.19 can be considered as two neighbouring point volume velocity sources (monopoles) of equivalent magnitude but opposite sign (phase). As such, the dipole source consists of a positive point monopole, $+Q_0e^{j\omega t}$, and negative point monopole, $-Q_0e^{j\omega t}$. These two neighbouring point sources of equal magnitude but opposite sign combine to apply an external force to the acoustic medium. This external force is significant as it causes bending effects in duct sections. Therefore, the response of the dipole source can be used to predict the response of the duct to a force distribution. This is important for engine-duct acoustics where compressor and turbine sources may often be modelled by force distributions [39].

In similar fashion, the quadrupole source shown in Fig. 4.19 may be described as an array of four equivalent point monopoles, two positive and two negative so that there is zero total monopole moment. Alternatively, a quadrupole may be regarded as two neighbouring, opposed dipoles. The interactions of the opposing dipoles apply an external stress to the acoustic medium, subsequently causing twisting effects in the duct walls.

To demonstrate the accuracy of the linear HEX8 element for modelling transverse modes such as the dipole and quadrupole modes, the eigenvalues were calculated for a rigid walled straight duct section with dimensions 0.5 m × 0.67 m × 1.0 m. Calculations were performed with 100 HEX8 elements assembled in the axial direction of the duct section so that the system is equivalent to having 404 degrees of freedom. The eigenvalues for a duct section with these dimensions have been calculated before [32], but only the first five eigenvalues were presented and the results for the quadrupole mode were not included. Eigenvalue results presented here include the quadrupole mode calculations. As was the case in Section 4.4, the exact modes have the form $\cos(l\pi x/l_x)\cos(m\pi y/l_y)\cos(n\pi z/l_z)$, where l_x, l_y and l_z are duct dimensions.

There is an effective fine mesh in the axial direction of the duct and thus the axial modes are predicted quite accurately as shown in Table 4.5; the (0,0,1) mode is exact to three decimal places while the (0,0,2) mode has an error of 0.02%. The cut-off frequencies of the dipole modes, (1,0,0) and (0,1,0), and the quadrupole mode (1,1,0) predicted by this mesh are about 10.27% higher than exact values due to the linear approximation in the transverse direction. Modes which include an axial component such as the (1,0,1) mode are predicted much more accurately than the purely transverse modes by this type of mesh due to the fact that this is an axial mesh with many elements assembled in that direction.

If dipole and quadrupole mode effects in duct acoustics are to be analysed using finite elements, the element mesh representing the duct must be constrained with these modes to produce higher order mode propagation in the duct. The constraints may be applied by pre and post multiplying the global finite element matrices by a Boolean transfer matrix $[B]$, which is composed of ones and zeros. This has the effect of reducing the number of degrees of freedom in the system.

Table 4.5: Exact and Calculated Eigenvalues for a Straight Duct Section

Mode Number l,m,n	Exact Eigenvalues, λ_c	100 HEX8 Elements	% Error
0,0,1	3.142	3.142	0.00
1,0,0	4.689	5.170	10.27
1,0,1	5.644	6.050	7.19
0,0,2	6.283	6.284	0.02
0,1,0	6.283	6.928	10.27
0,1,1	7.025	7.607	8.29
1,0,2	7.840	8.138	3.80
1,1,0	7.840	8.645	10.27

Consider the simple straight duct network consisting of two HEX8 elements and 12 DOF shown in Fig. 4.20. The duct inlet is at the 1, 2, 3 and 4 nodes while the duct outlet is at the 9, 10, 11 and 12 nodes. If plane wave propagation exists in this duct , the pressure distribution is uniform across the duct cross-section (refer to Fig. 4.19) and may be represented by components of equal magnitude and phase at the pressure nodes. Therefore, this equivalent pressure distribution may be represented by values of unity at the pressure nodes.

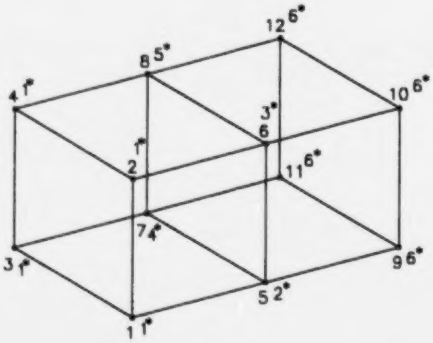

Figure 4.20: Straight Duct Section; Unconstrained and Constrained (*) Pressure Nodes

These constraints may be applied to the global element mesh by the following procedure. The pressure nodes are renumbered using $*$ notation as shown in Fig. 4.20 and the global pressure vector can be rewritten as

$$\{p\}=[B]\{p^*\} \tag{4.24}$$

$$\begin{Bmatrix} p_1 \\ p_2 \\ p_3 \\ p_4 \\ p_5 \\ p_6 \\ p_7 \\ p_8 \\ p_9 \\ p_{10} \\ p_{11} \\ p_{12} \end{Bmatrix} = \begin{bmatrix} 1 & 0 & 0 & 0 & 0 & 0 \\ 1 & 0 & 0 & 0 & 0 & 0 \\ 1 & 0 & 0 & 0 & 0 & 0 \\ 1 & 0 & 0 & 0 & 0 & 0 \\ 0 & 1 & 0 & 0 & 0 & 0 \\ 0 & 0 & 1 & 0 & 0 & 0 \\ 0 & 0 & 0 & 1 & 0 & 0 \\ 0 & 0 & 0 & 0 & 1 & 0 \\ 0 & 0 & 0 & 0 & 0 & 1 \\ 0 & 0 & 0 & 0 & 0 & 1 \\ 0 & 0 & 0 & 0 & 0 & 1 \\ 0 & 0 & 0 & 0 & 0 & 1 \end{bmatrix} \begin{Bmatrix} p_1^* \\ p_2^* \\ p_3^* \\ p_4^* \\ p_5^* \\ p_6^* \end{Bmatrix}$$

where $[B]$ is the Boolean transfer matrix. Notice that in the first and sixth columns of matrix $[B]$, a series of ones has been placed representing plane wave propagation at the inlet and outlet nodes of the duct section. Using this procedure, the number of DOF for this element mesh has been reduced from 12 to 6 DOF to allow for the plane wave constraints applied to the duct. Similarly, the Boolean transfer matrix may be applied to the global finite element equations in the following form

$$\left([B]^T\left([S]-k^2[P]\right)[B]\right)\{p^*\}=\rho\omega^2\{Q^*\} \tag{4.25}$$

where the superscript T denotes a matrix transpose.

Dipole and quadrupole constraints can be applied to a duct using the same procedure. If the aforementioned duct section was constrained with the (0,1) dipole mode shown in Fig. 4.19, its global pressure vector would be written in this form.

$$\begin{Bmatrix} p_1 \\ p_2 \\ p_3 \\ p_4 \\ p_5 \\ p_6 \\ p_7 \\ p_8 \\ p_9 \\ p_{10} \\ p_{11} \\ p_{12} \end{Bmatrix} = \begin{bmatrix} 1 & 0 & 0 & 0 & 0 & 0 \\ 1 & 0 & 0 & 0 & 0 & 0 \\ -1 & 0 & 0 & 0 & 0 & 0 \\ -1 & 0 & 0 & 0 & 0 & 0 \\ 0 & 1 & 0 & 0 & 0 & 0 \\ 0 & 0 & 1 & 0 & 0 & 0 \\ 0 & 0 & 0 & 1 & 0 & 0 \\ 0 & 0 & 0 & 0 & 1 & 0 \\ 0 & 0 & 0 & 0 & 0 & 1 \\ 0 & 0 & 0 & 0 & 0 & 1 \\ 0 & 0 & 0 & 0 & 0 & -1 \\ 0 & 0 & 0 & 0 & 0 & -1 \end{bmatrix} \begin{Bmatrix} p_1^* \\ p_2^* \\ p_3^* \\ p_4^* \\ p_5^* \\ p_6^* \end{Bmatrix}$$

Notice the presence of positive and negative values in columns one and six of the Boolean transfer matrix. These represent the opposing point monopoles which produce the dipole at the duct inlet and outlet. A quadrupole mode may be produced using this method as well.

It has been demonstrated that a simple finite element mesh consisting of axially connected HEX8 elements may be used to calculate cut-off frequencies of dipole and quadrupole modes with an accuracy of 10.27%. In the following sections, the propagation of these modes is examined to illustrate the effect of cut-off frequencies on the attenuation of these modes. Various geometries are considered including chambers, duct bends, curved sections and junctions. The results show that higher mode effects may be analysed for very complicated geometries using this method.

4.5.2.1 Chambers

In Chapter 2 of this thesis, transmission loss results for various expansion chambers were presented to demonstrate the effectiveness of the pipe element in modelling acoustic ducts with plane wave propagation. In this section, the simple HEX8 element is implemented to model dipole and quadrupole mode propagation in expansion chambers with the results also being presented in terms of transmission loss. Since the T.L. of the chamber is calculated over a frequency range, the effects of cut-off frequency on a mode's propagation is clearly illustrated by the T.L. calculations.

A model consisting of 12 HEX8 elements representing an expansion chamber with dimensions 0.13 m × 0.30 m × 0.50 m is shown in Fig. 4.21. The elements have been assembled only in the axial direction and the model was assumed to be part of an infinite transmission line (ρc termination). A dipole mode (1,0) was prescribed at the inlet and outlet of the chamber to analyse its propagation and attenuation; prescription of the dipole mode at the outlet was necessary to avoid noise in the T.L. calculations. T.L. values are presented in Fig. 4.22 for this system. For these particular chamber dimensions, the (1,0) mode has an exact cut-off frequency, $f_c = c/(2l_x)$, of 1391.23 Hz where the speed of sound is 343 m/s. The cut-off frequency calculated by the finite element model is 1455 Hz, which is approximately 10.27% greater than the exact frequency. The extremely high T.L. values which appear before the cut-off frequency indicate that the mode is being strongly attenuated and is not propagating in this frequency range. In this frequency region, only the fundamental mode (plane wave) can propagate. For driving frequencies greater than the cut-off frequency, the mode is attenuated significantly less and will propagate as a wave, causing bending forces in the chamber.

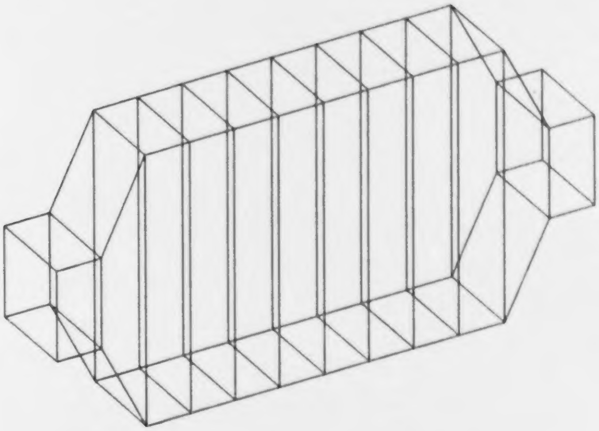

Figure 4.21: Finite Element Model of Expansion Chamber; 12 HEX8 Elements

The other dipole mode (0,1) and the quadrupole mode (1,1) were also prescribed to the chamber to determine their attenuation and propagation. T.L. values for the (0,1) mode are presented in Fig. 4.23. An exact cut-off frequency, $f_c = c/(2l_y)$, of 571.67 Hz was calculated for these dimensions. The cut-off frequency as determined from the finite element calculations was 630 Hz, which is 10.27% greater than the exact frequency as expected. High T.L. values appearing before the cut-off frequency indicate strong

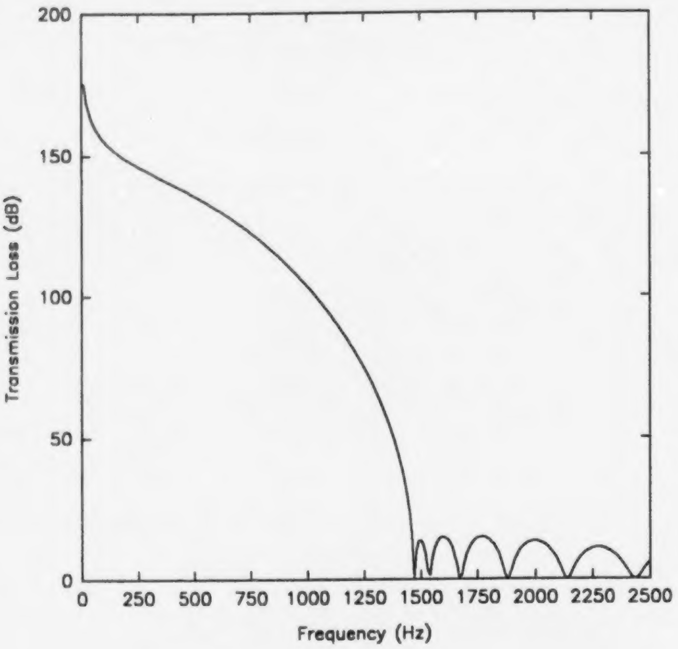

Figure 4.22: T.L. Values for an Expansion Chamber; Dipole Mode (1,0) Propagation

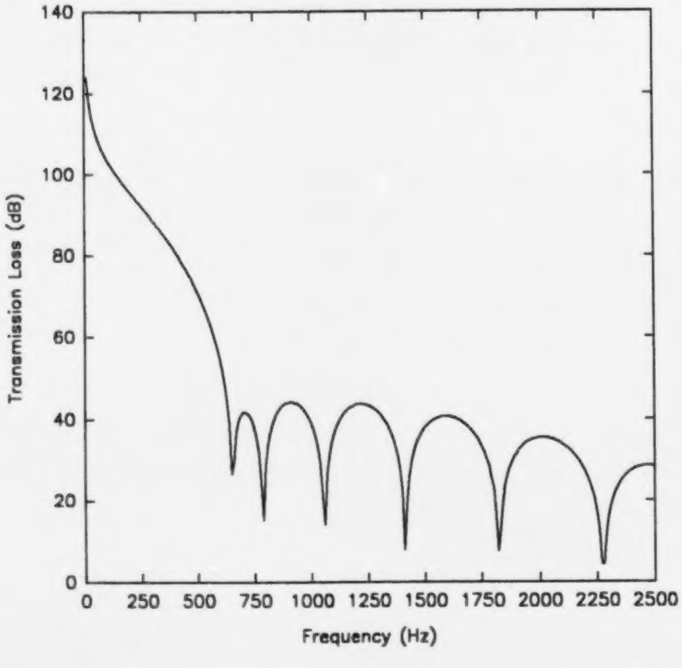

Figure 4.23: T.L. Values of an Expansion Chamber; Dipole Mode (0,1) Propagation

attenuation and the mode is not propagating in this frequency region. Above the cut-off frequency, the mode propagates causing bending forces in the chamber.

Lastly, a quadrupole mode (1,1) was prescribed to the chamber with the subsequent T.L. calculations appearing in Fig. 4.24. The exact cut-off frequency for the (1,1) mode for this system is 1437.77 Hz as calculated by the formulae, $f_c = c/2((1/l_x)^2 + (1/l_y)^2)^{1/2}$. The cut-off frequency had a value of 1585 Hz as determined from the finite element calculations; this was 10.27% greater than the exact cut-off frequency. Attenuation of the mode is significant below the cut-off frequency as indicated by the extremely high T.L. values. The mode propagates for driving frequencies greater than the cut-off frequency, causing torsional stresses in the chamber.

It should be noted that the extremely high T.L. values presented here represent pressures which are well beyond the range of any instrument. As such, the high T.L. values are purely academic, they only indicate that the mode is being attenuated and is not propagating.

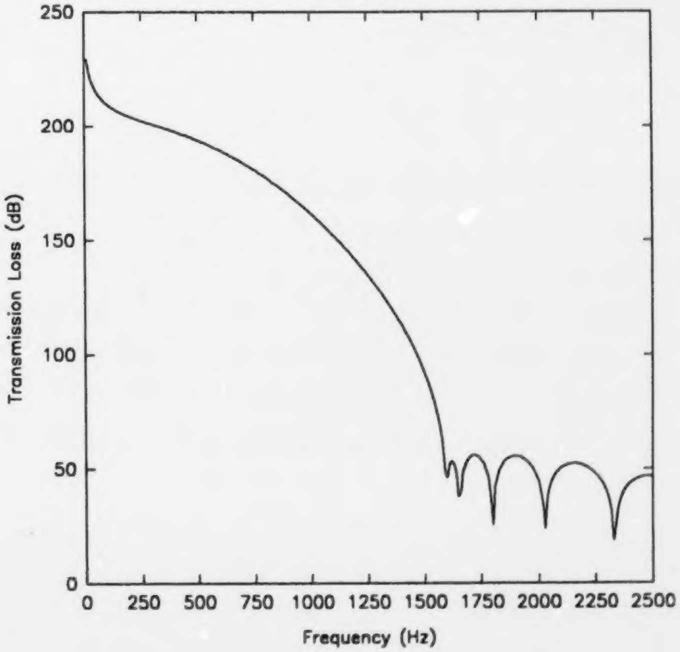

Figure 4.24: T.L. Values of an Expansion Chamber; Quadrupole Mode (1,1) Propagation

Curious results appear when the element used to model the inlet and outlet of the chamber has cubic dimensions. Peaks representing sidebranch resonator effects show up in the T.L. curves in the region where there is strong mode attenuation. These peaks are a purely academic phenomenon as they appear in the frequency region of high T.L. (below cut-off frequency). Their appearance seems to be determined entirely by the dimensions of the element used to model the chamber inlet and outlet.

Consider the 14 HEX8 element mesh representing an expansion chamber with dimensions of 0.15 m × 0.45 m × 0.75 m as shown in Fig. 4.25. The element used to model the chamber inlet and outlet has a length of 0.15 m.

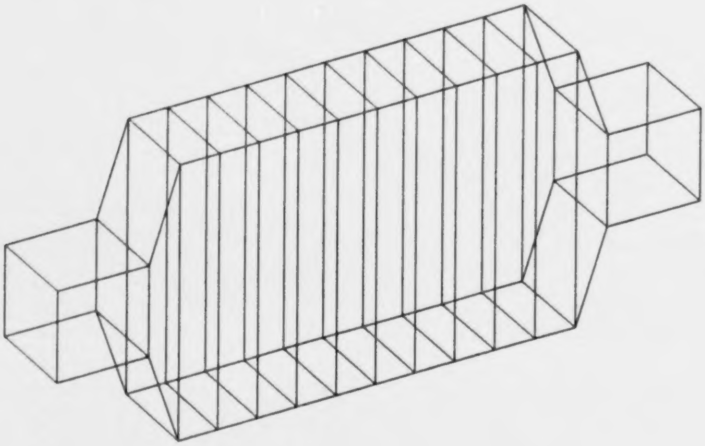

Figure 4.25: Finite Element Model of an Expansion Chamber; 14 HEX8 Elements

Dipole mode (1,0) propagation was considered for this chamber with the T.L. values presented in Fig. 4.26. This mode has an exact cut-off frequency of 1143.33 Hz and a cut-off frequency of 1261 Hz as calculated by the finite element model, which is 10.27% greater than the exact value. Mode attenuation and propagation for this system are as described earlier. At a frequency of 888 Hz, a strong sidebranch resonator effect appears, dramatically increasing mode attenuation. The mechanism responsible for this attenuation increase has not been determined, but is interesting from an academic point of view. In practice, attenuation is high in the frequency region below the mode cut-off frequency irregardless of this sidebranch resonator effect. Increasing the width of model to 0.20 m has the effect of moving the location of the sidebranch resonator peak to a lower frequency of 320 Hz as shown in Fig. 4.27; the change in dimension lowered the cut-off frequency to a value of 946 Hz as well.

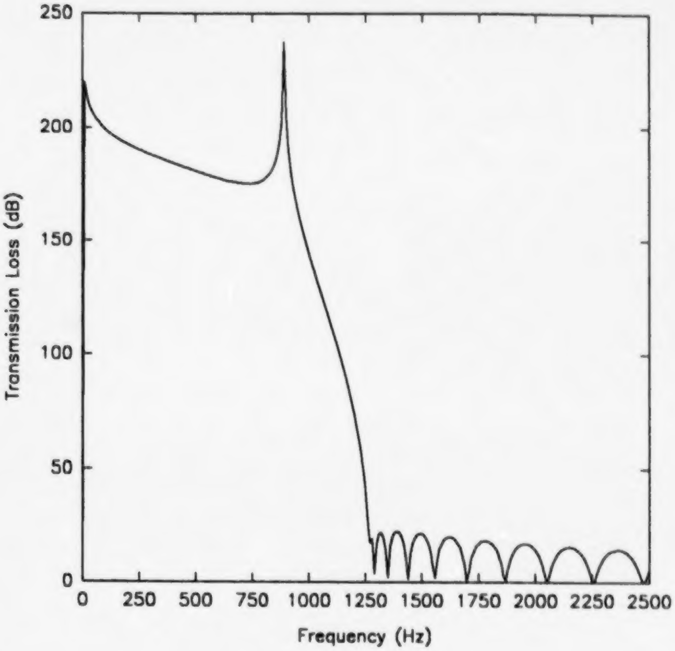

Figure 4.26: T.L. Values for an Expansion Chamber; Dipole Mode (1,0) Propagation

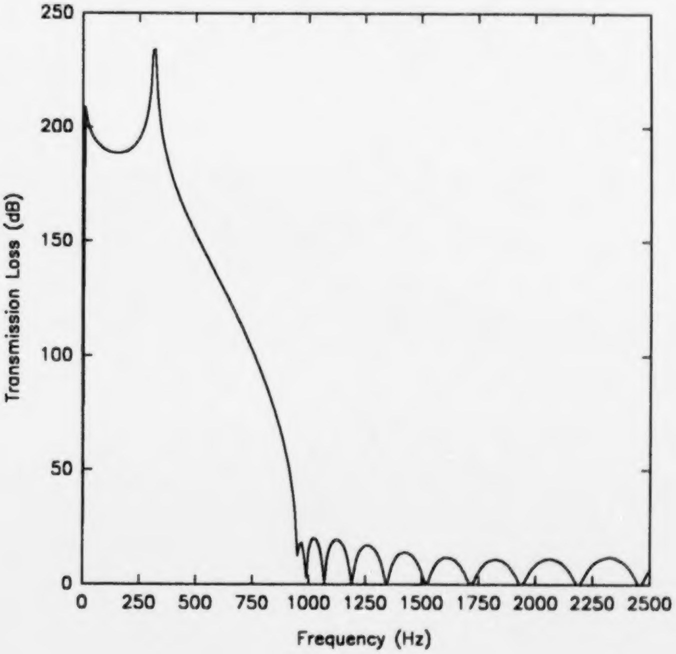

Figure 4.27: T.L. Values of an Expansion Chamber; Dipole Mode (1,0) Propagation

A similar situation occurs when propagation of the dipole mode (0,1) is considered. A large sidebranch resonator peak appears at a frequency of 888 Hz as shown in Fig. 4.28. This is significant as it appears at a frequency greater than the cut-off frequency of 420 Hz.

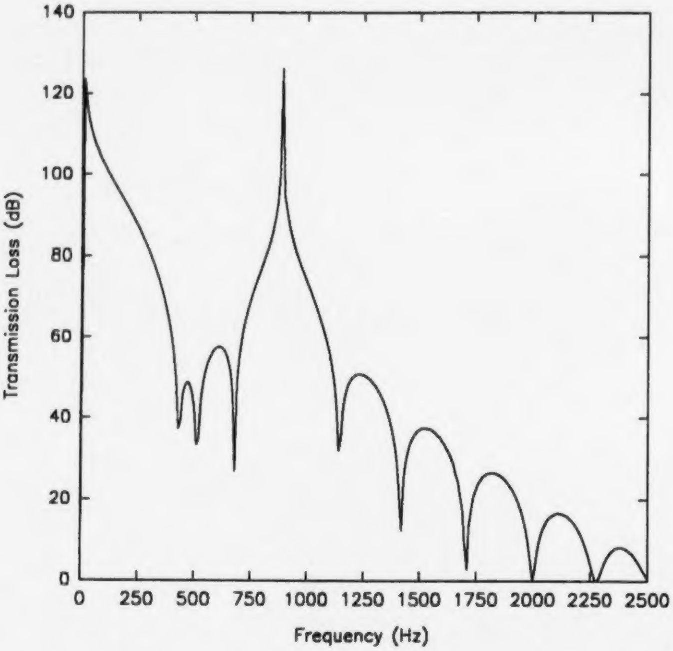

Figure 4.28: T.L. Values of an Expansion Chamber; Dipole Mode (0,1) Propagation

Increasing the chamber inlet height to 0.20 m has the effect of moving back the peak to a frequency of 320 Hz as shown in Fig. 4.29. The cut-off frequency for the chamber has not changed as the dimensions of the chamber itself have not changed, only the inlet/outlet dimensions have been altered. Clearly, the dimensions of the chamber have no effect on the appearance of these peaks in the T.L. curves, only the dimensions of the element modelling the inlet/outlet are relevant. These peaks did not appear in the response curves of the chamber presented earlier. For these cases, the length of the element modelling the inlet/outlet regions of the chamber was not the same as any of the cross-sectional dimensions of the element. This appears to be necessary for these sidebranch peaks to appear in the chamber response curves.

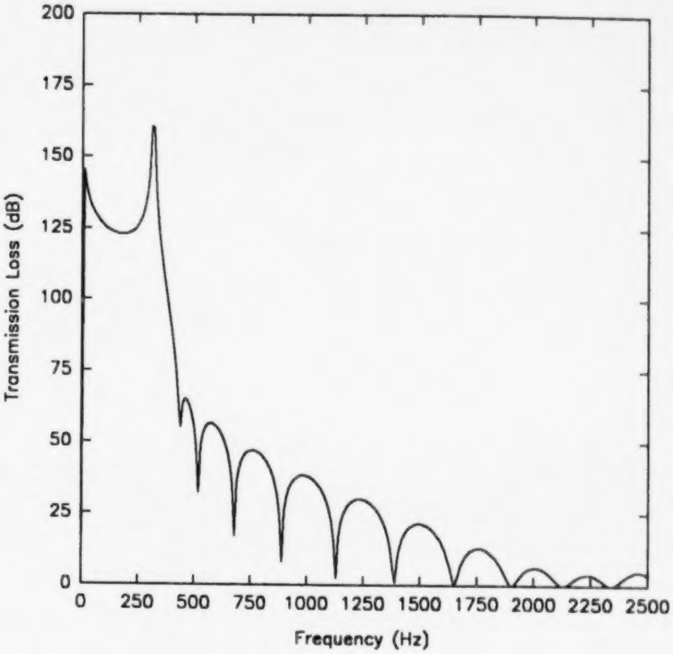

Figure 4.29: T.L. Values of an Expansion Chamber; Dipole Mode (0,1) Propagation

The propagation of the quadrupole mode (1,1) for this chamber was also examined and the large sidebranch resonator peaks again were present in the response curves. When the chamber inlet/outlet cross-section had dimensions 0.15 m × 0.15 m, a sidebranch peak appeared at a frequency of 1540 Hz as shown in Fig. 4.30. The width of the model was increased to 0.20 m and the peak appeared at 1300 Hz as shown in Fig. 4.31. The cut-off frequencies for the quadrupole mode were 1329 Hz and 1035 Hz respectively for these situations.

In some cases, the large sidebranch resonator peaks appear in the frequency region beyond the cut-off frequency and this is important as they attenuate the mode in this region, which is not as one would expect. The appearance of these peaks in the frequency region below the cut-off frequency has no practical influence on the propagation of the mode in this region as it is being strongly attenuated. More research in this area is necessary to determine the forcing mechanism responsible for the sidebranch resonator peaks appearing in the response curves for these chambers. These peaks have not appeared for any of the other geometries considered in this thesis.

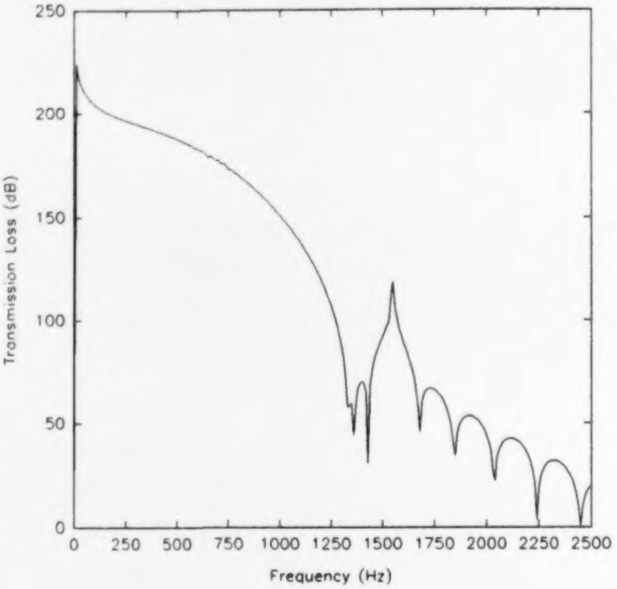

Figure 4.30: T.L. Values of an Expansion Chamber; Quadrupole Mode (1,1) Propagation

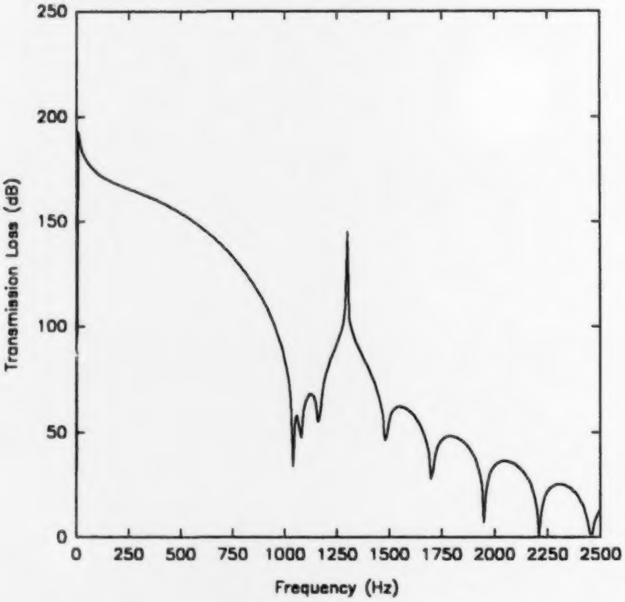

Figure 4.31: T.L. Values of an Expansion Chamber; Quadrupole Mode (1,1) Propagation

4.5.2.2 Duct Bends

The propagation of sound waves in duct bends has been studied extensively by previous researchers [15, 16, 34, 35, 76, 77] so a detailed discussion of this topic is not presented in this section. The propagation of plane waves, dipole and quadrupole modes in 90° duct bends will be considered in this section using the methods described in Section 4.5.2.1.

A simple finite element mesh consisting of 36 HEX8 elements assembled along the axial direction of a 90° duct bend is shown in Figure 4.32.

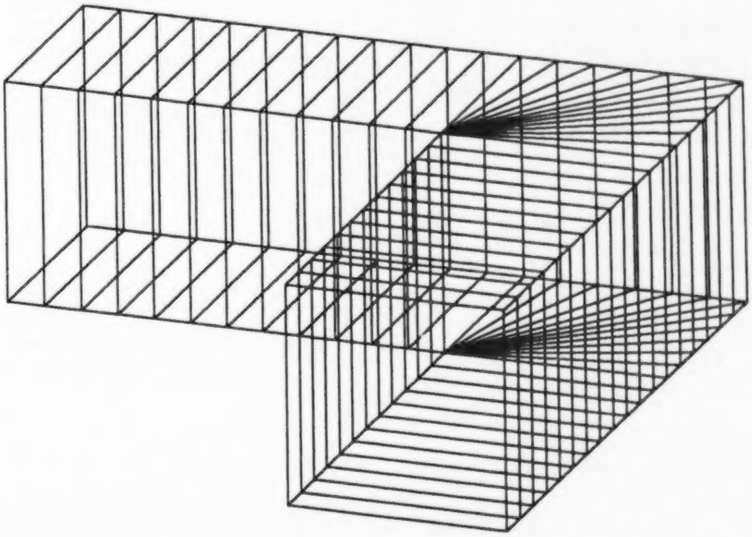

Figure 4.32: Finite Element Model of a 90° Duct Bend; 36 HEX8 Elements

The duct has cross-sectional dimensions of 0.15 m × 0.15 m and was assumed to be part of an infinite transmission line (ρc termination). Plane wave propagation was first considered to demonstrate that simply connected HEX8 elements can be used to successfully model the low frequency response of a complicated geometry such as a duct bend. Transmission loss values for plane wave propagation are presented in Fig. 4.33 and the results are similar to those presented by [61]. It may be assumed that this type of element mesh provides acceptable modelling of the low frequency acoustics of a duct bend.

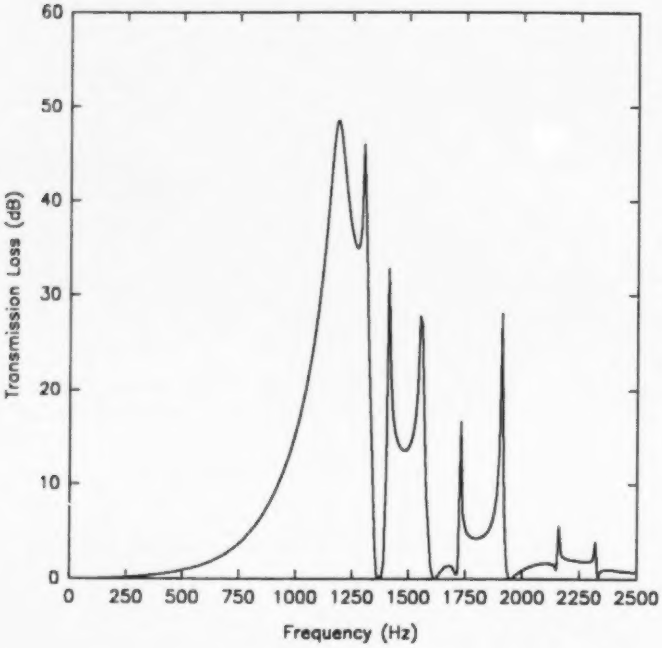

Figure 4.33: T.L. Values for a 90° Duct Bend; Plane Wave Propagation

Propagation and attenuation of the two dipole modes, (1,0) and (0,1), was also considered for this duct bend with the results shown in Figures 4.34 and 4.35. The exact cut-off frequency for this duct is 1143.33 Hz for a speed of sound of 343 m/s. The cut-off frequency as calculated by the finite element model was 1260 Hz which is 10.27% greater than the exact frequency as expected. Attenuation of the mode is strong below the cut-off frequency as indicated by the high transmission loss values in this frequency region. Here, the mode does not propagate as a wave. For frequencies above the cut-off frequency, attenuation of the mode is not very strong and it propagates along the duct bend, causing bending forces in the duct.

Quadrupole mode (1,1) propagation and attenuation was also examined for this duct section with the T.L. values being presented in Fig. 4.36. The calculated cut-off frequency is 1783 Hz which is 10.27% greater than the exact cut-off frequency of 1616.92 Hz. Attenuation is strong below the cut-off frequency and the mode does not propagate in this region; above the cut-off frequency, the mode propagates causing torsional stresses in the duct. The method presented in this chapter of prescribing dipole and quadrupole modes in ducts to study the propagation and attenuation of these modes has proven successful for complicated geometries such as duct bends.

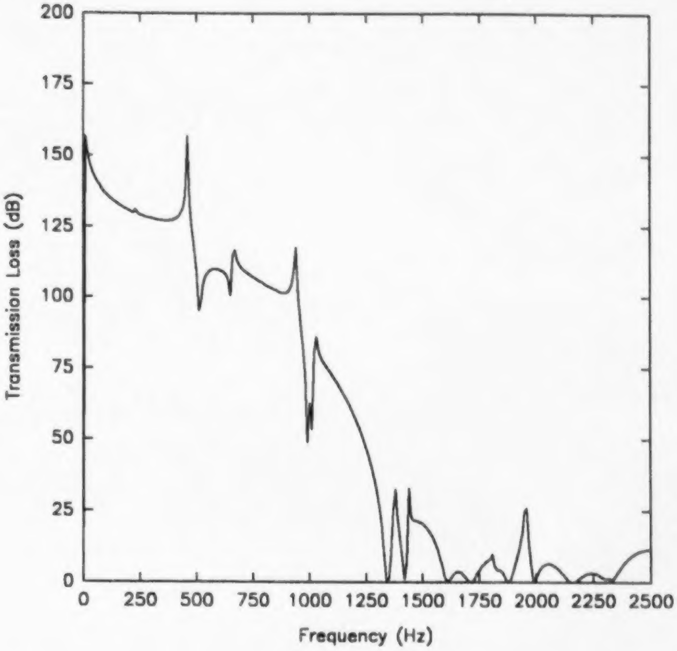

Figure 4.34: T.L. Values for a 90° Duct Bend; Dipole Mode (1,0) Propagation

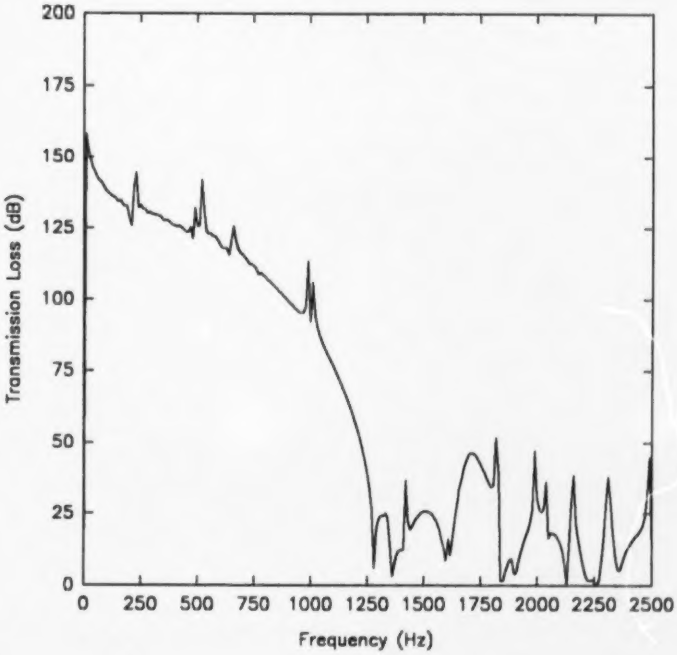

Figure 4.35: T.L. Values for a 90° Duct Bend; Dipole Mode (0,1) Propagation

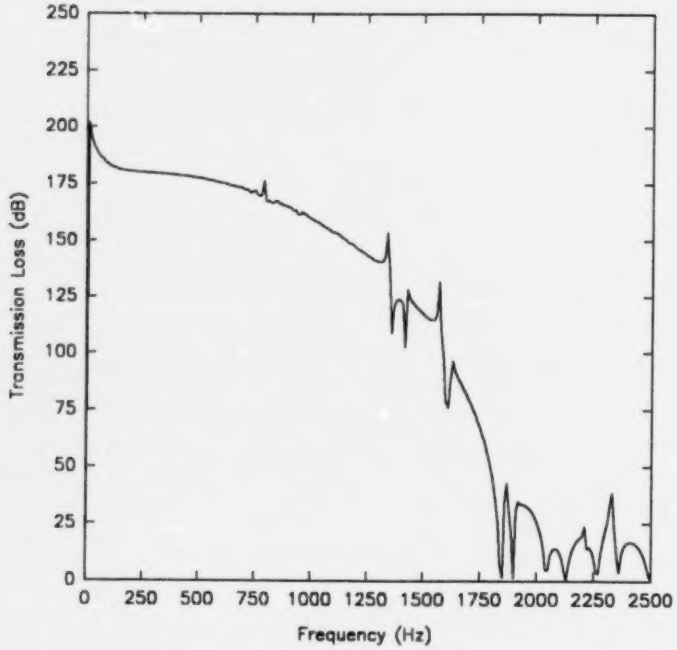

Figure 4.36: T.L. Values for a 90° Duct Bend; Quadrupole Mode (1,1) Propagation

4.5.2.3 Curved Duct Sections

As was the case with sound propagation in duct bends, the propagation of sound waves in curved duct sections has been extensively studied [19, 34, 56, 77, 86, 87, 88]. The propagation of the plane wave mode, dipole and quadrupole modes in curved waveguides is examined here using simple element meshes consisting of chain-assembled HEX8 elements based on the methods described in Section 4.5.2.1.

A 90° curved duct section with cross-section dimensions 0.15 m × 0.15 m and radius of curvature $R_1 = 0.30$ m and $R_2 = 0.45$ m was considered. A simple chain-assembled finite element mesh representing this duct section consisted of 36 HEX8 elements with 148 DOF as shown in Fig. 4.37. Again, the duct was assumed to be part of an infinite transmission line so that there would be no reflections back from the end of the duct section.

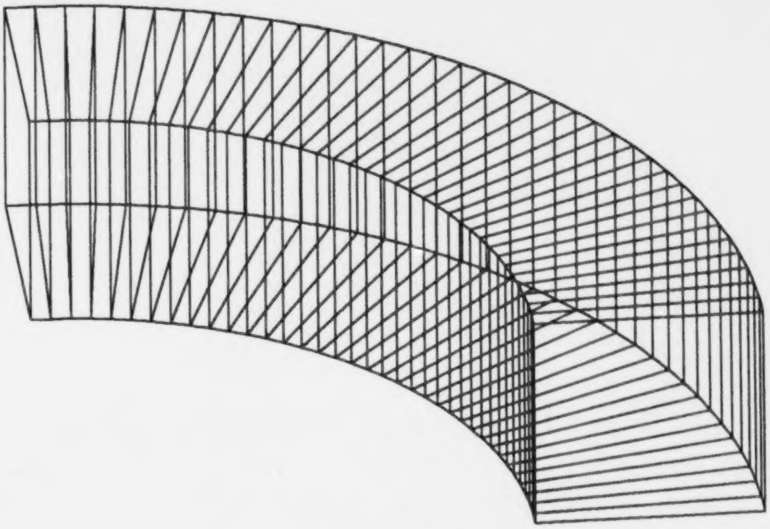

Figure 4.37: Finite Element Model of a 90° Curved Duct Section; $R_1 = 0.30$ m, $R_2 = 0.45$ m; 36 HEX8 Elements

Transmission loss values for plane wave propagation are presented in Fig. 4.38, clearly showing that there is minimal attenuation of the plane wave for the low frequencies considered here. This result is not unexpected as long waves in a narrow curved waveguide propagate as if the waveguide were straight [84, 86]. As the frequencies of interest increase, radial reflections from the curved section decrease the amplitude of the transmitted wave causing increased attenuation of the wave.

Dipole mode (1,0), (0,1) propagation and attenuation was examined for the curved duct section using the element mesh described above with T.L. results being presented in Figures 4.39 and 4.40. The calculated cut-off frequency for this duct section was 1260 Hz which is 10.27% greater than the exact cut-off frequency of 1143.33 Hz. There is strong attenuation of the modes below the cut-off frequency and the mode will not propagate as a wave. Above the cut-off frequency, there is much less attenuation and the modes propagate, causing bending stresses in the walls of the duct section. Sidebranch resonator effects appear in the response curve of the (1,0) mode below the cut-off frequency. The forcing mechanism responsible for this is not fully understood and the results are presented here as an interesting phenomena only. Further research could be undertaken to determine the source of the sidebranch resonator effects but this was considered beyond the original scope of the thesis.

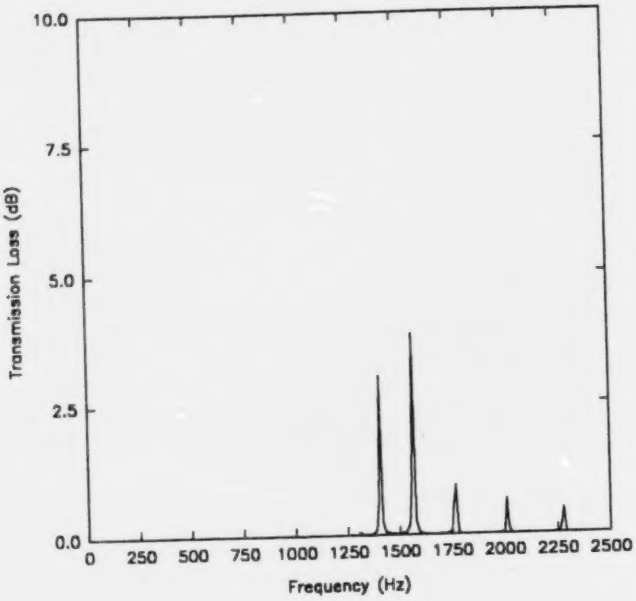

Figure 4.38: T.L. Values for a 90° Curved Duct Section; Plane Wave Propagation

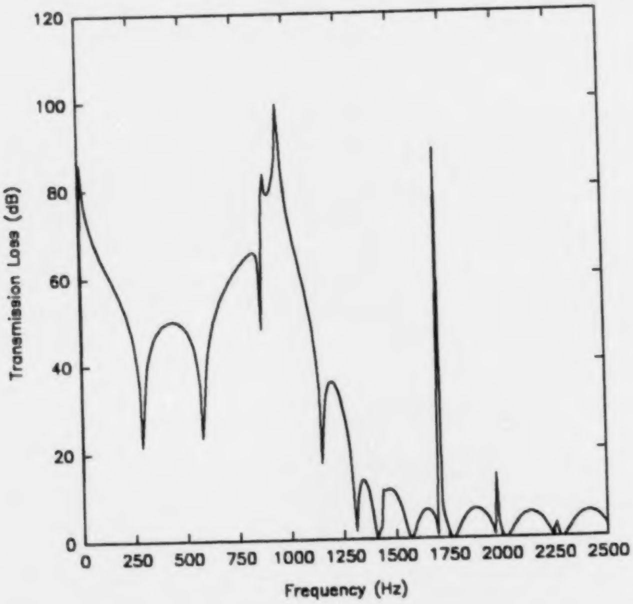

Figure 4.39: T.L. Values for a 90° Curved Duct Section; Dipole Mode (1,0) Propagation

Propagation and attenuation of the quadrupole mode (1,1) was examined for the curved duct section with T.L. values presented in Fig. 4.41. As with the duct bend considered in the previous section, the calculated cut-off frequency of the mode was 1783 Hz. This is exactly 10.27% greater than the exact cut-off frequency of 1616.92 Hz as expected. There is strong attenuation of the mode below the cut-off frequency and the mode does not propagate in this frequency region. For frequencies greater than cut-off, the mode propagates causing torsional stresses in the walls of the duct. A large sidebranch resonator peak appeared in the T.L. curve in the frequency range below the cut-off frequency. This peak is of academic interest only as it appears in the region of strong mode attenuation. The method of chain-assembling HEX8 elements together to form simple element meshes to study dipole and quadrupole mode propagation in curved duct sections provides expected accuracies when calculating the cut-off frequencies of these modes.

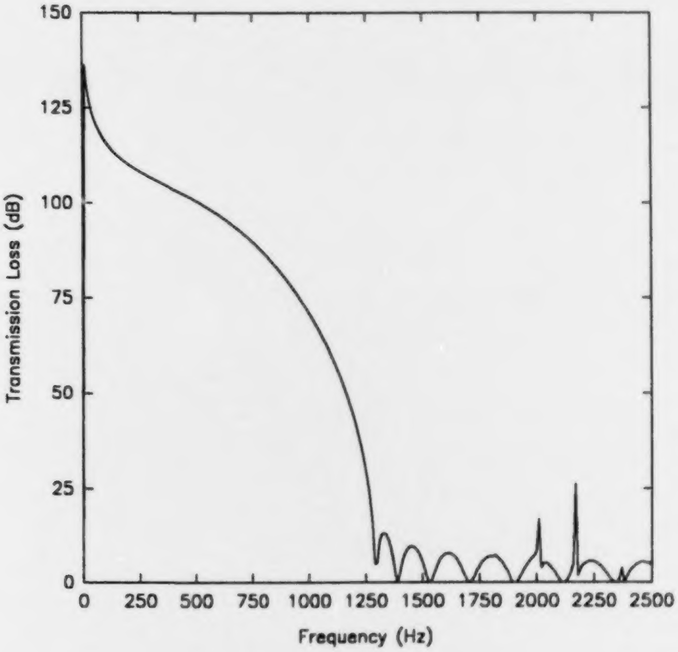

Figure 4.40: T.L. Values for a 90° Curved Duct Section; Dipole Mode (0,1) Propagation

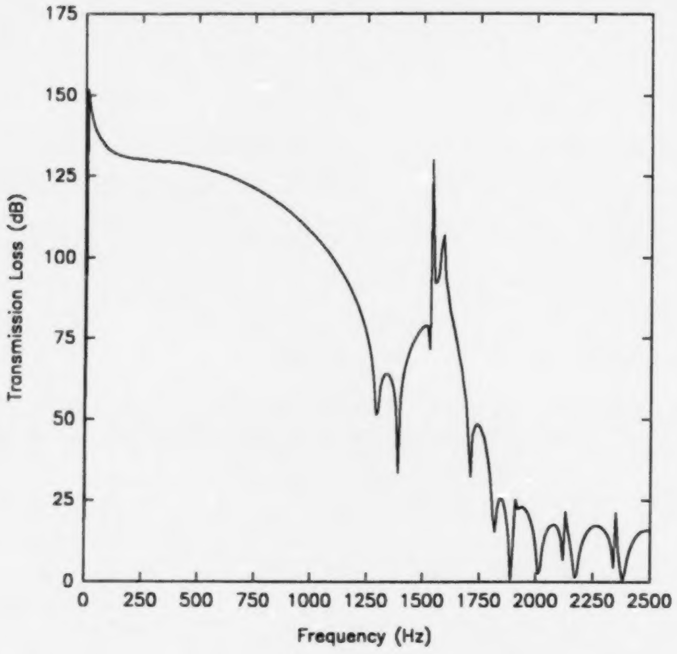

Figure 4.41: T.L. Values for a 90° Curved Duct Section; Quadrupole Mode (1,1) Propagation

4.5.2.4 Junctions

There has been a relatively small amount of research done on sound propagation through duct junctions where three or more sections join at a common intersection. The remainder of this chapter demonstrates that simple HEX8 elements chain-assembled together may be used to approximate the junction problem where anechoically terminated duct sections meet at a junction.

It is necessary to use three-dimensional elements when modelling complex duct junctions. The pipe element introduced in Chapter 2 is able to approximate duct junctions on a very limited scale. With that element, the acoustic pressure at the junction is treated as a single nodal quantity and cannot take into account reflections and diffractions present at the junction. As such, sidebranches with various offset angles are not accurately modelled. Using the HEX8 element, sidebranches of any offset angle may be modelled and the reflections and diffractions present at the junction may be accurately represented. It was found that a single HEX8 element was usually sufficient to model the junction; for the low frequencies considered here, results were identical to those obtained with a fine element mesh in the junction area.

Plane wave, dipole and quadrupole mode propagation was considered for a duct junction with 45° sidebranch as shown in Fig. 4.42. The finite element model consisted of 38 HEX8 elements with 150 DOF; cross-sectional dimensions were 0.15 m × 0.15 m. A mesh with fewer elements in the straight duct sections would be acceptable as well.

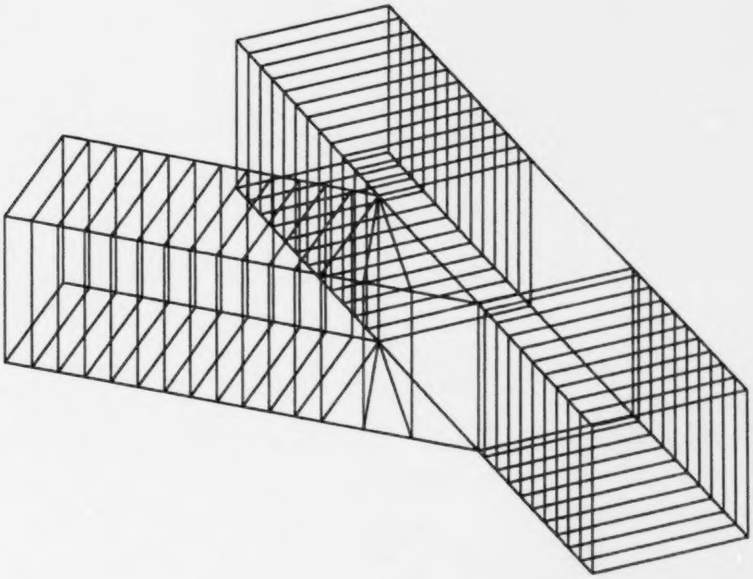

Figure 4.42: Finite Element Model of Junction with 45° Sidebranch; 38 HEX8 Elements

Transmission loss values for plane wave propagation through the junction is shown in Fig. 4.43, indicating very little attenuation for the low frequencies considered. Response curves for dipole mode propagation and quadrupole mode propagation are presented in Figures 4.44-4.46. The cut-off frequencies for the junction are identical to those for the duct bend and curved section considered earlier. More complicated junctions could be considered but the purpose of this section was only to introduce the procedure for examining dipole and quadrupole mode propagation using simple HEX8 elements.

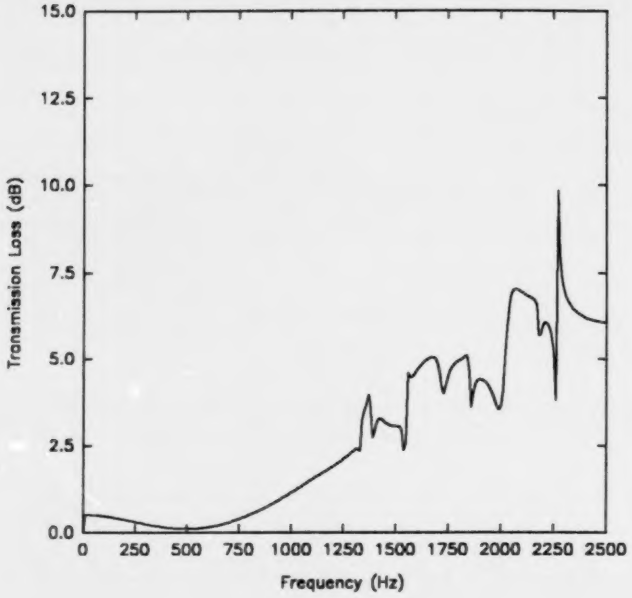

Figure 4.43: T.L. Values for Junction with 45° Sidebranch; Plane Wave Propagation

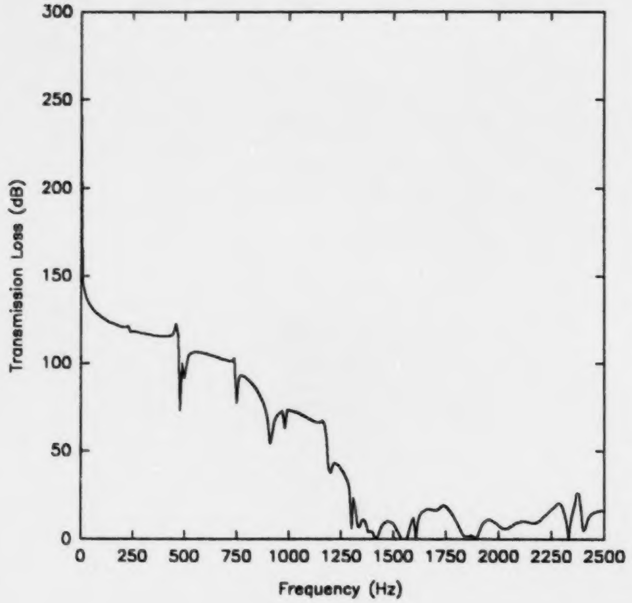

Figure 4.44: T.L. Values for Junction with 45° Sidebranch; Dipole Mode (1,0) Propagation

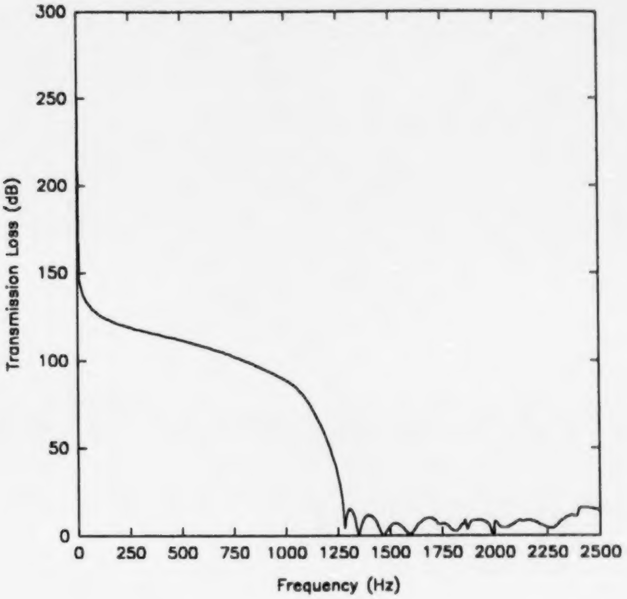

Figure 4.45: T.L. Values for Junction with 45° Sidebranch; Dipole Mode (0,1) Propagation

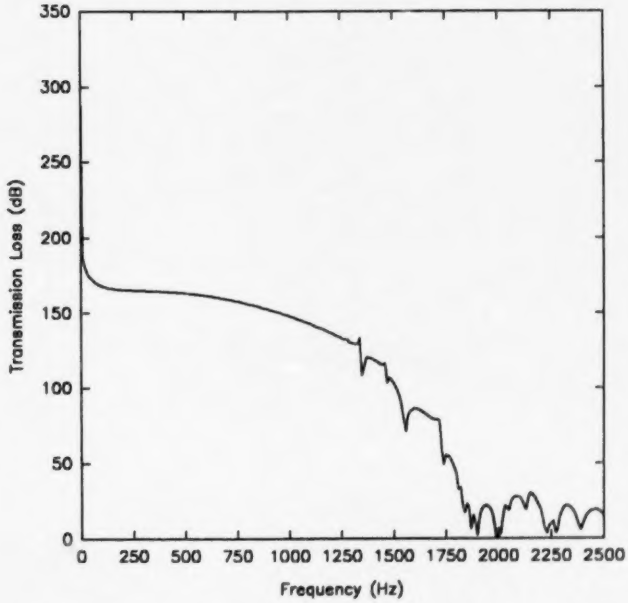

Figure 4.46: T.L. Values for Junction with 45° Sidebranch; Quadrupole Mode (1,1) Propagation

Chapter 5

A Three-Dimensional HEX8 Finite Element with Flexible Boundaries

5.1 Introduction

If fluid motion normal to a surface is possible, there will be wave motion in that surface. For certain cases, various parts of the surface are not strongly coupled together and the motion normal to the surface, of any one portion of the surface, is dependent only on the acoustic pressure which is incident on that surface portion. It is independent of the motion of any other part of the surface [71]. For such cases, the surface is said to be *locally reacting*. The three-dimensional HEX8 acoustic element discussed in Chapter 4 will be modified here to allow suitable approximation of locally reacting surfaces, this being an extension of previous research [26] where hexahedral elements were used to study the effects of boundary flexibility on normal modes and natural frequencies. The locally reacting assumption follows the basic goal of this thesis; to provide simple finite element methods for the acoustics engineer concerned with duct acoustics.

When surface reaction at one point depends on the motion of neighbouring points, so that the reaction is different for various incident waves, the surface is *extended reacting*. Surfaces such as ones which are membrane-like, ones with laminated structure, ones where waves penetrate into the surface material and surfaces where waves propagate parallel to the surface may all be considered extended reacting. Theoretical treatment of an extended reacting surface involves considering surface motion as being governed by the unsteady plate equation. This must be coupled with equations governing the acoustics of the duct in the finite element model. This is not a trivial undertaking.

The interaction between sound waves and a locally reacting surface is defined by specifying its acoustic impedance as a function of frequency. Simplifying assumptions are usually made by workers in acoustics concerning surface impedance, usually that the surface impedance be either mass, stiffness or damping controlled. Damping is usually very slight at low frequencies and only mass controlled or stiffness controlled surfaces were considered here.

A linear isoparametric two-dimensional finite element with four pressure nodes is formulated using Galerkin's method of weighted residuals to model surface motion and is coupled to the HEX8 element. This procedure does not add any new degrees of freedom to the system as the HEX8 element has only four pressure nodes on any of its surfaces. The effects of mass or stiffness controlled surface motion on wave propagation are considered by determining the eigenvalues of a closed tube with flexible side walls and rigid ends. Comparison is made with the flexible walled pipe element developed in Chapter 3.

5.2 3-D Hexahedral Element with Flexible Walls

The HEX8 element presented in Chapter 4 is modified here to allow for not only rigid duct walls but locally reacting flexible walls as well and is shown in Fig. 5.1. Essentially, acoustic wave motion will be approximated using the three-dimensional HEX8 element but the wall motion of any of the surfaces of the element will be approximated using linear isoparametric two-dimensional surface elements. In this way, any combination of rigid and locally reacting flexible duct walls may be modelled using a combination of simple linear elements while not increasing the number of degrees of freedom in the system.

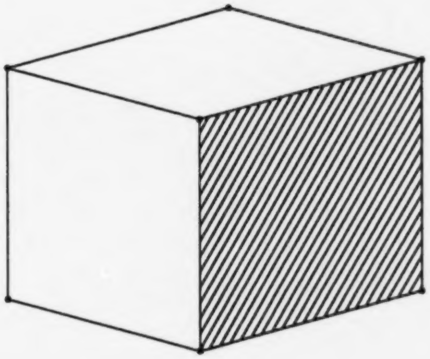

Figure 5.1: HEX8 Element with Flexible Walls

The three-dimensional Helmholtz equation governs the acoustic wave motion in any duct

$$\frac{\partial^2 p}{\partial x^2}+\frac{\partial^2 p}{\partial y^2}+\frac{\partial^2 p}{\partial z^2}+k^2 p=0, \tag{5.1}$$

together with the boundary conditions, $\nabla p=0$ on any rigid surface, $\nabla p=j\rho\omega v$ on any flexible surface. Here, p is the acoustic pressure, v is the velocity of the moving boundary, ρ is the density of the acoustic medium, ω is the angular frequency and the gradient operator has the usual form, $\nabla=\partial/\partial x+\partial/\partial y+\partial/\partial z$. The governing finite element equations used to approximate the Helmholtz equation with corresponding rigid and flexible walled boundary conditions are formulated using Galerkin's method of weighted residuals as presented in Chapter 4. With respect to efficiency, only the formulation of the element equations is presented here; the linear polynomial, transformation matrix and Jacobian for the HEX8 element have been given previously in Section 4.3.

Galerkin's method of weighted residuals is used to formulate the finite element approximations to the Helmholtz equation. The residual, R, may be written as

$$R=\left\{F_x''\right\}^T\left[T^{-1}\right]\left\{p_e\right\}+\left\{F_y''\right\}^T\left[T^{-1}\right]\left\{p_e\right\}+\left\{F_z''\right\}^T\left[T^{-1}\right]\left\{p_e\right\}+k^2\{F\}^T\left[T^{-1}\right]\left\{p_e\right\} \tag{5.2}$$

where the vector $\left\{F_x''\right\}$ denotes $\partial^2 F/\partial x^2$, $\left\{F_y''\right\}$ denotes $\partial^2 F/\partial y^2$ and $\left\{F_z''\right\}$ denotes $\partial^2 F/\partial z^2$. As before, Galerkin's equation has the form

$$\iiint_V \{f\}\,R\,dx\,dy\,dz=0 \tag{5.3}$$

where

$$\{f\}=\left[T^{-1}\right]^T\{F\}.$$

Substitution of the residual into Galerkin's equation results in the following equation.

$$\iiint_V\Big(\left[T^{-1}\right]^T\{F\}\left\{F_x''\right\}^T\left[T^{-1}\right]+\left[T^{-1}\right]^T\{F\}\left\{F_y''\right\}^T\left[T^{-1}\right]+\left[T^{-1}\right]^T\{F\}\left\{F_z''\right\}^T\left[T^{-1}\right]+$$

$$+k^2\left[T^{-1}\right]^T\{F\}\{F\}^T\left[T^{-1}\right]\Big)\left\{p_e\right\}dx\,dy\,dz=0$$

In this form, the matrices in the first three terms are null and non-symmetric and there are no surface terms representing the wall motion of the element. Greens first theorem

$$\int_V \{F\}\{F_n''\}^T dV = \int_S \{F\}\left\{\frac{\partial F}{\partial \bar{n}}\right\} dS - \int_V \{F_n'\}\{F_n'\}^T dV$$

can be used to make the matrices symmetric and also introduce the surface terms into the equation,

$$\begin{aligned} &\iiint_V \Big(\left[T^{-1}\right]^T \{F_x'\}\{F_x'\}^T \left[T^{-1}\right] + \left[T^{-1}\right]^T \{F_y'\}\{F_y'\}^T \left[T^{-1}\right] + \left[T^{-1}\right]^T \{F_z'\}\{F_z'\}^T \left[T^{-1}\right] - \\ &-k^2 \left[T^{-1}\right]^T \{F\}\{F\}^T \left[T^{-1}\right]\Big)\{p_e\}\, dx\, dy\, dz + j\rho\omega \int_S (pv)\, dS = 0 \end{aligned} \tag{5.4}$$

with the previously mentioned rigid and flexible wall boundary conditions.

The surface terms of Eq. (5.4) need to be modelled with some finite element other than the three-dimensional HEX8 element. A linear isoparametric two-dimensional element with four pressure nodes was chosen to model the motion of any of the surfaces of the HEX8 element and will be referred to as the *surface element*. This is a logical choice as any particular surface of the isoparametric HEX8 element has only four pressure nodes. The surface element is deformable to any geometry, has linear pressure variations between its four node points and is shown in Fig. 5.2 in its local (*r*, *s*) and global (*x*, *y*) coordinate systems. Similar to the HEX8 element, the surface element remains a fixed square in its local coordinate system with coordinates varying between −1 and +1. The element may be deformed to almost any geometry in its global coordinates, the restriction being that all interior angles be less than 180° to avoid singularities in the Jacobian matrix. All integrations for the surface element are performed numerically between ±1 limits, conforming with the Gauss quadrature technique.

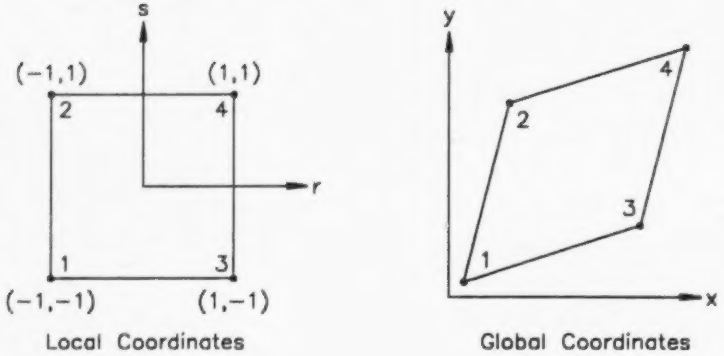

Figure 5.2: Linear Isoparametric Surface Element in Local and Global Coordinate Systems

The linear pressure distribution between the nodes on any surface of the surface element may be represented by a simple polynomial

$$p = a_1 + a_2 r + a_3 s + a_4 rs \tag{5.5}$$

which can be expressed in matrix form as

$$p = \{F\}_S^T \{\alpha\} \tag{5.6}$$

where the subscript S denotes the surface element and

$$\{F\}_S^T = \{1 \quad r \quad s \quad rs\}$$

$$\{\alpha\} = \begin{Bmatrix} a_1 \\ a_2 \\ a_3 \\ a_4 \end{Bmatrix}$$

The pressure is expressed in terms of generalised coordinates $a_1 \cdots a_4$ which govern the contribution of each of the terms of the simple polynomial. They are related to the acoustic pressures at the individual node points of the element by inserting boundary values for each nodal pressure. Insertion of the boundary values for each nodal pressure results in a system of four equations and four unknowns which can be expressed in matrix form as

$$\{p_e\}_S = [T]_S\{\alpha\} \text{ or } \{\alpha\} = \left[T^{-1}\right]_S \{p_e\}_S$$

where the transformation matrix for the surface element is

$$[T]_S = \begin{bmatrix} 1 & -1 & -1 & 1 \\ 1 & -1 & 1 & -1 \\ 1 & 1 & -1 & -1 \\ 1 & 1 & 1 & 1 \end{bmatrix}$$

The pressure at any point (r, s) within the element may now be written in terms of the nodal pressures

$$p = \{F\}_S^T \left[T^{-1}\right]_S \{p_e\}_S. \tag{5.7}$$

For an isoparametric acoustic finite element, the variation in geometry is governed by the same polynomials which govern the variation in pressure, allowing the element to be distorted to any geometry. The regular geometry in the local coordinate system is transformed to a distorted geometry in the global system; the relationship between local and global coordinates can be determined by applying rules of partial differentiation

$$\frac{\partial}{\partial r} = \frac{\partial x}{\partial r}\frac{\partial}{\partial x} + \frac{\partial y}{\partial r}\frac{\partial}{\partial y}$$

$$\frac{\partial}{\partial s} = \frac{\partial x}{\partial s}\frac{\partial}{\partial x} + \frac{\partial y}{\partial s}\frac{\partial}{\partial y}.$$

Following the steps presented in Section 4.3, the relationship between global coordinate derivatives and local coordinate derivatives is written as

$$\begin{Bmatrix} \dfrac{\partial}{\partial x} \\ \dfrac{\partial}{\partial y} \end{Bmatrix} = \left[J^{-1}\right]_S \begin{Bmatrix} \dfrac{\partial}{\partial r} \\ \dfrac{\partial}{\partial s} \end{Bmatrix}$$

where $[J]_S$ denotes the Jacobian matrix for the surface element. Transformation of the coordinate systems is given by, $dx\,dy = \|J\|_S\,dr\,ds$, where $\|J\|_S$ denotes the absolute value of the determinant of the surface Jacobian matrix. Using Galerkin's method of weighted residuals, the equations representing the surface element may be introduced into Eq. (5.4). Subsequently, the respective Jacobians for the HEX8 and surface elements can also be introduced into Eq. (5.4) to transform the equations to local coordinates.

$$\begin{aligned}
&\int_{-1}^{+1}\int_{-1}^{+1}\int_{-1}^{+1}\left([T^{-1}]^T[G]^T[J^{-1}]^T[J^{-1}][G][T^{-1}]\|J\|\right)\{p_e\}\,dr\,ds\,dt - \\
&-k^2\int_{-1}^{+1}\int_{-1}^{+1}\int_{-1}^{+1}\left([T^{-1}]^T\{F\}\{F\}^T[T^{-1}]\|J\|\right)\{p_e\}\,dr\,ds\,dt + \\
&+j\rho\omega v\int_{-1}^{+1}\int_{-1}^{+1}\left([T^{-1}]_S^T\{F\}_S\{F\}_S^T[T^{-1}]_S\|J\|_S\right)\{p_e\}_S\,dr\,ds = 0
\end{aligned}$$

If the relationship, $v = p / Z_w$ (Z_w being the wall impedance), is substituted for the velocity of the moving surface, the above equation may be rewritten in terms of the wall impedance

$$\begin{aligned}
&\int_{-1}^{+1}\int_{-1}^{+1}\int_{-1}^{+1}\left([T^{-1}]^T[G]^T[J^{-1}]^T[J^{-1}][G][T^{-1}]\|J\|\right)\{p_e\}\,dr\,ds\,dt - \\
&-k^2\int_{-1}^{+1}\int_{-1}^{+1}\int_{-1}^{+1}\left([T^{-1}]^T\{F\}\{F\}^T[T^{-1}]\|J\|\right)\{p_e\}\,dr\,ds\,dt + \qquad , \\
&+j\frac{\rho\omega}{Z_w}\int_{-1}^{+1}\int_{-1}^{+1}\left([T^{-1}]_S^T\{F\}_S\{F\}_S^T[T^{-1}]_S\|J\|_S\right)\{p_e\}_S\,dr\,ds = 0
\end{aligned} \tag{5.8}$$

or in more compact form, it may be written as

$$\left(\left([S] - k^2[P]\right) + j\frac{\rho\omega}{Z_w}[A]\right)\{p\} = \{0\} \tag{5.9}$$

which is the approximate finite element equation of motion for an acoustic system with locally reacting flexible walls [26]. This equation is only suitable for undamped systems where there is no energy dissipation; this was not a significant handicap for this work as for most low frequency acoustic problems the damping is slight. As usual, Eq. (5.8) may be separated into the square symmetric 8×8 kinetic $[S]$ and potential $[P]$ energy matrices respectively. As well, the surface term is represented by the square symmetric 4×4 matrix $[A]$.

$$[S] = \int_{-1}^{+1}\int_{-1}^{+1}\int_{-1}^{+1}\left(\left[T^{-1}\right]^T [G]^T \left[J^{-1}\right]^T \left[J^{-1}\right][G]\left[T^{-1}\right]\|J\|\right)\{p_e\}\,dr\,ds\,dt \tag{5.10}$$

$$[P] = \int_{-1}^{+1}\int_{-1}^{+1}\int_{-1}^{+1}\left(\left[T^{-1}\right]^T \{F\}\{F\}^T \left[T^{-1}\right]\|J\|\right)\{p_e\}\,dr\,ds\,dt \tag{5.11}$$

$$[A] = \int_{-1}^{+1}\int_{-1}^{+1}\left(\left[T^{-1}\right]_S^T \{F\}_S \{F\}_S^T \left[T^{-1}\right]_S \|J\|_S\right)\{p_e\}_S\,dr\,ds \tag{5.12}$$

The global kinetic and potential energy matrices are assembled in the usual way; the surface elements are assembled based on the nodal configuration of the global system of HEX8 elements. As such, the global surface element matrix will have the same number of degrees of freedom as the global kinetic and potential energy matrices, irregardless of which surfaces are considered flexible and independent of the number of surface elements in the element mesh; this procedure does not increase the number of degrees of freedom of the system.

The selected values for the acoustic wall impedance, Z_w, were purely hypothetical and were chosen only to demonstrate the effects of mass or stiffness-controlled locally reacting flexible walls. These particular impedances to not have any specific references to the properties of a specific material. Consider the case where the wall motion is mass controlled. The velocity of the moving surface can be written as [26]

$$v = \frac{jp}{\omega m_w} \tag{5.13}$$

where m_w is the generalised wall mass. Making use of the relationship $v = p/Z_w$, Eq. (5.13) can be written in terms of the wall impedance

$$Z_w = \frac{\omega m_w}{j}. \tag{5.14}$$

Substituting the mass controlled wall impedance into Eq. (5.9), the approximate equation of motion becomes

$$\left(\left([S]-\frac{\rho}{m_w}[A]\right)-k^2[P]\right)\{p\}=\{0\}. \tag{5.15}$$

It would appear as though the mass controlled terms are subtracted from the kinetic energy matrix. Actually, the globally assembled coefficients of $[A]$ are negative, thus the mass controlled terms are added to the kinetic energy matrix. This has the effect of increasing the natural frequencies of the system.

Alternatively, wall motion may be stiffness controlled. Wall surface velocity is represented by [26]

$$v=-\frac{j\omega p}{c^2 k_w} \tag{5.16}$$

where k_w is the generalised wall stiffness term. Again, Eq. (5.16) can be written in terms of the wall impedance

$$Z_w=-\frac{c^2 k}{j\omega}. \tag{5.17}$$

This result is now substituted into Eq. (5.9) and the approximate equation of motion now becomes

$$\left([S]-k^2\left([P]-\frac{\rho}{k_w}[A]\right)\right)\{p\}=\{0\}. \tag{5.18}$$

The globally assembled coefficients of $[A]$ are negative, therefore the stiffness controlled terms are added to the potential energy matrix. This has the effect of decreasing the natural frequencies of the system. Examination of Eqs. (5.15) and (5.18) shows that if the generalised wall mass or generalised wall stiffness terms are increased indefinitely, the terms added to the kinetic and potential energy matrices approach zero, corresponding to the limiting rigid wall condition.

The HEX8 element is assembled using the method described in Section 4.3.1. The surface element is assembled for any non-rigid surface using the nodal connectivity information of the HEX8 element. Mass or stiffness controlled terms added to the global kinetic and potential energy matrices have the same degrees of freedom. Continuity and convergence conditions are both satisfied for the coupled HEX8-surface element by the arguments presented in Section 4.3.2.

5.3 Element Testing

The effects of a flexible boundary on the frequencies of a closed straight duct section with flexible side walls and rigid ends are demonstrated by considering the wall motion to be either mass or stiffness controlled; eigenvalue results are compared with the rigid case and with results obtained for a similar tube using the flexible walled pipe element. The results presented here are entirely numerical in nature as no experimentally determined natural frequencies exist in the literature for ducts with locally reacting surfaces.

5.3.1 Eigenvalue Models

Finite element models consisting of 80 HEX8 elements with 324 DOF were chain assembled to represent a closed straight duct section with flexible side walls and stationary medium as shown in Fig. 5.3. The shaded areas represented the non-rigid surfaces. The duct section was unit length with cross-section dimensions 0.1 m × 0.1 m.

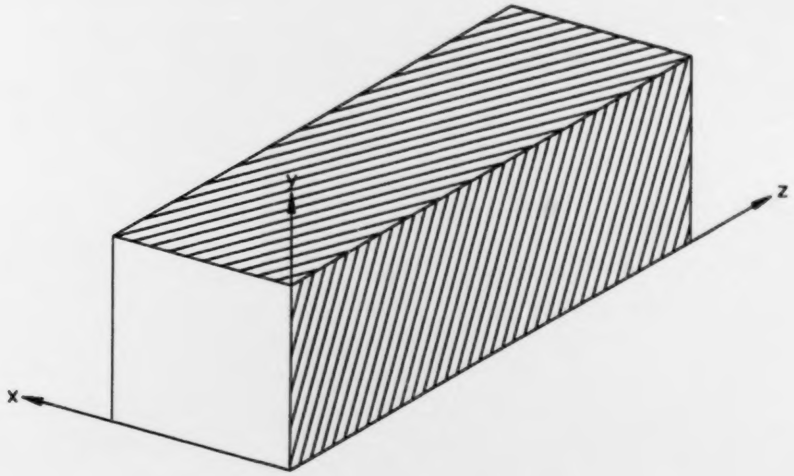

Figure 5.3: Closed Straight Duct Section with Flexible Side Walls and Rigid Ends

For the case where the flexible walls are mass-controlled, eigenvalue results are presented in Table 5.1. These results demonstrate that a mass controlled flexible boundary increases the natural frequencies of a system. The eigenvalues converge from above to the rigid walled case as the generalised mass term is increased. For the case where m_w = 10000, the limiting condition has almost been reached and the side walls are very nearly rigid; the eigenvalues are nearly identical to the rigid walled case. Results for wall masses m_w = 1 and m_w = 10 display the expected characteristics where the natural frequencies are increased by the mass controlled walls, increasing as the generalised wall mass decreases. This may be summarised by stating that the motion of the mass controlled walls is out of phase with the acoustic pressure, pushing the waves along at a quicker pace than they would travel in free space.

When the flexible walls are stiffness controlled, eigenvalue results are presented in Table 5.2. Clearly, stiffness controlled flexible boundaries decrease the natural frequencies of a system. The eigenvalues converge from below the rigid walled case as the generalised stiffness term is increased. When k_w = 10000, the limiting condition has almost been reached and the side walls are very nearly rigid. For wall masses k_w = 1 and k_w = 10, eigenvalues are decreased, increasing as the generalised stiffness term increases as expected. Wall motion is out of phase with the acoustic pressure and the wave progresses down the duct at a slower pace than they would travel in free space.

A similar duct section was modelled in Chapter 3 using the flexible walled pipe element for mass and stiffness controlled walls. Comparison of the results show similar trends for the natural frequencies for nearly rigid cases but as the duct walls become more flexible, the difference in natural frequencies is more dramatic. This difference arises since the pipe element models duct sections as tubes and for any length of duct, the surface area of the tube is less than a square duct section. The added surface area accounted for by the coupled HEX8-surface element increases the values of the terms added to the kinetic and potential energy matrices, therefore the difference in natural frequencies.

Table 5.1: Eigenvalues of a Closed Straight Duct Section of Unit Length with Mass Controlled Flexible Walls

Mode Number, n	Rigid Walled	Flex-Wall $m_w = 0.01$	Flex-Wall $m_w = 1$	Flex-Wall $m_w = 10$	Flex-Wall $m_w = 10000$
1	9.87	4849.87	58.27	14.71	9.88
2	39.50	4879.50	87.90	44.34	39.50
3	88.93	4928.93	137.33	93.77	88.93
4	158.23	4998.24	206.64	163.08	158.24
5	247.53	5087.53	295.93	252.37	247.54
6	356.95	5196.95	405.35	361.79	356.96

Table 5.2: Eigenvalues of a Closed Duct Section of Unit Length with Stiffness Controlled Flexible Walls

Mode Number, n	Rigid Walled	Flex-Wall $k_w = 0.01$	Flex-Wall $k_w = 1$	Flex-Wall $k_w = 10$	Flex-Wall $k_w = 10000$
1	9.87	0.002	0.20	1.69	9.82
2	39.50	0.008	0.80	6.76	39.31
3	88.93	0.02	1.80	15.23	88.50
4	158.23	0.03	3.20	27.10	157.48
5	247.53	0.05	5.01	42.39	246.34
6	356.95	0.07	7.23	61.12	355.23

CHAPTER 6

The Hypercube Element

6.1 Introduction

Disturbances such as turbulence in fluids or thermal fluctuations produce equivalent volume source distributions, generating acoustic waves (continuous distributions of monopole sources over a finite region) [64]. Intense acoustic waves can generate turbulence or thermal disturbances in a fluid as well. Compressor fans or turbine stages do not behave like a simple source and are usually represented by a distribution of point sources over a certain region of the duct; often as a dipole source [39]. Noise generated by a turbulent jet can be regarded as being caused by a distribution of equivalent acoustic quadrupole sources over the jet mixing region. In summary, aerodynamic sound can be described in terms of equivalent dipole and quadrupole source distributions and therefore it may be said that the important higher order point multipole sources are the dipole and quadrupole.

In Chapter 4, a method was introduced where a simple HEX8 finite element was constrained to represent higher order dipole and quadrupole mode effects in a duct. In this chapter, a hybrid element known as the *hypercube** is developed to model various dipole and quadrupole source configurations in a duct section. The hypercube consists of 7 HEX8 elements, assembled in such a way as to form a "cube within a cube" shape, similar to the four-dimensional cube used to represent the principle of parallel processing. This element allows various sources of aerodynamic sound in a duct to be modelled and is easily connected to a chain assembly of simple HEX8 elements.

All duct systems considered in this chapter are based on the assumption of a rigid walled duct with stationary medium and all duct sections were considered to be part of an infinite transmission line (anechoically terminated). Computations with the hypercube element were carried out on an IBM RS/6000 320H workstation using FORTRAN source code with extremely fast computation times. The hypercube element is described in detail in the subsequent section followed by the modelling of various dipole and quadrupole sources using a mesh of HEX8 and hypercube elements.

6.2 The Hypercube Element

Consider an elementary source distribution present in a duct as shown in Fig. 6.1.

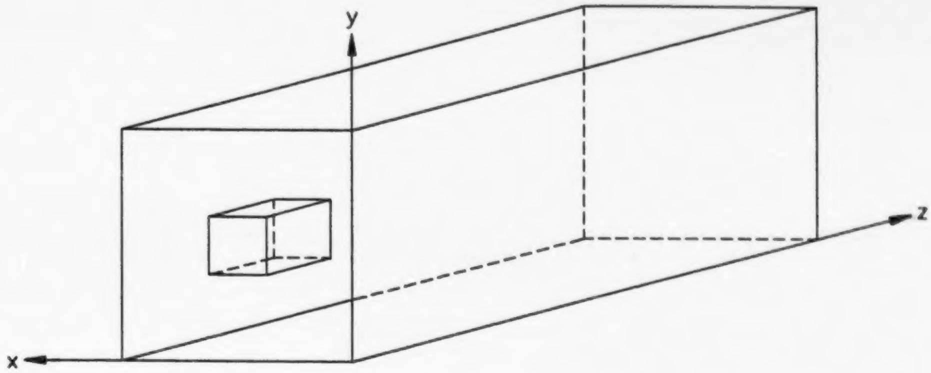

Figure 6.1: Elementary Source Distribution in a Duct

The linear dimensions of the source are small compared with the acoustic wavelength and therefore the shape of the source region is not critical [39]; for a rectangular duct, the region is assumed to be cubic in nature.

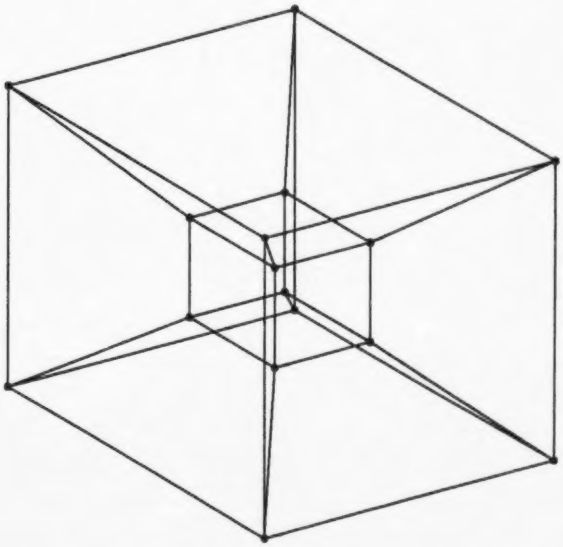

Figure 6.2: Hypercube Element (7 Assembled HEX8 Elements)

* The hypercube element was formulated to model multiple sources in duct acoustics based on suggestion from Dr. A. Craggs, Department of Mechanical Engineering, University of Alberta, Edmonton, Canada.

The assumption that the source region be cubic in nature lends itself perfectly to the hypercube element. A hypercube element is actually an assembly of 7 HEX8 elements with 16 nodes or DOF to form a "cube within a cube" as shown in Fig. 6.2. In this configuration, a source region is represented by the inner cube of the element. The element has only four pressure nodes on any of its outer faces, thus allowing only plane wave, dipole and quadrupole modes of propagation. This makes the element ideal for connecting into a mesh of chain assembled HEX8 elements, keeping with the goal of providing simple finite element techniques for the acoustics engineer.

To represent sources of dipole and quadrupole order, appropriate mode constraints are applied to the faces of the inner cube using the procedure of pre and post multiplying the global finite element matrices by a Boolean transfer matrix. By this method, axial and transverse sources in the duct may be modelled by constraining the faces of the inner cube as shown in Fig. 6.3. It should be noted that this is an isoparametric element and the inner cube may be formulated to represent a source of any size and can even be rotated if desired.

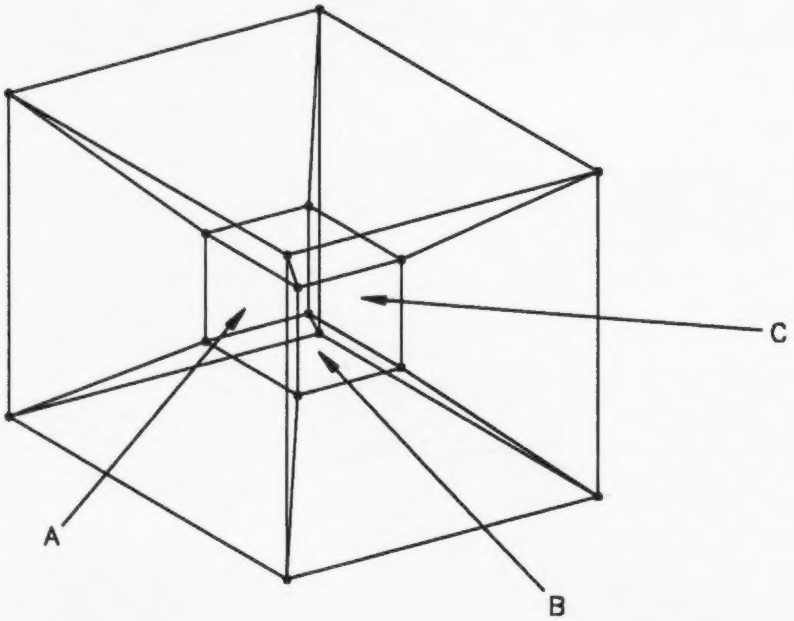

Figure 6.3: Surfaces of the Inner Cube Representing Axial and Transverse Sources in a Duct

6.3 Modelling Dipole and Quadrupole Source Distributions

In this section, various dipole and quadrupole sources are considered for a straight duct section using a mesh of a hypercube element and HEX8 elements. Results are presented in terms of transmission loss, clearly illustrating the effects of cut-off frequency on higher order mode propagation.

A finite element model approximating a source in a straight duct section with dimensions 0.2 m × 0.2 m × 1.0 m is shown in Fig. 6.4. A hypercube element is used to model the source while 8 HEX8 elements represent the remainder of the duct section; the mesh has 48 DOF. The source (inner cube) has dimensions 0.05 m × 0.05 m × 0.05 m and is located in the centre of the duct. One end of the duct section is assumed to be rigid while the other end is anechoically terminated.

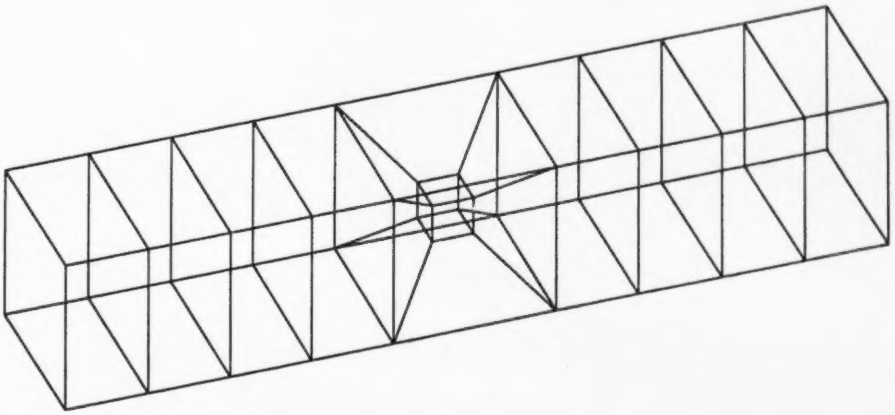

Figure 6.4: Hypercube Element Representing a Sound Source in a Straight Duct Section

First, an axial dipole (1,0) source was considered by constraining a face of the inner cube (face A shown in Fig. 6.3) with transmission loss results being shown in Fig. 6.5. A dipole (1,0) was also applied to the outlet of the duct section (anechoically terminated end). For these particular duct dimensions, the dipole mode has an exact cut-off frequency of 857.5 Hz. The cut-off frequency calculated with the finite element model is 945.6 Hz which is 10.27% greater than the exact value as expected based on results presented in Chapter 4. Mode propagation is entirely dependent on the dimensions of the duct, not on the configuration of the source.

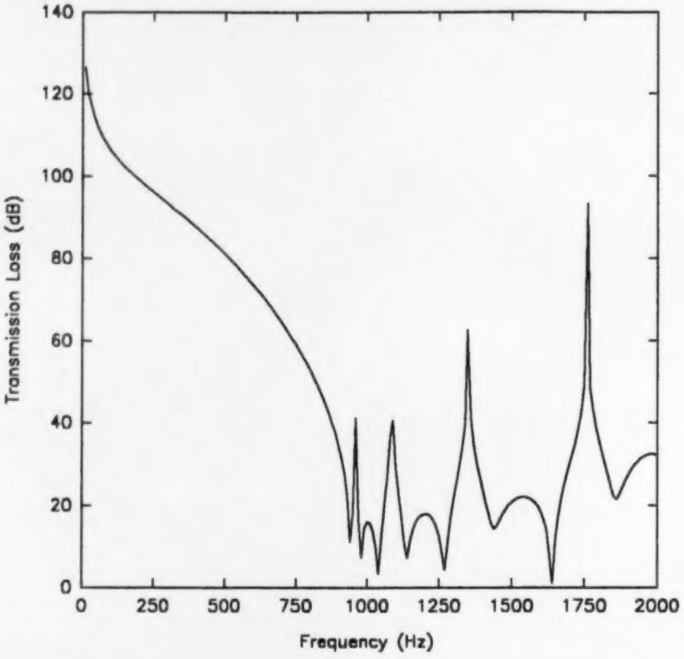

Figure 6.5: Axial Dipole (1,0) Source; Dipole (1,0) Prescribed at Outlet

An axial quadrupole (1,1) source was also considered with a quadrupole being prescribed at the outlet of the duct section. T.L. results are presented in Fig. 6.6, clearly illustrating the effects of cut-off frequency on propagation of the mode. Below the calculated cut-off frequency of 1337.2 Hz, the mode is strongly attenuated and does not propagate as a wave. Above the cut-off frequency, the mode is attenuated much less and propagates, introducing torsional stresses in the walls of the duct. For the remainder of the work presented in this chapter, the duct dimensions will be 0.2 m × 0.2 m × 1.0 m and the calculated cut-off frequencies for the dipole and quadrupole modes will be 945.6 Hz and 1337.2 Hz respectively.

It should be noted that the mode applied to the outlet of the duct section is particularly important. If a dipole (1,0) source is considered and an opposing dipole (0,1) is applied at the duct outlet, the opposing modes essentially nullify each other, producing a destructive interference effect as shown in Fig. 6.7.

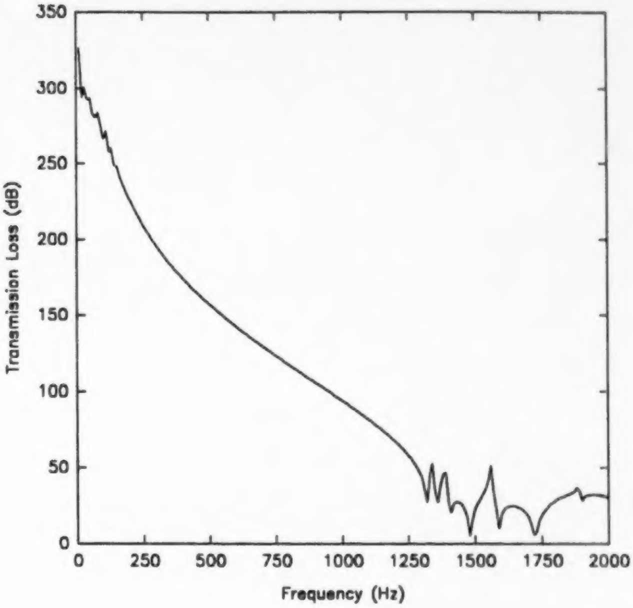

Figure 6.6: Axial Quadrupole (1,1) Source; Quadrupole (1,1) Prescribed at Outlet

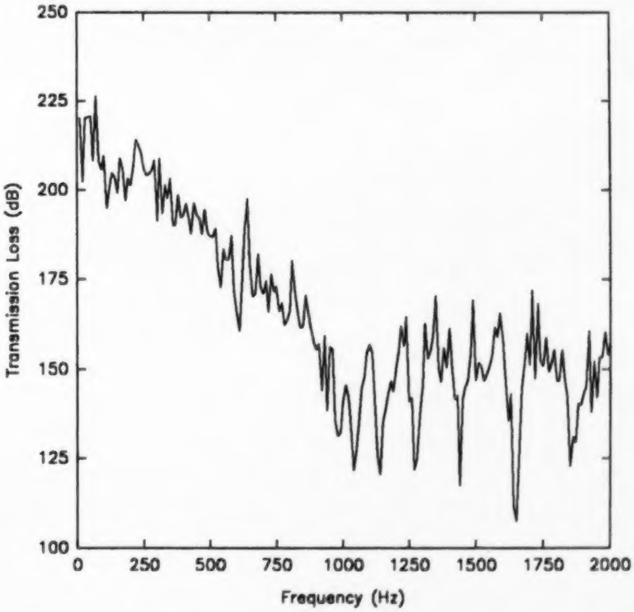

Figure 6.7: Axial Dipole (1,0) Source; Dipole (0,1) Prescribed at Outlet

Transverse sources may also be modelled by constraining face B of the inner cube as shown in Fig. 6.3. A transverse dipole (1,0) source was considered with a plane wave prescribed at the duct outlet. T.L. results presented in Fig. 6.8 demonstrate that care must be taken when applying modes at the termination of the duct as they may destructively interfere with the propagation of both axial and transverse source modes. As such, no cut-off frequencies were calculated with this finite element model. Similarly, a transverse dipole (0,1) source was considered with a plane wave again being prescribed at the duct outlet. For this case, interference appears to be much greater than when the other dipole (1,0) source was considered as shown by the T.L. results presented in Fig. 6.9. This is probably due to the manner in which each of these modes reflects from the duct walls because of the transverse source distribution. If transverse dipole and quadrupole sources are considered with corresponding dipoles and quadrupoles applied at the duct outlet, mode propagation is the same as if the sources were axial as shown in Figures 6.10 and 6.11, again demonstrating that mode propagation depends only on the duct configuration, not on the source, based on the assumptions mentioned at the beginning of the chapter.

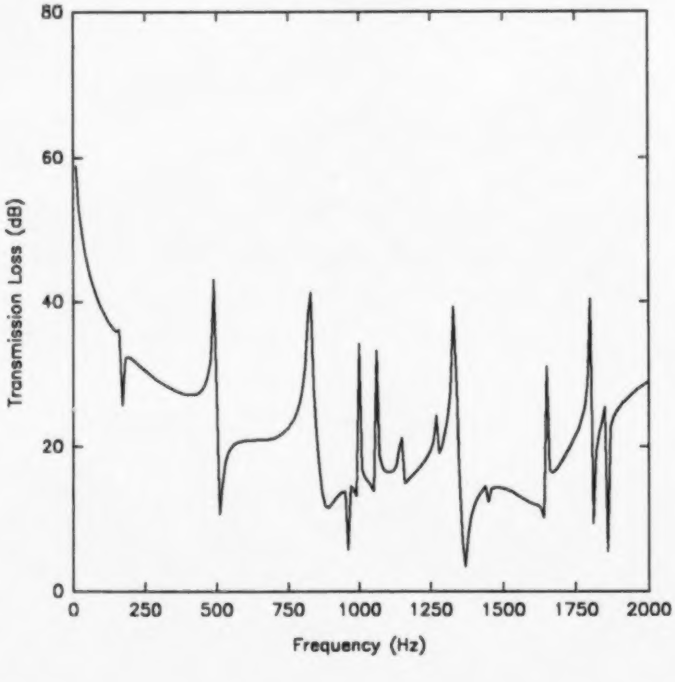

Figure 6.8: Transverse Dipole (1,0) Source; Plane Wave Prescribed at Outlet

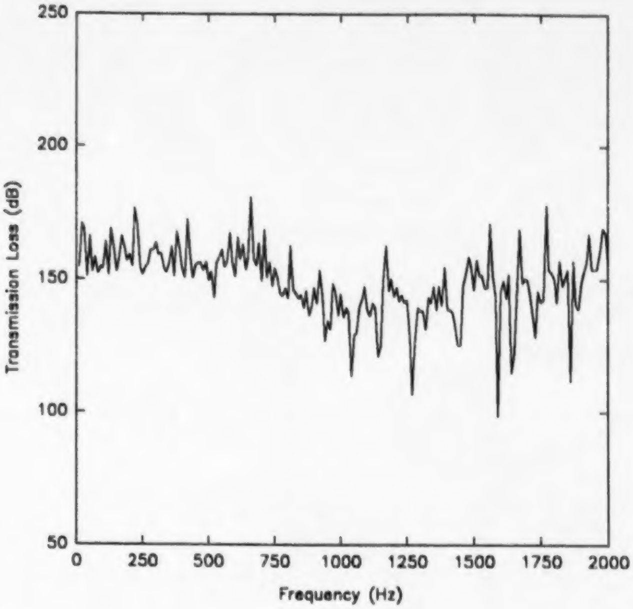

Figure 6.9: Transverse Dipole (0,1) Source; Plane Wave Prescribed at Outlet

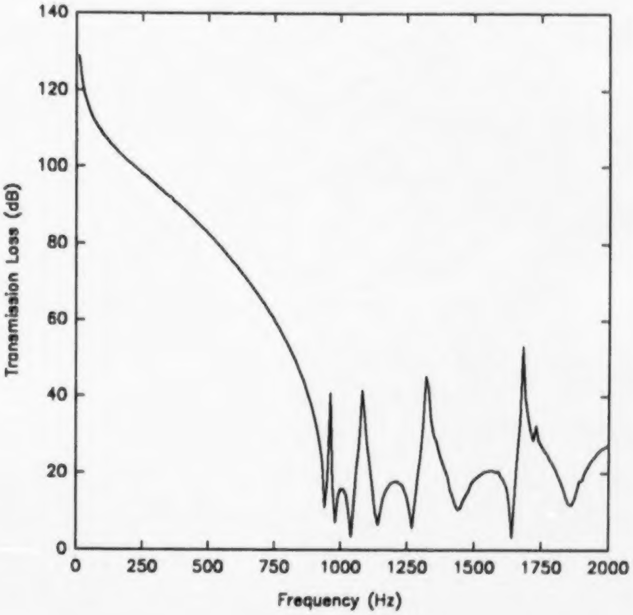

Figure 6.10: Transverse Dipole (1,0) Source; Dipole (1,0) Prescribed at Outlet

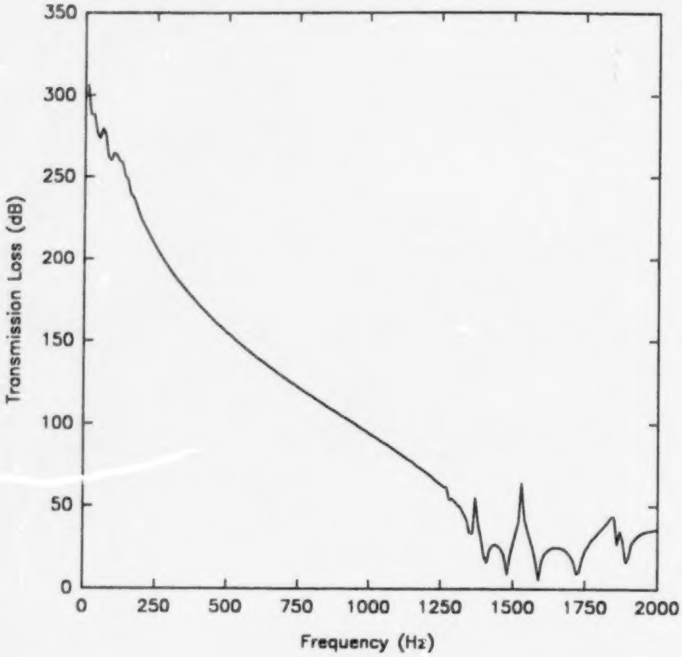

Figure 6.11: Transverse Quadrupole (1,1) Source; Quadrupole (1,1) Prescribed at Outlet

The inner cube of the hypercube may be offset to any position within the larger cube to represent any type of source located within the duct. It may even be rotated by some angle less than 45° as well. Axial propagation from an offset higher order source was considered as shown in Fig. 6.12. A dipole (1,0) source was considered with a dipole (1,0) being prescribed at the duct outlet with T.L. results being presented in Fig. 6.13. Propagation and cut-off effects of the dipole mode are similar to those presented earlier but within the frequency range below the cut-off frequency, a sidebranch resonator peak appears, probably due to reflections caused by the offset source. This peak appears in the region of strong mode attenuation and thus is of no practical interest. Therefore, the mechanism responsible for this peak has not been examined in this thesis work.

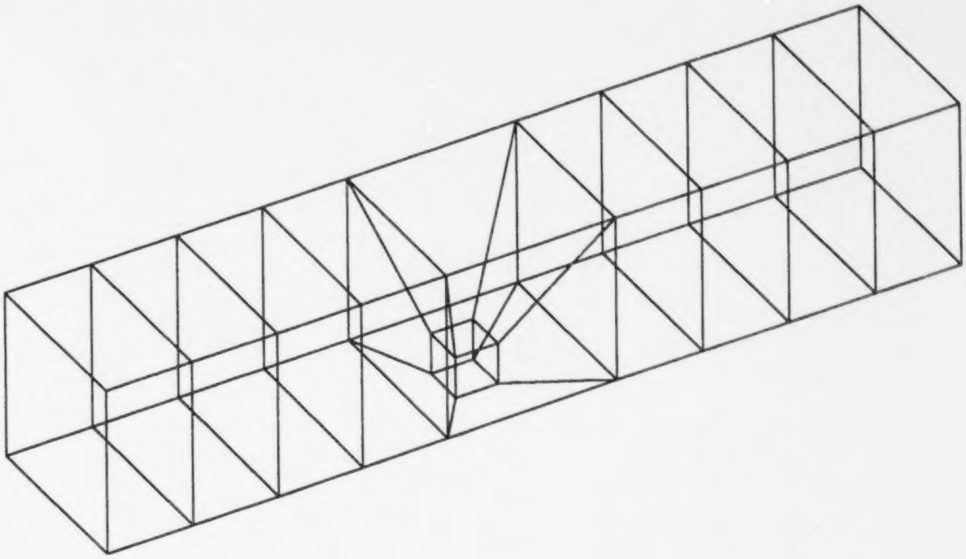

Figure 6.12: Offset Source in a Straight Duct Section

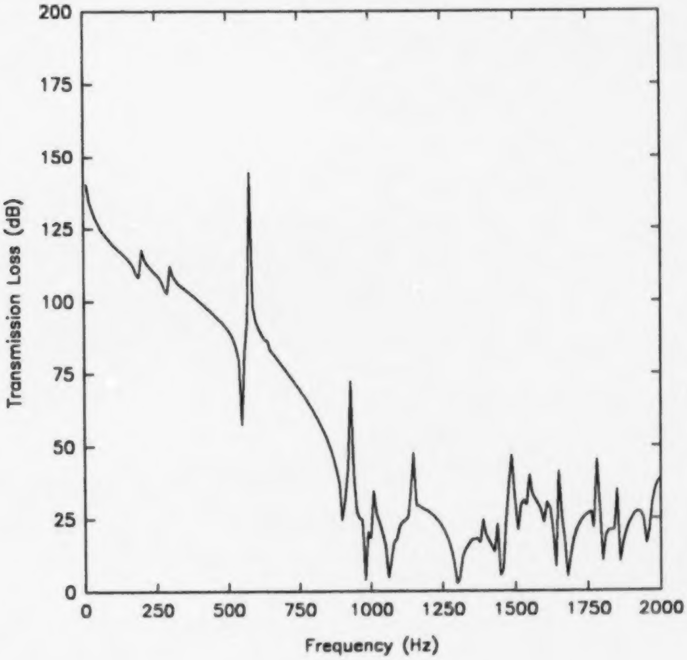

Figure 6.13: Offset Axial Dipole (1,0) Source; Dipole (1,0) Prescribed at Outlet

A larger sound source in a straight duct section was also considered with the source having dimensions of 0.1 m × 0.1 m × 0.1 m as shown in Fig. 6.14. As before, both axial and transverse dipole and quadrupole sources are examined.

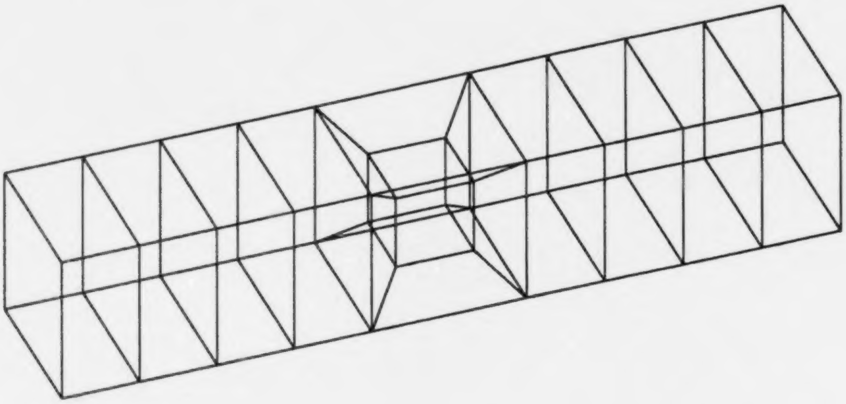

Figure 6.14: Large Source in a Straight Duct Section

An axial dipole (1,0) source was prescribed to face A of the inner cube (refer to Fig. 6.3) with the same dipole set at the duct outlet. T.L. results for this case are presented in Fig. 6.15; the calculated mode cut-off frequency is 857.5 Hz, demonstrating once again that the mode cut-off frequency is independent of source configuration. The same modes were considered for a transverse source with T.L. results shown in Fig. 6.16. For this case, the mode cut-off frequency is not distinct and the general shape of the T.L. curve in the frequency region below 1000 Hz suggests that many reflections are present in this duct section. Clearly, the size of the sound source is the cause of the added reflection in the duct section. Although theory suggests that the shape of the source region is not critical [39], care must be taken that the criterion stating the linear dimensions of the source be small compared with the acoustic wavelength is not violated.

If a dipole (1,0) source is prescribed to all faces of the inner cube with the same dipole being applied to the duct outlet, the result is that the source just pulsates and no sound propagates down the duct, as the destructive interference present in Fig. 6.17 suggests.

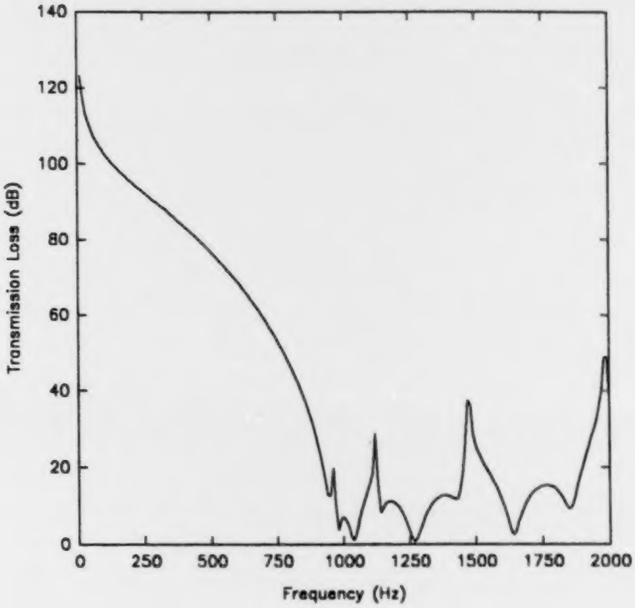

Figure 6.15: Large Axial Dipole (1,0) Source; Dipole (1,0) Prescribed at Outlet

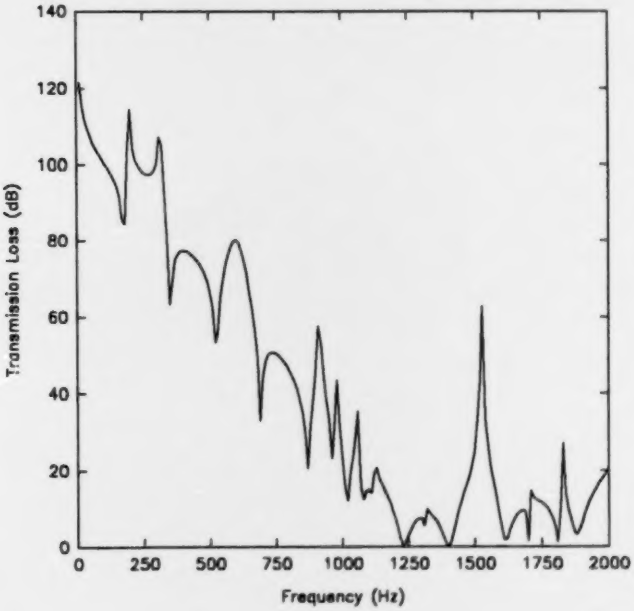

Figure 6.16: Large Transverse Dipole (1,0) Source; Dipole (1,0) Prescribed at Outlet

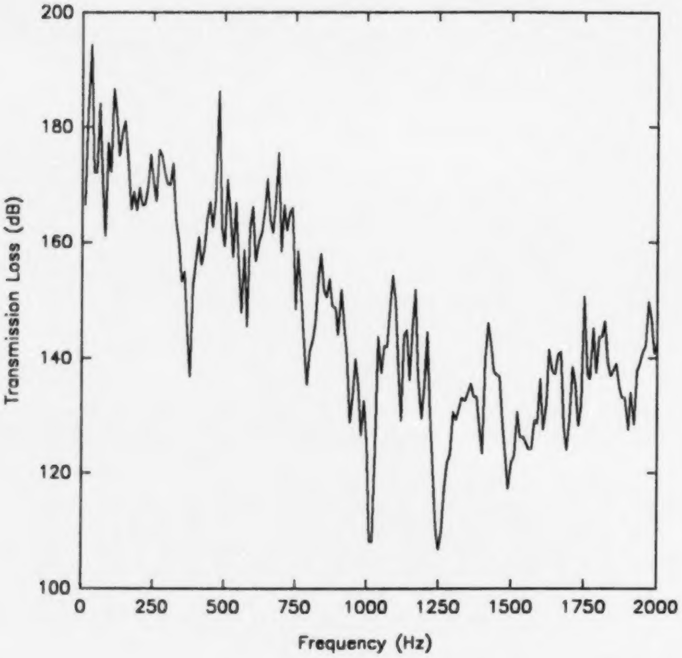

Figure 6.17: Dipole (1,0) Prescribed to all Surfaces of Inner Cube; Dipole (1,0) Prescribed at Outlet

Very small sound sources were also considered for a straight duct section where the linear dimensions of the inner cube were 0.001 m and 0.000001 m respectively. This configuration is shown in Fig. 6.18.

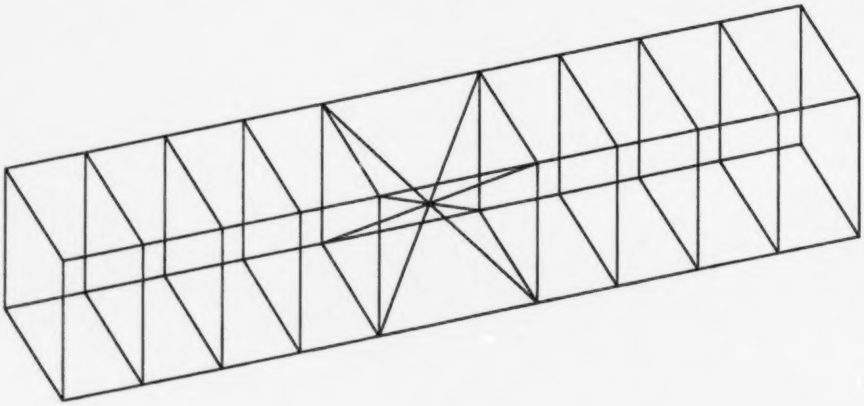

Figure 6.18: Small Source in a Straight Duct Section

Dipole and quadrupole sources were considered by applying these modes to all faces of the inner cube with respective modes being prescribed at the duct outlet. T.L. results for these cases are presented in Figures 6.19 and 6.20, clearly illustrating the effects of cut-off frequency and mode propagation. In these configurations, the source pulsates and there is very little sound propagation as indicted by the elevated pressure losses beyond the respective cut-off frequencies. If the dimensions of the source are reduced to 0.000001 m and a mode is applied to all faces of the inner cube, the source begins to pulsate completely and there is no sound propagation as indicated by the T.L. results and destructive interference patterns presented in Fig. 6.21. Again, theory states that the shape of the source is not critical for cases where the dimensions of the source distribution are small compared with the acoustic wavelength. Care must be taken when using these assumptions in conjunction with finite element approximations.

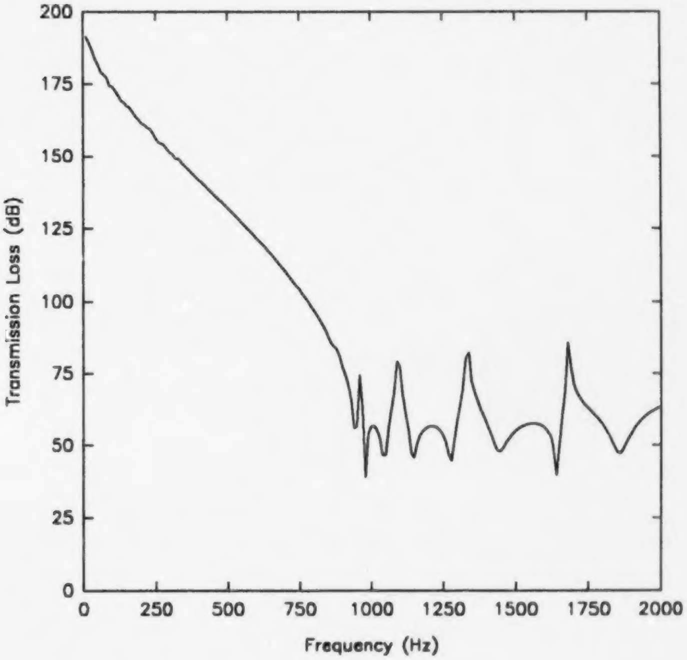

Figure 6.19: Dipole (1,0) Source; Dipole (1,0) Prescribed at Outlet

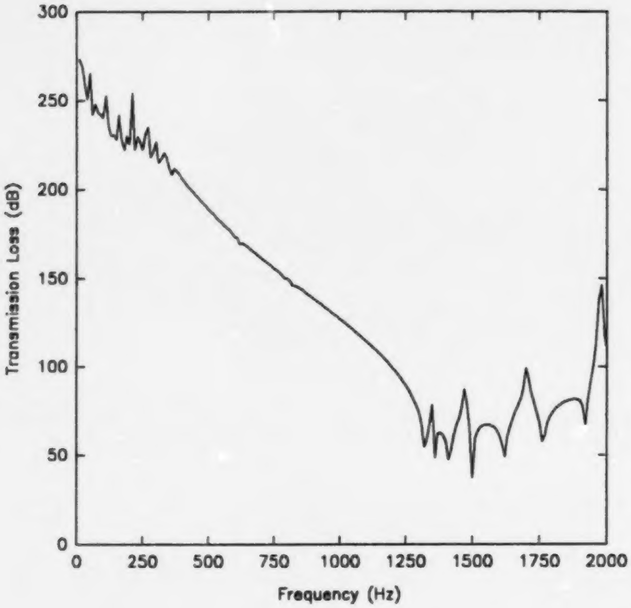

Figure 6.20: Quadrupole (1,1) Source; Quadrupole (1,1) Prescribed at Outlet

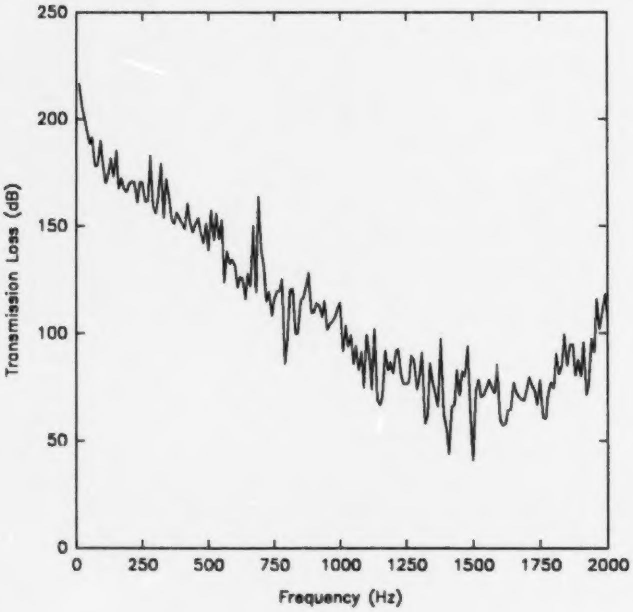

Figure 6.21: Small Dipole (1,0) Source (0.000001 m × 0.000001 m × 0.000001 m); Dipole (1,0) Prescribed at Outlet

CHAPTER 7

Conclusions

This thesis has presented a variety of simple one and three-dimensional finite element methods for studying low frequency duct acoustics. These methods are directed at the acoustics engineer who needs more accurate methods than the "rules of thumb" he may be using to design acoustic duct systems and provide him with uncomplicated finite element models which require only limited computer resources. First, a quadratic one-dimensional finite element is formulated for studying plane wave acoustics for rigid and flexible walled ducts with anechoic termination and stationary flow. Second, a linear isoparametric three-dimensional element is formulated to study low frequency plane wave, dipole and quadrupole mode propagation in ducts for rigid and flexible walled cases with anechoic termination and stationary flow. Last, the three-dimensional element is modified to form a hybrid element suitable for modelling aerodynamic sound sources in ducts.

The second chapter of this thesis introduced a one-dimensional quadratic finite element (pipe element) to model plane wave acoustics, the restriction being that the transverse dimensions of the element be small compared with the acoustic wavelength. The element is formulated based on quadratic pressure and cross-sectional area variations using Galerkin's method of weighted residuals. This method is more general than energy methods such as the Rayleigh-Ritz variational method allowing Galerkin's method to be more applicable to a wider range of problems. A reflective filter is one which removes low frequencies from a system while an absorptive filter is more useful for removing higher frequencies form a system. The finite element used in this chapter was formulated for plane wave or low frequency acoustics and thus only reflective systems were considered. Absorptive systems which dissipate energy were not analysed with this element. The damped equations of motion for an acoustic system were formulated using Galerkin's method as well. While only undamped reflective systems were considered here, various sources of dissipation could be considered in future work using these equations. All systems were considered to be rigid walled with stationary flow.

Element accuracy was determined by calculating the eigenvalues of a standing wave in a closed tube. Using thirteen pipe elements, the sixth natural frequency of the tube was calculated with an error of 0.6%. The frequency response of a variety of one-dimensional systems including area expansions, chambers, sidebranches, resonators, finite length horns and junctions were considered. For low frequencies where only the plane wave mode propagates, only a few elements were necessary to effectively model the system. A limitation of the pipe element is that it is only one-dimensional and therefore cannot model offsets or junctions where the branch angle is important. This element is particularly useful for determining the initial low frequency response of a system which could subsequently be analysed by three-dimensional elements.

For most practical duct configurations, wall thickness is finite and may not always be considered as being completely rigid. The pipe element is modified in Chapter 3 to include the effects of locally reacting mass and stiffness controlled duct walls. A mass controlled duct wall increases the natural frequencies of a system by adding terms to the kinetic energy matrix while a stiffness controlled wall decreases the natural frequencies of a system by adding terms to the potential energy matrix. As wall mass is increased, the limiting rigid wall case is approached; as wall stiffness is increased, the limiting rigid walled case is approached.

In Chapter 4, the HEX8 element was formulated using Galerkin's method of weighted residuals, a method which is much more general than a variational energy formulation such as the Rayleigh-Ritz method and thus Galerkin's method is applicable to a wider range of problems. The HEX8 element is isoparametric in nature meaning that it is deformable to almost any shape as long as all interior angles are less than 180°. The accuracy of this element in deformed shape was determined by calculating the eigenvalues of a cylindrical enclosure.

On any face of the HEX8 element, there are only four pressure nodes meaning that only four modes of propagation are allowed; the plane wave, two dipole modes and the quadrupole mode. For low frequency acoustics, these modes cannot be neglected as they cause bending forces and torsional stresses in the walls of the duct. By applying appropriate pressure constraints to a duct section, mode propagation and attenuation can be examined using the methods introduced in this chapter. For the simple element meshes consisting of HEX8 elements chain assembled together, there is only a linear approximation in the transverse direction, thus the cut-off frequencies of the dipole and quadrupole modes are calculated as being 10.27% greater than exact values. Various duct configurations including chambers, bends, curves and junctions were considered using simple chain assembled element meshes with low frequency results being extremely good for the first four modes of propagation. Even in the region of a junction, only one HEX8 element was necessary because only up to the fourth mode was propagating, greatly simplifying the element mesh.

Significant low frequency 3-D wave effects including mode propagation and attenuation can be examined using only simple chain assembled HEX8 elements, leading to subsequent reduction in the usage of computer resources. Higher order elements could be constrained with these modes to study propagation and attenuation of more complicated systems but that would be the subject of future work.

Similar to the procedure presented in Chapter 3, the HEX8 element is modified in Chapter 5 to include locally reacting mass and stiffness controlled wall effects. This is a simplified approach to approximating wall motion on the acoustics of the duct. A much more difficult approach is to allow wall motion to be governed by the unsteady plate equation and couple it to the acoustic model. Here, locally reacting mass and stiffness controlled wall effects are approximated using a linear, two-dimensional isoparametric element coupled to the surfaces of a HEX8 element. Again, a mass controlled wall increases natural frequencies while a stiffness controlled wall causes a decrease in the natural frequencies of the system. A straight rectangular duct section was modelled with both the flexible walled HEX8 element and the flexible walled pipe element. The calculated eigenvalues showed similar trends but values differed slightly because the surface area modelled with the three-dimensional element was greater than for the pipe element, which considered the duct section as a tube. Experimental work could be undertaken to determine the validity of locally reacting mass and stiffness controlled wall approximations as compared to wall motion governed by the unsteady plate equation. The method presented here is a much simpler approach.

A hybrid finite element known as the *hypercube* was introduced in Chapter 6. Based on the "cube within a cube" description used to represent parallel processing theory, the element actually consists of seven assembled HEX8 elements. The major advantage of this is that the element is easily connected to a chain assembly of simple HEX8 elements. Aerodynamic sound can be represented by continuous distributions of monopole sources over a finite region and thus thermal fluctuations, compressor fans, turbine stages and turbulence may be represented by equivalent dipole or quadrupole source distributions. By constraining the hypercube element with appropriate dipole or quadrupole modes, various sources of aerodynamic sound can be approximated by the finite element method including offset and rotated sources. Preliminary results presented in this thesis indicate that mode propagation is entirely dependent on the dimensions of the duct, not on the configuration of the source as long as the linear dimensions of the source are small compared with the acoustic wavelength. The hypercube is in its infancy and much further work could be done with the element including considering systems with more complicated geometries than a straight duct section and systems with multiple sources. This element may prove particularly useful in the future for representing turbulent sources generated in ducts with high Mach number flow. There has only been limited work thus far in this area.

Hopefully, the finite element methods presented in this thesis work will be beneficial to the practical analysis of low frequency acoustic systems, particularly to future work in the field of turbulent noise generated in ducts with flow. Listings of computers programs will be published as a departmental report.

REFERENCES

[1] Allaire, P.E., *Basics of the Finite Element Method,* Wm. C. Brown, Dubuque, Iowa, 1985.

[2] Alfredson, R.J., "The propagation of sound in a circular duct of continuously varying cross-sectional area", *Journal of Sound and Vibration,* 23(4):433-442, 1972.

[3] Alfredson, R.J. and P.O.A.L. Davies, "Performance of exhaust silencer components", *Journal of Sound and Vibration,* 15(2):175-196, 1971.

[4] Astley, R.J., "A finite element, wave envelope formulation for acoustical radiation in moving flows", *Journal of Sound and Vibration,* 103(4):471-485, 1985.

[5] Astley, R.J. and A. Cummings, "A finite element scheme for acoustic transmission through the walls of rectangular ducts: Comparison with experiment", *Journal of Sound and Vibration,* 92(3):387-409, 1984.

[6] Astley, R.J., Cummings, A. and N. Sormaz, "A finite element scheme for acoustic propagation in flexible-walled ducts with bulk reacting liners, and comparison with experiment", *Journal of Sound and Vibration,* 150(1):119-138, 1991.

[7] Astley, R.J. and W. Eversman, "A finite element method for transmission in non-uniform ducts without flow: Comparison with the method of weighted residuals", *Journal of Sound and Vibration,* 57(3):367-388, 1978.

[8] Astley, R.J. and W. Eversman, "A finite element formulation of the eigenvalue problem in lined ducts with flow", *Journal of Sound and Vibration,* 65(1):61-74, 1979.

[9] Astley, R.J. and W. Eversman, "The finite element duct eigenvalue problem: An improved formulation with Hermitian elements and no-flow condensation", *Journal of Sound and Vibration*, 69(1):13-25, 1980.

[10] Astley, R.J. and W. Eversman, "Acoustic transmission in non-uniform ducts with mean flow, Part II: The finite element method", *Journal of Sound and Vibration*, 74(1):103-121, 1981.

[11] Bathe, K.J., *Finite Element Procedures in Engineering Analysis*, Prentice-Hall, Englewood Cliffs, N.J., 1982.

[12] Beranek, L.L., *Acoustics*, American Institute of Physics, 1986.

[13] Beranek, L.L., *Noise and Vibration Control*, McGraw-Hill, 1971, See Chapter 12.

[14] Burnett, D.S., *Finite Element Analysis from Concepts to Applications*, Addison-Wesley, Reading, Massachusetts, 1987.

[15] Cabelli, A., "The acoustic characteristics of duct bends", *Journal of Sound and Vibration*, 68(3):369-388, 1980.

[16] Cabelli, A., "The influence of flow on the acoustic characteristics of a duct bend for higher order modes - a numerical study", *Journal of Sound and Vibration*, 82(1):131-149, 1982.

[17] Cabelli, A., "Application of the time dependent finite difference theory to the study of sound and vibration interactions in ducts", *Journal of Sound and Vibration*, 103(1):13-23, 1985.

[18] Cabelli, A., "The propagation of sound in a square duct with a non-rigid side wall", *Journal of Sound and Vibration*, 103(3):379-394, 1985.

[19] Cabelli, A. and I.C. Shepherd, "The influence of geometry on the acoustic characteristics of duct bends for higher order modes", *Journal of Sound and Vibration*, 78(1):119-129, 1981.

[20] Cabelli, A. and I.C. Shepherd, "Duct acoustics - a numerical technique for the higher order mode solution of three-dimensional problems with rigid walls and no flow", *Journal of Sound and Vibration*, 92(3):419-426, 1984.

[21] Cheng, C.Y.R., Seybert, A.F. and T.W. Wu, "A multidomain boundary element solution for silencer and muffler performance prediction", *Journal of Sound and Vibration*, 151(1):119-129, 1991.

[22] Chung, J.Y. and D.A. Blaser, "Transfer function method of measuring in-duct acoustic properties. I. Theory", *Journal of the Acoustical Society of America*, 68(3):907-913, 1980.

[23] Chung, J.Y. and D.A. Blaser, "Transfer function method of measuring in-duct acoustic properties. II. Experiment", *Journal of the Acoustical Society of America*, 68(3):914-921, 1980.

[24] Craggs, A., "The transient response of a coupled plate-acoustic system using plate and acoustic finite elements", *Journal of Sound and Vibration*, 15(4):509-528, 1971.

[25] Craggs, A., "The use of simple three dimensional acoustic finite elements for determining the natural modes and frequencies of complex shaped enclosures", *Journal of Sound and Vibration*, 23(3):331-339, 1972.

[26] Craggs, A., "An acoustic finite element approach for studying boundary flexibility and sound transmission between irregular enclosures", *Journal of Sound and Vibration*, 30(3):343-357, 1973.

[27] Craggs, A., "A finite element method for damped acoustic systems: An application to evaluate the performance of reactive mufflers", *Journal of Sound and Vibration*, 48(3):377-392, 1976.

[28] Craggs, A., "A finite element method for modeling dissipative mufflers with a locally reactive lining", *Journal of Sound and Vibration*, 54(2):285-296, 1977.

[29] Craggs, A., "A finite element model for rigid porous absorbing materials", *Journal of Sound and Vibration*, 61(1):101-111, 1978.

[30] Craggs, A., "Coupling of finite element acoustic absorption models", *Journal of Sound and Vibration*, 66(4):605-613, 1979.

[31] Craggs, A., "A note on the theory and application of a simple pipe acoustic element", *Journal of Sound and Vibration*, 85(2):292-295, 1982.

[32] Craggs, A., "The application of the transfer matrix and matrix condensation methods with finite elements to duct acoustics", *Journal of Sound and Vibration*, 132(2):393-402, 1989.

[33] Craggs, A. and D.C. Stredulinsky, "Analysis of acoustic wave transmission in a piping network", *Journal of the Acoustical Society of America*, 88(1):542-547, 1990.

[34] Cummings, A., "Sound transmission in curved duct bends", *Journal of Sound and Vibration*, 35(4):451-477, 1974.

[35] Cummings, A., "Sound transmission in 180° duct bends of rectangular section", *Journal of Sound and Vibration*, 41(3):321-334, 1975.

[36] Cummings, A., "Design charts for low frequency acoustic transmission through the walls of rectangular ducts", *Journal of Sound and Vibration*, 78(2):269-289, 1981.

[37] Davis Jr., D.D., "Acoustical filters and mufflers, Chapter 21", *Handbook of Noise Control*, C.M. Harris (editor), McGraw-Hill, New York, 1975.

[38] De Rosa, S. and G. Pezzullo, "One-dimensional wave equation: Finite element eigenanalysis", *Journal of Sound and Vibration*, 150(2):335-337, 1991.

[39] Doak, P.E., "Excitation, transmission and radiation of sound from source distributions in hard-walled ducts of finite length (I): The effects of duct cross-section geometry and source distribution space-time pattern", *Journal of Sound and Vibration*, 31(1):1-72, 1973.

[40] Doak, P.E., "Excitation, transmission and radiation of sound from source distributions in hard-walled ducts of finite length (II): The effects of duct length", *Journal of Sound and Vibration*, 31(2):137-174, 1973.

[41] Doak, P.E., "Cylindrical wave propagation in a cylindrical diffuser", *Journal of Sound and Vibration*, 155(3):541-544, 1992.

[42] Doak, P.E., "Acoustic wave propagation in a homentropic, irrotational, low mach number mean flow", *Journal of Sound and Vibration*, 155(3):545-548, 1992.

[43] Doak, P.E. and P.G. Vaidya, "Attenuation of plane wave and higher order mode sound propagation in lined ducts", *Journal of Sound and Vibration*, 12(2):201-224, 1970.

[44] Dowling, A.P. and J.E. Ffowcs Williams, *Sound and Sources of Sound*, Ellis Horwood, Chichester, West Sussex, 1983.

[45] Eisner, E., "Complete solutions of the Webster horn equation", *Journal of the Acoustical Society of America*, 41(4):1126-1146, 1967.

[46] El-Sharkawy, A.I. and A.H. Nayfeh, "Effect of an expansion chamber on the propagation of sound in circular ducts", *Journal of the Acoustical Society of America*, 63(3):667-674, 1978.

[47] Eriksson, L.J., "Higher order mode effects in circular ducts and expansion chambers", *Journal of the Acoustical Society of America*, 68(2):545-550, 1980.

[48] Eriksson, L.J., "Effect of inlet/outlet locations on higher order modes in silencers", *Journal of the Acoustical Society of America*, 72(4):1208-1211, 1982.

[49] Eriksson, L.J., Anderson, C.A., Hoops, R.H. and K. Jayaraman, "Finite length effects on higher order mode propagation in silencers", 11^e *Congres International D'Acoustique*, pp. 329-332, Paris, 1983.

[50] Eversman, W., "Computation of axial and transverse wave numbers for uniform two-dimensional ducts with flow using a numerical integration scheme", *Journal of Sound and Vibration*, 41(2):252-255, 1975.

[51] Eversman, W., "A reciprocity relationship for transmission in non-uniform hard walled ducts without flow", *Journal of Sound and Vibration*, 47(4):515-521, 1976.

[52] Eversman, W., "Acoustic energy in ducts: Further observations", *Journal of Sound and Vibration*, 62(4):517-532, 1979.

[53] Eversman, W. and R.J. Astley, "Acoustic transmission in non-uniform ducts with mean flow, Part I: The method of weighted residuals", *Journal of Sound and Vibration*, 74(1):89-101, 1981.

[54] Eversman, W., Cook, E.L. and R.J. Beckemeyer, "A method of weighted residuals for the investigation of sound transmission in non-uniform ducts without flow", *Journal of Sound and Vibration*, 38(1):105-123, 1975.

[55] Ford, R.D., *Introduction to Acoustics*, Elsevier, London, 1970.

[56] Fuller, C.R. and D.A. Bies, "Propagation of sound in a curved bend containing a curved axial partition", *Journal of the Acoustical Society of America*, 63(3):681-686, 1978.

[57] Gladwell, G.M.L., "A finite element method for acoustics", 5^e *Congres International D'Acoustique*, Paper No. L33, Liege, 1965.

[58] Gladwell, G.M.L., "On energy and complementary energy formulations of acoustic and structural vibration problems", *Journal of Sound and Vibration*, 3(3):233-241, 1966.

[59] Gladwell, G.M.L., "A variational formulation of damped acousto-structural vibration problems", *Journal of Sound and Vibration*, 4(2):172-186, 1966.

[60] Gladwell, G.M.L., "Variational calculation of the impedance of a lossy, non-uniform mechanical transmission line", *Journal of Sound and Vibration*, 7(2):200-219, 1968.

[61] Ih, J.G., "The reactive attenuation of rectangular plenum chambers", *Journal of Sound and Vibration*, 157(1):93-122, 1992.

[62] Ih, J.G. and B.H. Lee, "Analysis of higher-order mode effects in the circular expansion chamber with mean flow", *Journal of the Acoustical Society of America*, 77(4):1377-1388, 1985.

[63] Kagawa, Y., Yamabuchi, T. and A. Mori, "Finite element simulation of an axisymmetric acoustic transmission system with a sound absorbing wall", *Journal of Sound and Vibration*, 53(3):357-374, 1977.

[64] Lighthill, M.J., "On sound generated aerodynamically. I. General theory.", *Proceedings of the Royal Society*, A 211, 564-587, 1952.

[65] Lippert, W.K.R., "The measurement of sound reflection and transmission at right-angled bends in rectangular tubes", *Acustica*, 4:313-319, 1954.

[66] Lippert, W.K.R., "Wave transmission around bends of different angles in rectangular ducts", *Acustica*, 5:274-278, 1955.

[67] Miles, J.W., "The diffraction of sound due to right-angled joints in rectangular tubes", *Journal of the Acoustical Society of America*, 19(4):572-579, 1947.

[68] Morfey, C.L., "Sound transmission and generation in ducts with flow", *Journal of Sound and Vibration*, 14(1):37-55, 1971.

[69] Morse, P.M., *Vibration and Sound*, American Institute of Physics, 1986.

[70] Morse, P.M., Boden, R.H. and H. Schecter, "Acoustic vibrations and internal engine performance (I): Standing waves in the intake pipe system", *Journal of Applied Physics*, Vol. 9, January, 1938.

[71] Morse, P.M. and K.U. Ingard, *Theoretical Acoustics*, McGraw-Hill, New York, 1968.

[72] Morse, P.M. and H. Feshbach, *Methods of Theoretical Physics*, McGraw-Hill, New York, 1953.

[73] Munjal, M.L., *Acoustics of Ducts and Mufflers with Application to Exhaust and Ventilation System Design*, John Wiley & Sons, New York, 1987.

[74] Munjal, M.L., "A simple numerical method for three-dimensional analysis of simple expansion chamber mufflers of rectangular as well as circular cross-section with a stationary medium", *Journal of Sound and Vibration*, 116(1):71-88, 1987.

[75] Olson, H.F., *Acoustical Engineering*, D. Van Nostrand Company, Princeton, N.J., 1957.

[76] Osborne, W.C., "Calculation of the angular propagation constant for a bend", *Journal of Sound and Vibration*, 37(1):65-77, 1974.

[77] Osborne, W.C., "Higher mode propagation of sound in short curved bends of rectangular cross-section", *Journal of Sound and Vibration*, 45(1):39-52, 1976.

[78] Panton, L., *Incompressible Flow*, John Wiley & Sons, New York, 1984.

[79] Peat, K.S., "Evaluation of four-pole parameters for ducts with flow by the finite element method", *Journal of Sound and Vibration*, 84(3):389-395, 1982.

[80] Peat, K.S., "The acoustical impedance at the junction of an extended inlet or outlet duct", *Journal of Sound and Vibration*, 150(1):101-110, 1991.

[81] Petyt, M. and G.H. Koopman, "A finite element method for determining the acoustic modes of irregular shaped cavities", *Journal of Sound and Vibration*, 45(4):495-502, 1976.

[82] Press, W.H., Flannery, B.P., Teukolsky, S.A. and W.T. Vetterling, *Numerical Recipes, The Art of Scientific Computing (Fortran Version)*, Cambridge University Press, Cambridge, 1990.

[83] Pyle Jr., R. W., "Effective length of horns", *Journal of the Acoustical Society of America*, 57(6):1309-1317, 1975.

[84] Rayleigh, Baron, *The Theory of Sound*, Dover, New York, 1945.

[85] Redmore, T.L. and K.A. Mulholland, "The application of mode coupling theory to the transmission of sound in the sidebranch of a rectangular duct system", *Journal of Sound and Vibration*, 85(3):323-331, 1982.

[86] Rostafinsky, W., "On propagation of long waves in curved ducts", *Journal of the Acoustical Society of America*, 52(5):1411-1420, 1972.

[87] Rostafinsky, W., "Analysis of propagation of waves of acoustic frequencies in curved ducts", *Journal of the Acoustical Society of America*, 56(1):11-15, 1974.

[88] Rostafinsky, W., "Acoustic systems containing curved duct sections", *Journal of the Acoustical Society of America*, 60(1):23-28, 1976.

[89] Sahasrabudhe, A.D., Anantharamu, S., and M.L. Munjal, "Matrix condensation techniques in the 3-D analysis of expansion chamber mufflers", *Journal of Sound and Vibration*, 147(3):371-394, 1991.

[90] Sengupta, G., "Finite element analysis of natural fequencies of acoustic enclosures with periodic properties", *Journal of Sound and Vibration*, 147(3):528-532, 1991.

[91] Shepherd, I.C. and A. Cabelli, "Transmission and reflection of higher order acoustic modes in a mitered duct bend", *Journal of Sound and Vibration*, 77(4):495-511, 1981.

[92] Stredulinsky, D.C., *An Isoparametric Hermitian Finite Element for Duct Acoustics with Flow*, Ph.D. Thesis, University of Alberta, 1990.

[93] Stredulinsky, D.C., Craggs, A. and M.G. Faulkner, "Acoustics of piping and ducts", *Canadian Acoustics*, 15(4):3-14, 1987.

[94] Stredulinsky, D.C. and A. Craggs, "Isoparametric finite element using cubic hermite polynomials for acoustics in duct components with flow", *Canadian Acoustics*, 19(3):3-15, 1991.

[95] Stumpf, F.B., *Analytical Acoustics*, Ann Arbor Science, Ann Arbor, 1980.

[96] Temkin, S., *Elements of Acoustics*, John Wiley & Sons, New York, 1981.

[97] Vo, P.T. and W. Eversman, "A method of weighted residuals with trigonometric basis functions for sound transmission in circular ducts", *Journal of Sound and Vibration*, 56(2):243-250, 1978.

[98] Young, C.J. and M.J. Crocker, "Prediction of transmission loss in mufflers by the finite-element method", *Journal of the Acoustical Society of America*, 57(1):144-148, 1975.

[99] Young, C.J. and M.J. Crocker, "Finite element acoustical analysis of complex muffler systems with and without wall vibrations", *Noise Control Engineering*, 9(2):86-93, 1977.

[100] Zienkiewicz, O.C. and R.L. Taylor, *The Finite Element Method, Fourth Edition*, McGraw-Hill, London, 1989.

APPENDIX A

A.1 The Jacobi Method

The Jacobi method was developed for the solution of standard eigenvalue problems and has been used extensively because of the method's simplicity and stability [11]; it is foolproof for all real, symmetric matrices. The method consists of a sequence of orthogonal similarity transformations of the form

$$\mathbf{A} \rightarrow \mathbf{P}_1^{-1} \cdot \mathbf{A} \cdot \mathbf{P}_1 \rightarrow \mathbf{P}_2^{-1} \cdot \mathbf{P}_1^{-1} \cdot \mathbf{A} \cdot \mathbf{P}_1 \cdot \mathbf{P}_2 \rightarrow \mathbf{P}_3^{-1} \cdot \mathbf{P}_2^{-1} \cdot \mathbf{P}_1^{-1} \cdot \mathbf{A} \cdot \mathbf{P}_1 \cdot \mathbf{P}_2 \cdot \mathbf{P}_3 \rightarrow etc. \qquad \text{(A.1)}$$

where **P** is some transformation matrix. These similarity transformations direct the matrix **A** towards a diagonal form. Each transformation is just a plane rotation (*Jacobi rotation*) designed to eliminate one of the off-diagonal matrix elements. Previously set zeros may be undone by successive transformations but the off-diagonal elements continue to be reduced until the matrix is diagonal to computer precision. The product of the transformations can be accumulated as follows to give the matrix of eigenvectors

$$\mathbf{X} = \mathbf{P}_1 \cdot \mathbf{P}_2 \cdot \mathbf{P}_2 \cdots \qquad \text{(A.2)}$$

and the elements of the final diagonal matrix are the eigenvalues.

Following the procedure and notation outlined in [82], a basic Jacobi rotation is a matrix of the form

$$\mathbf{P}_{pq} = \begin{bmatrix} 1 & & & & & & \\ & \cdots & & & & & \\ & & c & \cdots & s & & \\ & & \vdots & 1 & \vdots & & \\ & & -s & \cdots & c & & \\ & & & & & \cdots & \\ & & & & & & 1 \end{bmatrix}$$

and is selected in such a way that an off-diagonal element in **A** is zeroed. All diagonal elements are unity except for two cosine elements c in rows and columns p and q. All off-diagonal elements are zero except for the two sine elements s and $-s$ in rows and columns p and q.

A plane rotation is used to transform the matrix **A** according to

$$\mathbf{A}' = \mathbf{P}_{pq}^{T} \cdot \mathbf{A} \cdot \mathbf{P}_{pq} \tag{A.3}$$

where the superscript T denotes a matrix transformation. The operation $\mathbf{P}_{pq}^{T} \cdot \mathbf{A}$ changes only rows p and q of **A**, while $\mathbf{A} \cdot \mathbf{P}_{pq}$ changes only columns p and q of **A**. Thus the changed elements of **A** are only in the p and q rows and columns

$$\mathbf{A}' = \begin{bmatrix} & \cdots & a'_{1p} & \cdots & a'_{1q} & \cdots & \\ \vdots & & \vdots & & \vdots & & \vdots \\ a'_{p1} & \cdots & a'_{pp} & \cdots & a'_{pq} & \cdots & a'_{pn} \\ \vdots & & \vdots & & \vdots & & \vdots \\ a'_{q1} & \cdots & a'_{qp} & \cdots & a'_{qq} & \cdots & a'_{qn} \\ \vdots & & \vdots & & \vdots & & \vdots \\ & \cdots & a'_{np} & \cdots & a'_{nq} & \cdots & \end{bmatrix}$$

The following explicit formulas can be determined by multiplying out Eq. (A.3) and making use of the symmetry of **A**

$$a'_{rp} = ca_{rp} - sa_{rq}$$

$$a'_{rq} = ca_{rq} + sa_{rp} \qquad r \neq p, \ r \neq q \tag{A.4}$$

$$a'_{pp} = c^2 a_{pp} + s^2 a_{qq} - 2sca_{pq} \tag{A.5}$$

$$a'_{qq} = s^2 a_{pp} + c^2 a_{qq} + 2sca_{pq} \tag{A.6}$$

$$a'_{pq} = \left(c^2 - s^2\right) a_{pq} + sc\left(a_{pp} - a_{qq}\right) \tag{A.7}$$

To set $a'_{pq} = 0$, Eq. (A.7) gives the following expression for the angle of the plane rotation

$$\theta \equiv \cot 2\phi \equiv \frac{c^2 - s^2}{2sc} = \frac{a_{qq} - a_{pp}}{2a_{pq}} \tag{A.8}$$

If we let $t \equiv s/c$, the definition of θ can be rewritten as

$$t^2 + 2t\theta - 1 = 0 \tag{A.9}$$

The smaller root of Eq. (A.9) corresponds to a rotation angle less than $\pi/4$, which gives the most stable reduction at each phase of the operation. Using the form of the quadratic formula with the discriminant in the denominator, the smaller root can be written as

$$t = \frac{\operatorname{sgn}(\theta)}{|\theta| + \sqrt{\theta^2 + 1}} \tag{A.10}$$

If θ is so large that θ^2 would overflow the computer, we set $t = 1/(2\theta)$. It follows that the cosine and sine terms can be rewritten as

$$c = \frac{1}{\sqrt{t^2 + 1}} \tag{A.11}$$

$$s = tc \tag{A.12}$$

When we use Eqs. (A.4-A.7) numerically, we rewrite them to minimize round-off error and Eq. (A.7) is replaced by a'_{pq}. The idea in the remaining equations is to set the new quantity equal to the old quantity plus a small correction. Therefore, we can eliminate a'_{qq} from Eq. (A.5), giving

$$a'_{pp} = a_{pp} - ta_{pq} \tag{A.13}$$

In similar fashion,

$$a'_{qq} = a_{qq} + ta_{pq} \tag{A.14}$$

$$a'_{rp} = a_{rp} - s\left(a_{rq} + \tau a_{rp}\right) \tag{A.15}$$

$$a'_{rq} = a_{rq} + s\left(a_{rp} - \tau a_{rq}\right) \tag{A.16}$$

where τ is defined by $\tau \equiv s/(1+c)$.

One can see the convergence of the Jacobi method by considering the sum of the squares of the off-diagonal elements.

$$S = \sum_{r \neq s} \left|a_{rs}\right|^2 \tag{A.17}$$

Equations (A.4-A.7) imply that

$$S' = S - 2\left|a_{pq}\right|^2 \tag{A.18}$$

Since the transformation is orthogonal, the sum of the squares of the diagonal elements increases correspondingly by $2\left|a_{pq}\right|^2$. Since the sequence is bounded below zero, and we can choose a_{pq} to be whatever we want, the sequence can be made to converge to zero.

Eventually, the matrix **D** becomes diagonal to computer precision. The diagonal elements give the eigenvalues of the original matrix **A**, since

$$\mathbf{D} = \mathbf{V}^T \cdot \mathbf{A} \cdot \mathbf{V} \tag{A.19}$$

where

$$\mathbf{V} = \mathbf{P}_1 \cdot \mathbf{P}_2 \cdot \mathbf{P}_3 \cdots \tag{A.20}$$

the $\mathbf{P}_i$'s being the successive Jacobi rotation matrices. The columns of **V** are the eigenvectors $(\mathbf{A} \cdot \mathbf{V} = \mathbf{V} \cdot \mathbf{D})$. They can be determined by considering

$$\mathbf{V}' = \mathbf{V} \cdot \mathbf{P}_i \tag{A.21}$$

at each stage of the calculation, where **V** is the identity matrix. In detail, Eq. (A.21) is

$$v'_{rs} = v_{rs} \qquad (s \neq p,\ s \neq q)$$

$$v'_{rp} = cv_{rp} - sv_{rq} \tag{A.22}$$

$$v'_{rq} = sv_{rp} + cv_{rq}$$

These equations are also rewritten in terms of τ to minimize round-off error.

The following routines listed in FORTRAN code are used to compute the eigenvalues and eigenvectors of a real, symmetric matrix. They are part of the IMSL reference library. Notice that the matrices must be in vector format.

```
      SUBROUTINE NROOT(M,A,B,XL,X)
C This routine computes the eigenvalues and eigenvectors of a real,
C symmetric matrix of the form B-inverse times A.  The routine
C EIGEN is used in combination with NROOT.  The matrices must be input
C as vectors.

C M - order of square matrices A, B and X.
C A - input vector (M x M).
C B - input vector (M x M).
C XL - output vector of length M containing eigenvalues of B-inverse
C       times A.
C X - output vector (M x M) containing eigenvectors columnwise.

      IMPLICIT REAL*8 (A-H,O-Z)
      IMPLICIT INTEGER*2 (I-N)
      REAL*8 A(M*M), B(M*M), XL(M), X(M*M), SUMV

C Compute eigenvalues and eigenvectors of B
      K=1
      DO 100 J=2,M
      L=M*(J-1)
      DO 100 I=1,J
      L=L+1
      K=K+1
  100 B(K)=B(L)

C The matrix B is a real symmetric matrix.
      MV=0
      CALL EIGEN(B,X,M,MV)

C Form reciprocals of square root of eigenvalues.  The results are
C premultiplied by the associated eigenvectors.
      L=0
      DO 110 J=1,M
      L=L+J
  110 XL(J)=1.0/DSQRT(DABS(B(L)))
      K=0
      DO 115 J=1,M
      DO 115 I=1,M
      K=K+1
  115 B(K)=X(K)*XL(J)

C Form (B**(-1/2))PRIME*A*(B**(-1/2))
      DO 120 I=1,M
      N2=0
      DO 120 J=1,M
      N1=M*(I-1)
      L=M*(J-1)+I
      X(L)=0.0
      DO 120 K=1,M
      N1=N1+1
      N2=N2+1
  120 X(L)=X(L)+B(N1)*A(N2)
      L=0
      DO 130 J=1,M
      DO 130 I=1,J
      N1=I-M
      N2=M*(J-1)
      L=L+1
      A(L)=0.0
      DO 130 K=1,M
      N1=N1+M
      N2=N2+1
  130 A(L)=A(L)+X(N1)*B(N2)

C Compute eigenvalues and eigenvectors of A.
      CALL EIGEN(A,X,M,MV)
      L=0
      DO 140 I=1,M
      L=L+I
  140 XL(I)=A(L)

C Compute the normalized eigenvectors
      DO 150 I=1,M
      N2=0
      DO 150 J=1,M
      N1=I-M
      L=M*(J-1)+I
      A(L)=0.0
      DO 150 K=1,M
      N1=N1+M
      N2=N2+1
  150 A(L)=A(L)+B(N1)*X(N2)
      L=0
      K=0
      DO 180 J=1,M
      SUMV=0.0
      DO 170 I=1,M
      L=L+1
  170 SUMV=SUMV+A(L)*A(L)
  175 SUMV=DSQRT(SUMV)
      DO 180 I=1,M
      K=K+1
  180 X(K)=A(K)/SUMV
      RETURN
      END

      SUBROUTINE EIGEN(A,R,N,MV)
C This routine computes the eigenvalues and eigenvectors of a real
C symmetric matrix.
C A - original matrix (symmetric), destroyed in computation.  Resultant
C     eigenvalues are developed in diagonal of matrix A in descending
C     order.
C R - resultant matrix of eigenvectors (stored columnwise, in same
C     sequence as eigenvalues).
C N - order of matrices A and R.
C MV - input code.
C       0   compute eigenvalues and eigenvectors.
C       1   compute eigenvalues only (R need not be dimensioned but
C     must still appear in calling sequence).

      IMPLICIT REAL*8 (A-H,O-Z)
      IMPLICIT INTEGER*2 (I-N)
      REAL*8 A(N,N), R(N,N)

C Generate identity matrix.
    5 RANGE=1.0E-012
      IF (MV-1) 10,25,10
   10 IQ=-N
      DO 20 J=1,N
       IQ=IQ+N
       DO 20 I=1,N
          IJ=IQ+I
          R(IJ)=0.0
          IF (I-J) 20,15,20
   15     R(IJ)=1.0
   20 CONTINUE

C Compute initial and final norms (anorm and anormx)
   25 ANORM=0.0
      DO 35 I=1,N
       DO 35 J=1,N
          IF (I-J) 30,35,30
   30     IA=I+(J*J-J)/2
          ANORM=ANORM+A(IA)*A(IA)
   35 CONTINUE
      IF (ANORM) 165,165,40
   40 ANORM=1.414*DSQRT(ANORM)
      ANRMX=ANORM*RANGE/DFLOAT(N)

C Initialize indicators and compute threshold, thr.
      IND=0
      THR=ANORM
   45 THR=THR/DFLOAT(N)
   50 L=1
   55 M=L+1

C Compute sin and cos
   60 MQ=(M*M-M)/2
      LQ=(L*L-L)/2
      LM=L+MQ
   62 IF (DABS(A(LM))-THR) 130,65,65
   65 IND=1
      LL=L+LQ
      MM=M+MQ
      X=0.5*(A(LL)-A(MM))
   68 Y=-A(LM)/DSQRT(A(LM)*A(LM)+X*X)
      IF (X) 70,75,75
   70 Y=-Y
   75 SINX=Y/DSQRT(2.0*(1.0+(DSQRT(1.0-Y*Y))))
      SINX2=SINX*SINX
   78 COSX=DSQRT(1.0-SINX2)
      COSX2=COSX*COSX
      SINCS=SINX*COSX

C Rotate L and M columns.
      ILQ=N*(L-1)
      IMQ=N*(M-1)
      DO 125 I=1,N
      IQ=(I*I-I)/2
      IF (I-L) 80,115,80
   80 IF (I-M) 85,115,90
   85 IM=I+MQ
      GOTO 95
   90 IM=M+IQ
   95 IF (I-L) 100,105,105
```

```
  100 IL=I+LQ
      GOTO 110
  105 IL=L+IQ
  110 X=A(IL)*COSX-A(IM)*SINX
      A(IM)=A(IL)*SINX+A(IM)*COSX
      A(IL)=X
  115 IF (MV-1) 120,125,120
  120 ILR=ILQ+I
      IMR=IMQ+I
      X=R(ILR)*COSX-R(IMR)*SINX
      R(IMR)=R(ILR)*SINX+R(IMR)*COSX
      R(ILR)=X
  125 CONTINUE
      X=2.0*A(LM)*SINCS
      Y=A(LL)*COSX2+A(MM)*SINX2-X
      X=A(LL)*SINX2+A(MM)*COSX2+X
      A(LM)=(A(LL)-A(MM))*SINCS+A(LM)*(COSX2-SINX2)
      A(LL)=Y
      A(MM)=X

C Tests for completion.
C Test for M = last column.
  130 IF (M-N) 135,140,135
  135 M=M+1
      GOTO 60

C Test for L = second from last column.
  140 IF (L-(N-1)) 145,150,145
  145 L=L+1
      GOTO 55
  150 IF (IND-1) 160,155,160
  155 IND=0
      GOTO 50

C Compare threshold with final norm.
  160 IF (THR-ANRMX) 165,165,45

C Sort eigenvalues and eigenvectors.
  165 IQ=-N
      DO 185 I=1,N
       IQ=IQ+N
       LL=I+(I*I-I)/2
       JQ=N*(I-2)
       DO 185 J=I,N
          JQ=JQ+N
          MM=J+(J*J-J)/2
          IF (A(LL)-A(MM)) 170,185,185
  170     X=A(LL)
          A(LL)=A(MM)
          A(MM)=X
          IF (MV-1) 175,185,175
  175     DO 180 K=1,N
          ILR=IQ+K
          IMR=JQ+K
          X=R(ILR)
          R(ILR)=R(IMR)
  180     R(IMR)=X
  185 CONTINUE
      RETURN
      END
```

A.2 LU Decomposition

Consider that the coefficent matrix **A** can be written as the product of two matrices,

$$\mathbf{L} \cdot \mathbf{U} = \mathbf{A} \tag{A.23}$$

where **L** is lower triangular (has elements only on the diagonal and below) and **U** is upper triangular (has elements only on the diagonal and above). For the case of a 3×3 matrix **A**, Eq. (A.23) has the form

$$\begin{bmatrix} \alpha_{11} & 0 & 0 \\ \alpha_{21} & \alpha_{22} & 0 \\ \alpha_{31} & \alpha_{32} & \alpha_{33} \end{bmatrix} \cdot \begin{bmatrix} \beta_{11} & \beta_{12} & \beta_{13} \\ 0 & \beta_{22} & \beta_{23} \\ 0 & 0 & \beta_{33} \end{bmatrix} = \begin{bmatrix} a_{11} & a_{12} & a_{13} \\ a_{21} & a_{22} & a_{23} \\ a_{31} & a_{32} & a_{33} \end{bmatrix}$$

We can use a decomposition such as Eq. (A.23) to solve the linear set of equations

$$\mathbf{A} \cdot \mathbf{x} = (\mathbf{L} \cdot \mathbf{U}) \cdot \mathbf{x} = \mathbf{L} \cdot (\mathbf{U} \cdot \mathbf{x}) = \mathbf{b} \tag{A.24}$$

by first solving for the vector **y** such that

$$\mathbf{L} \cdot \mathbf{y} = \mathbf{b} \tag{A.25}$$

and then solving

$$\mathbf{U} \cdot \mathbf{x} = \mathbf{y} \tag{A.26}$$

The advantage of breaking up one linear set into two successive ones is that the solution of a triangular set of equations is quite trivial. Thus, Eq. (A.25) can be solved by *forward elimination* as follows,

$$y_1 = \frac{b_1}{\alpha_{11}}$$

$$y_i = \frac{1}{\alpha_{ii}}\left[b_i - \sum_{j=1}^{i-1}\alpha_{ij}y_j\right] \qquad i = 2,3,\ldots,N \tag{A.27}$$

while Eq. (A.26) can then be solved by *backsubstitution* as follows,

$$x_N = \frac{y_N}{\beta_{NN}}$$

$$x_i = \frac{1}{\beta_{ii}}\left[y_i - \sum_{j=i+1}^{N}\beta_{ij}x_j\right] \qquad i = N-1,\ N-2,\ldots,1 \tag{A.28}$$

Notice that once we have the *LU* decomposition of **A** we can solve with as many right-hand sides as we then care to, one at a time. This is a distinct advantage over the methods of Gauss-Jordan elimination and Gauss elimination with backsubstitution.

The following routines listed in FORTRAN code are used in combination to solve sets of linear equations and are listed in reference [82]. As well, the routines may be used to determine the inverse of a matrix as well as its determinant.

```
      SUBROUTINE Ludcmp(A,N,INDX,D)
C Given an N by N matrix A with physical dimension NP, this routine
C replaces it by the LU decomposition of a rowwise permutation of
C itself.  A and N are input.  INDX is an output vector which records
C the row permutation effected by the partial pivoting; D is output as
C +- 1 depending on whether the number of row interchanges was odd or
C even.  This routine is used in combination with LUBKSB to solve
C linear equations or invert a matrix.  (See Numerical Recipes, Fortran
C Version, p. 35)
      IMPLICIT REAL*4 (A-H,O-Z)
      IMPLICIT INTEGER*2 (I-N)
      PARAMETER (NMAX=500,TINY=1.0E-20)
      REAL*4 A(N,N), VV(NMAX)
      INTEGER*2 INDX(N)
      D=1.0
      DO I=1,N
         AAMAX=0.0
         DO J=1,N
          IF (ABS(A(I,J)).GT.AAMAX) AAMAX=ABS(A(I,J))
         END DO
         IF (AAMAX.EQ.0.0) PAUSE 'Singular matrix.'
         VV(I)=1.0/AAMAX
      END DO
      DO J=1,N
         DO I=1,J-1
            SUM=A(I,J)
            DO K=1,I-1
               SUM=SUM-A(I,K)*A(K,J)
            END DO
            A(I,J)=SUM
         END DO
         AAMAX=0.0
         DO I=J,N
            SUM=A(I,J)
            DO K=1,J-1
               SUM=SUM-A(I,K)*A(K,J)
            END DO
            A(I,J)=SUM
          DUM=VV(I)*ABS(SUM)
            IF (DUM.GE.AAMAX) THEN
               IMAX=I
               AAMAX=DUM
            ENDIF
         END DO
         IF (J.NE.IMAX) THEN
            DO K=1,N
               DUM=A(IMAX,K)
               A(IMAX,K)=A(J,K)
               A(J,K)=DUM
            END DO
            D=-D
            VV(IMAX)=VV(J)
         ENDIF
         INDX(J)=IMAX
         IF (A(J,J).EQ.0.0) A(J,J)=TINY
C If the pivot element is zero the matrix is singular (at least to the
C precision of the algorithm).  For some applications on singular
C matrices, it is desirable to substitute TINY for zero.
         IF (J.NE.N) THEN
            DUM=1.0/A(J,J)
            DO I=J+1,N
               A(I,J)=A(I,J)*DUM
            END DO
         ENDIF
      END DO
      RETURN
      END


      SUBROUTINE Lubksb(A,N,INDX,B)
C Solves the set of N linear equations A*x=B.  Here A is input, not as
C the matrix A but as its LU decomposition, determined by the routine
C LUDCMP.  INDX is input as the permutation vector returned by LUDCMP.
C B is input as the right-hand side vector B, and returns with the
C solution vector X.  A, N, NP and INDX are not modified by this routine
C and can be left in place for successive calls with different right-
C hand sides B.  This routine takes into account the possibility that B
C will begin with many zero elements, so it is efficient for use in
C matrix inversion. (See Numerical Recipes, Fortran Version, p. 36).
      IMPLICIT REAL*4 (A-H,O-Z)
      IMPLICIT INTEGER*2 (I-N)
      REAL*4 A(NP,NP), B(N)
      INTEGER*2 INDX(N)
      II=0
      DO I=1,N
         LL=INDX(I)
         SUM=B(LL)
         B(LL)=B(I)
         IF (II.NE.0) THEN
            DO J=II,I-1
               SUM=SUM-A(I,J)*B(J)
            END DO
         ELSE IF (SUM.NE.0.0) THEN
            II=I
         ENDIF
         B(I)=SUM
```

```
END DO
DO I=N,1,-1
   SUM=B(I)
   DO J=I+1,N
      SUM=SUM-A(I,J)*B(J)
   END DO
   B(I)=SUM/A(I,I)
END DO
RETURN
END
```